UNIVERSITY OF LONDON THESIS

Degree PhD Year 2008 Name of Author SPEARPOINT, Philip Anthony

Structure-Function Studies of the Influenza A M2 Proton Channel

By Philip Spearpoint

ProQuest LLC
789 East Eisenhower Parkway
P.O. Box 1346
Ann Arbor, MI 48106-1346

Acknowledgements

I would like to thank all the people who have given me a vast amount of help both academic and otherwise in the years it has taken to write this thesis. Firstly a big thank you to my Alan Hay who has been my stalwart supervisor throughout the process. Secondly and equally a big thankyou to Dr Steve Martin for at times, having to act as another supervisor. Within the lab, without the help of Peter Czabotar, Patrick Collins, Malini Menon, Steve Wharton and Seti Grambasl would have no doubt have been lost. Lastly, but not least a big thank you to my family for all their support and especially Jayne Smith-Palmer and my father for taking the time to read parts of this thesis.

Abstract

The influenza A virus M2 protein is a minor component of the virus membrane, it forms a homotetrameric, pH-activated, proton-selective channel and is the target of the anti-influenza drugs, amantadine and rimantadine. Two projects were undertaken to study the structure-function relationships of M2 and the mechanism of its inhibition. Firstly, an M2 protein with a pH-sensitive GFP fused to the C-terminus was constructed to determine whether it could be used to measure directly M2 proton conduction. The pH probe was responsive to rimantadine-sensitive changes in the pH gradient which were detected but were small. This was in part due to reduced proton conductance of the protein possibly due to altered conformation of the M2 pore, but may also reflect the low sensitivity of the GFP probe to local pH in the vicinity of the plasma membrane. Secondly tryptophan fluorescence studies of purified, E.coli-expressed M2 protein in detergent micelles investigated the mechanism of proton conduction and inhibition by anti-M2 drugs. Shifts in emission maxima and fluorescence intensity measurements relating to the tryptophans in the M2 pore indicated a molecular interaction between histidine 37 (His37) and tryptophan 41 (Trp41). pKa values from these experiments correlated with previously reported proton-mediated activation and permeation of the M2 channel. Acrylamide quenching showed that upon histidine protonation, Trp41 was more solvent accessible while polarisation measurements indicated a more restricted environment for Trp41 at low pH. Red-edge excitation measurements suggested a proteinaceous pore in which water molecules were highly immobile when the channel was closed, yet could freely reorientate upon channel activation. The M2 inhibitor rimantadine reversed these phenomena either fully or partially. Equilibrium and time-resolved measurements of this drug-induced

reversal permitted the determination of both association and dissociation rate constants and the affinities of drug interaction with M2. These results provide further support for an allosteric mechanism of amantadine inhibition.

Contents

List of Figures

Abbreviation List

APTS	Ammonium Persulphate
$BK_{410/470}$ measurements	Fluorescence microscopy background
BL21	Protein expressing *Escherichia coli*
$CaCl_2$	Calcium Chloride
C41	Protein expressing *Escherichia coli*
CD	Circular Dichriosm
Cl	Chloride
CMC	Critical Micelle Concentration
CO_2	Carbon Dioxide
Cu	Copper
Cys	Cysteine (an amino acid)
cDNA	copy Deoxyribonucleic acid
DE3	Designation for type of *Escherichia coli*
D	Drug

Abbreviation List

DH5α	*Escherichia coli used for* Deoxyribonucleic acid work
DMSO	Dimethyl Sulfoxide
DMPC	1.2-dimyristoyl-sn-glycero-3-phosphocholine
DMPG	1,2-dimyristoyl-sn-glycero-3-phosphoglycerol
DNA	Deoxyribonucleic acid
DPC	Dodecylphosphocholine
DTT	Dithiothreitol
EDTA	Ethylenediamine Tetraacetic acid
F	Phenylalanine
FACS	Flow cytometry
FCS	Foetal Calf Serum
FPLC	Fast Protein Liquid Chromatography
GFP	Green Fluorescent Protein
H^+	Protons
HA	Haemagluttinin
Hb	Haemoglobin
HCl	Hydrochloric Acid
HEPES	4-(2-hydroxyethyl)-1-piperazineethanesulfonic acid
H37A	M2 mutant
His	Histidine
IC	Internal Conversion
IgG	Immunoglobulin G
IPTG	Isopropyl β-D-1-thiogalactopyranoside
K_d	Dissociation Constant
$k_T(r)$	Rate of Energy Transfer
k_{nr}	Non-Radiative Decay Rate
k_{obs}	Observed binding constant
k_{on}	On-Rate
k_{off}	Off-Rate
k_q	Stern-Volmer Constant
^1L_a	Tryptophan Transition State
^1L_b	Tryptophan Transition State
LB	Liquid Broth
LCR	Locus Control Region
LDAO	N,N-Dimethyldodecylamine-N-oxide
MES	2-(*N*-morpholino)ethanesulfonic acid
MIC	Minimum Inhibitory Concentration
M2-GFP	M2-GFP Fusion Protein
M2-TM	M2 Trans-Membrane Domain Peptide
MEL	Mouse Erythrocyte Luekaemia Cells
MEM	Minimal Essential Media
$MgCl_2$	Magnesium Chloride
NA	Neuraminidase
NaCl	Sodium Chloride
NMDG	N-methyl-d-glucamine
NIMR	National Institute for Medical Research
NMR	Nuclear Magnetic Resonance
ssNMR	Solid-State Nuclear Magnetic Resonance
NP	Nucleoprotein
OD	Optical Density
ORF	Open Reading Frame
PBS	Phosphate Buffered Saline

Abbreviation List

PCR	Polymerase Chain Reaction
Phe	Phenylalanine
PISEMA	Polarisation Inversion Spin at the Magic Angle
pK_a	Acid Dissociation Constant
PM	Plasma Membrane
PMSF	Phenylmethylsulphonyl fluoride
Q	Quantum Yield
[Q]	Quenching Concentration
$R_{410/470}$	GFP excitation wavelengths
R_o	Fórster Distance
RET	Resonance Energy Transfer
RNA	Ribonucleic Acid
mRNA	Messenger Ribonucleic Acid
vRNA	Viral Nucleic Acid
RNP	Ribonucleoprotein
S_n	Vibrational Energy Levels
SDS	Sodium Dodecyl Sulphate
SDS-PAGE	Sodium Dodecyl Sulphate Polyacrylamide Gel Electrophoresis
SNARF1-AM	Seminaphtorhodafluor-1-acetoxymethylester
TBE	Tris-Borate-EDTA Buffer
TEMED	Tetramethylethylenediamine
TGN	*Trans-Golgi* network
Trp	Tryptophan
Tyr	Tyrosine
UV-CD	Ultra-Violet Circular Dichriosm
V27A	M2 Mutant
W	Tryptophan
WHO	World Health Organisation
WM2	Weybridge M2
Γ	Emissive Rate of Fluorophore
τ_n	Fluorescence Lifetime
τ_o	Bio-Molecular Quenching constant
I_Π	Vertical Polarised Fluorescence emission intensity
$I_\perp$	Horizontal Polarised Fluorescence emission intensity

Chapter 1:Introduction

In 1933, in the shadow of the 1918 Influenza pandemic, waves of a "flu-like" disease spread across London. The impact of the 1918 Influenza pandemic had been monumental, the resulting devastation unprecedented since the black death of the Middle Ages. The 1933 "flu like" illness aroused the interest of scientists based at the National Institute for Medical Research (NIMR) who focused their attention on identifying the causative agent.

Using canine distemper study facilities the infectious agent was identified as the Influenza virus. This was done by using infected colleagues from the outbreak at the time, taking throat washings which were filtered and inoculating into ferrets with the washings, resulting in influenza-like symptoms. Transmission to other ferrets was observed by induced immunity (Smith, 1933). Finally, Koch's postulates were fulfilled almost serendipitously when a ferret, infected with an adapted influenza virus sneezed at a scientist. The scientist subsequently developed flu-like symptoms, and the virus isolated from his throat washings proved to be the same virus to which the ferret was exposed (Smith and Stuart-Harris, 1936).

Influenza pandemics occur at varying intervals, this is due to the emergence of a new antigenic subtype, which is capable of human circulation and result from the emergence of novel A virus subtype to which the human population has little or no pre-existing immunity, facilitating their rapid spread. The pandemic of 1918-1919 killed an estimated 40-60 million people, while other pandemics

such as those in 1957 and 1968 were less severe (with approximately 1 million deaths worldwide), but were still major causes of morbidity and mortality. Annual epidemics of influenza are the result of antigenic variation of flu viruses but the mechanisms for this are distinct from those for pandemic viruses (see later). Influenza epidemics affect 10-20% of the population each year and are responsible for 3000-5000 deaths in England and Wales each year (Tillett *et al.*, 1980).

1.1: Influenza Virus Classification

Influenza viruses belong to the virus family *Orthomyxoviridae*, (from the Greek, *orthos* meaning "correct", and *myxo* "mucus"). The virion is enveloped and the genome consists of segmented, negative single-stranded RNA. Three types of human Influenza viruses exist, types A, B and C, based on the antigenicity of their respective nucleopcapsid (NP) and matrix (M1) proteins (World Health Organisation; WHO, 1953). A fourth arthropod-borne virus, *Thogotovirus* has also been classified in the *Orthomyxoviridae;* however, this classification is disputed. There are many differences between this virus and the three genera of Influenza (Neumann *et al.,* 2004). *Thogotovirus* are not discussed further in this thesis. Influenza B and C viruses have been primarily isolated from humans while Influenza A infects a variety of species, but its main host is aquatic birds.

Influenza A viruses are further divided into subtypes based on the antigenicity of two of their surface glycoproteins, haemagglutinin (HA) and neuraminidase (NA). Sixteen HA subtypes and nine NA subtypes have been identified to date (Schild *et al.,* 1985, Fouchier *et al.*, 2005). Whereas all sixteen HA subtypes circulate in aquatic birds, only three have evolved in humans (H1, H2, H3), two in pigs (H1, H3) and two in horses (H3, H7) (Webster, 1992).

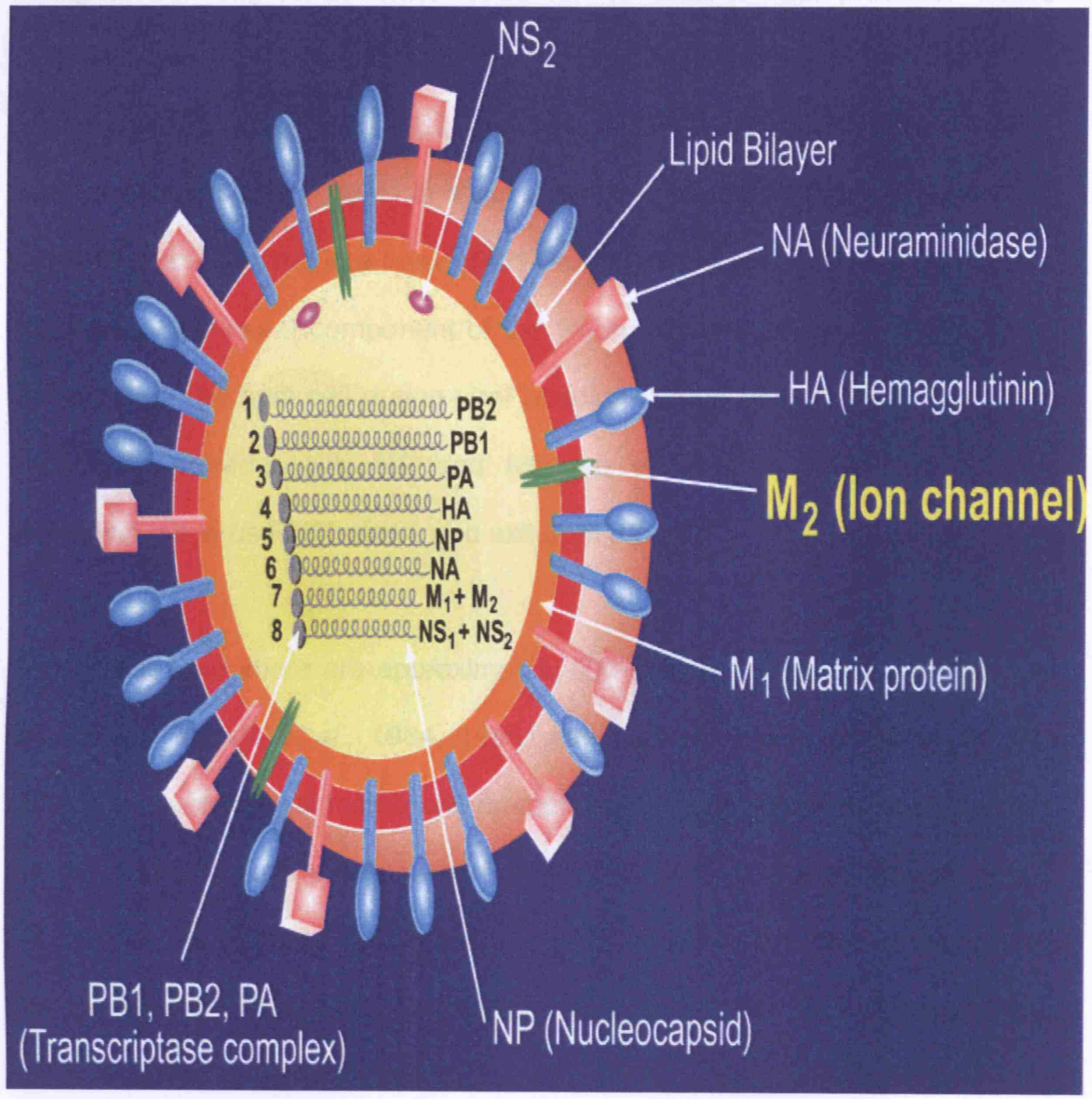

Figure 1.1: A schematic representation of a single Influenza A virion. The RNPs (RNA, NP, PB1, PB2 and PA) constitute a self-replicating complex, and are encased in matrix protein, which is covered by a lipid bilayer. HA, NA and M2 are inserted in the membrane and facilitate the transport of the transcriptase complex into and out of the cell.

1.2: Influenza Virion Structure

A diagram of an Influenza A virion is shown in Figure 1.1. The genome consists of eight RNA segments, which code for 11 distinct viral proteins. These segments are each associated with nucleoprotein (NP) and the viral RNA polymerase proteins (PB1, PB2 and PA) to form ribonucleoprotein (RNP) particles (Hagen *et al.*, 1994) in a coiled hairpin structure (Pons *et al.*, 1969). The RNP's are covered in a layer of M1 protein (Schulze, 1970 and 1972). This is the major structural component of the virion, which underlies a lipid bilayer, derived from the host cell during viral budding (Kates *et al.*, 1961). The three membrane proteins, HA, NA and M2 are embedded within this bilayer, facilitating the virus RNP's entry and exit from the cell.

In a typical virion there are approximately 600-800 HA molecules, 100-200 NA molecules (Ruigrok *et al.*, 1984, 1998) and typically 20-40 copies of the M2 protein, a minor integral membrane protein which forms an ion channel (Sugrue and Hay, 1991). All these proteins are found within the viral membrane. Both HA and NA are found to accumulate in lipid rafts within the plasma membrane (Nayak, Hui and Barman, 2004); M2is not found in lipid rafts, hence the low levels found in the virion (Lesser and Lamb, 2005). Influenza virus particles are typically 80-120nm in diameter, spherical in shape with membrane glycoproteins protruding from the surface (Figure 1.2) (Taylor, 1943). However, virions can also be filamentous (Mosley, 1946; Roberts, Lamb and Compans, 1998). Clinical human isolates are predominantly filamentous (Chu *et al.*, 1949), and a gradual shift from filamentous to spherical morphology has been observed upon serial passage in embryonated hens eggs (Choppin and Tamm, 1960).

1.3: The Influenza Virus Replication Cycle

Influenza viruses bind to cells via an interaction between HA and sialylated receptors (Gottschalk, 1959), which leads to receptor-mediated endocytosis and internalization of the virus (Figure 1.2) (Matlin *et al.,* 1981; Sieczkarski and Whittaker, 2002). During transmission along the endosomal pathway the virus is exposed to increasing acidity. This acidity causes M2 to conduct protons into the virion, lowering the intra-virion pH and causing M1 to dissociate from the RNP's (Martin and Helenius, 1991; Wharton *et al.,* 1994). The high acidity of the endosome triggers a conformational change in the HA molecule, resulting in fusion between the viral and endosomal membranes (Skehel *et al.,* 1982), which permits release of RNP's into the cytoplasm and import to the nucleus (Bukrinskaya *et al.,* 1982).

Once in the nucleus, the RNP's are transcribed into messenger RNA (mRNA) and replicated by the polymerase complex, comprising proteins PA, PB1, PB2 (Hay *et al.,* 1977; Braam, Ulmanen and Krug., 1983; Honda *et al.*, 2002). In addition to the polymerase proteins, NP is required for the replication of the vRNA (Beaton and Krug, 1986; Portela and Digard, 2002). mRNAs are translated into the viral proteins, including HA, NA and M2 which are synthesized at the endoplasmic reticulum (ER) by ER-associated ribosomes (Compans, 1973; Zebedee, Richardson and Lamb, 1985). HA, NA and M2 are inserted into the cell plasma membrane (Webster., 1995; Sugrue, Belshe and Hay., 1990). Upon assembly of the replicated viral genome and its associated proteins, progeny virions are released by budding from lipid rafts at the plasma

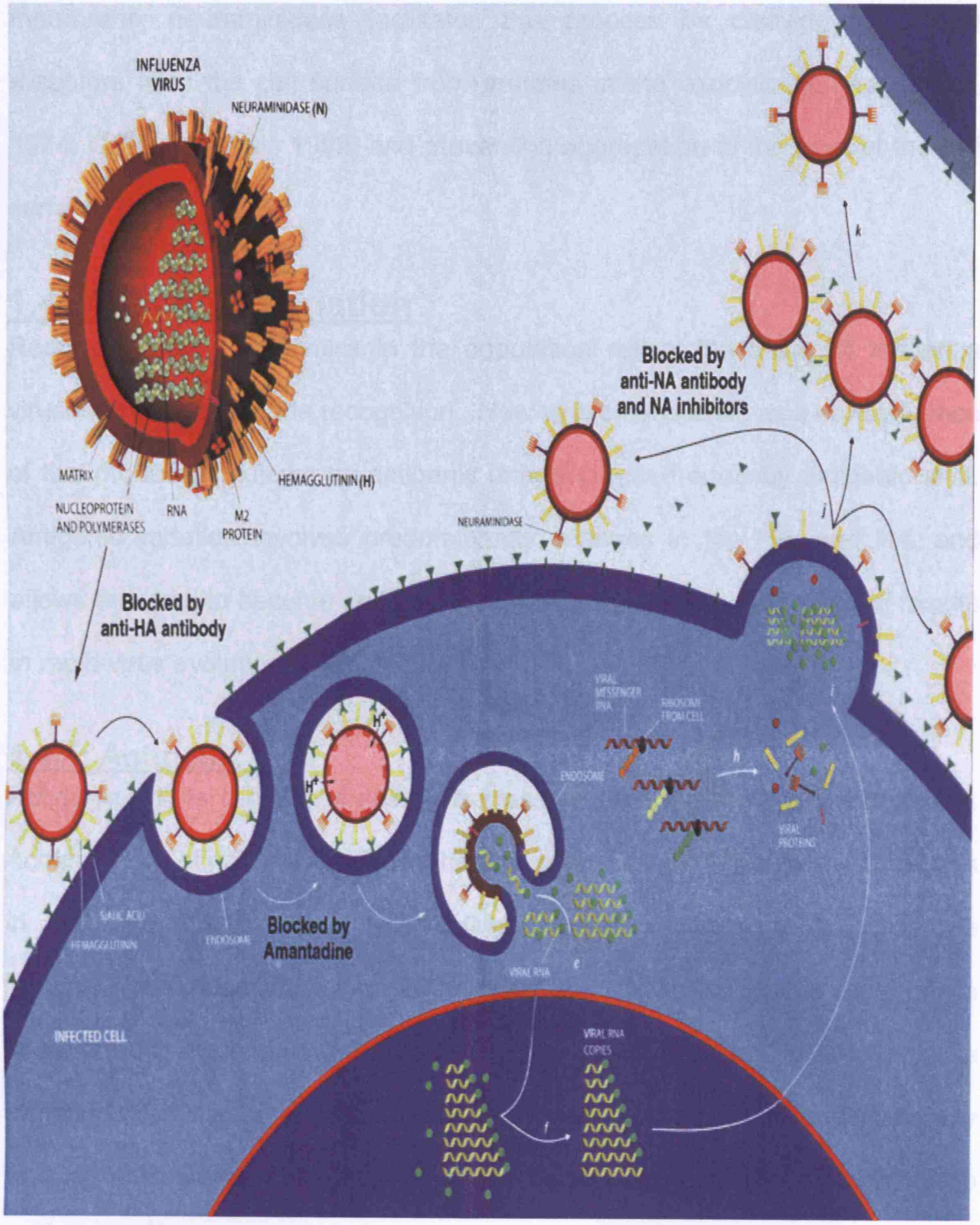

Figure 1.2: The replication cycle of Influenza A virus. The process from cell entry to exit is shown. A detailed explanation is given in the text. The points at which the two classes of anti-Influenza drugs are known to inhibit are also shown (Adapted from Scientific American Lancer and Webster, 1999)

membrane; neuraminidase facilitates this process by cleaving sialic acid receptors from the cell surface from proteins in the exocytic pathway. (Hay, 1974; Gallagher et al., 1992) and preventing aggregation of the virus at the cell surface (Palese, 1974)

1.4: Antigenic Variation

Recurrent annual epidemics in the population reflect the ability of Influenza viruses to evade immune recognition. New viral strains arise as a consequence of two processes, known as antigenic drift, and less frequently antigenic shift. Antigenic variation involves predominantly changes in the HA, and NA, and allows the virus to become undetected by the host defence systems and results in rapid virus evolution.

1.4.1: Antigenic Drift

Antigenic drift is a result of selection pressure from the host immune system. Accumulation of point mutations in the viral genome lead to amino acid changes in the HA and NA proteins, by selecting a dominant circulating strain from the "quasispecies" (Domingo *et al.,* 2001; Domingo, 2003) and viral evasion of the host immune system is permitted (Figure 1.3). The rate at which these mutations occur is high since the RNA polymerase lacks proof-reading activity and introduces errors in the range of 10^{-3} to 10^{-4} per nucleotide, in contrast to 10^{-8} to 10^{-11} for DNA polymerases. The surface proteins are the fastest evolving proteins within the Influenza virus. HA is more variable than NA with most accumulated changes located within the antigenic sites in the HA1 region of the protein (Both et al., 1981). Furthermore, these amino acid substitutions were observed to occur more frequently at antigenic sites, suggesting positive mutant selection through immune surveillance (Ina and Gojobori, 1994; Fitch *et al.,* 1997; Bush *et al.,* 1999).

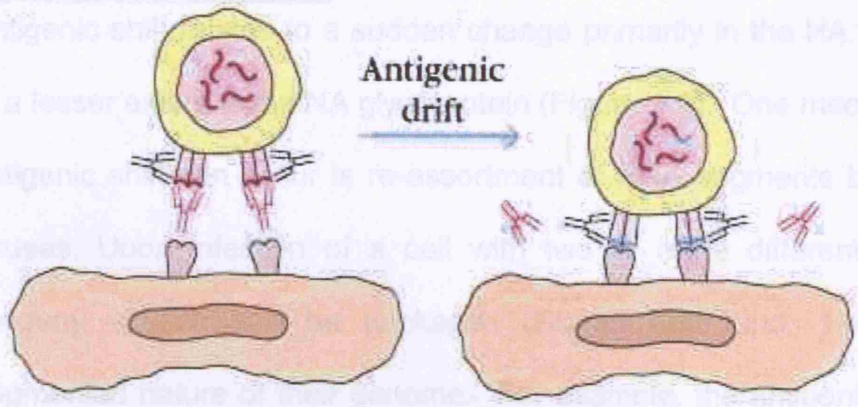

Antigenic Drift

- Minor change with subtype
- Point mutations
- Occur in A and B subtypes
- May cause epidemics
- Example: drifted A/H3N2/Fujian circulated vs A/H3N2/Panama (vaccine strain) in 2003-2004

Figure 1.3: A proposed mechanism by which antigenic drift occurs within Influenza virus due to immunological pressure. This force compels a change in the HA thereby interfering with antibody binding and allowing the newly mutated virus to infect the host.

Phylogenetic analysis has shown that HA of the H3 subtype incorporates mutations leading to evolution of this protein several times faster than the non-structural proteins (Fitch *et al.,* 1991).

1.4.2: Antigenic Shift

Antigenic shift relates to a sudden change primarily in the HA glycoprotein and to a lesser extent in the NA glycoprotein (Figure 1.4). One mechanism by which antigenic shift can occur is re-assortment of RNA segments between different viruses. Upon infection of a cell with two or more different viruses, hybrid progeny viruses can be packaged (Burnet and Lind, 1949) due to the segmented nature of their genome. For example, the antigenic shift which led to the Hong Kong influenza pandemic in 1968 was due to the production of a recombinant virus containing an avian H3 subtype HA gene and the remaining seven RNA segments from an H2N2 virus that was circulating within the human population at the time (Kawaoka *et al.,* 1989).

In addition to reassortment, antigenic shift may occur by direct cross-species transmission of a virus containing a novel HA, for instance, infections of humans by avian viruses (Peiris *et al.,* 1999; Fouchier *et al.,* 2004). The avian H5N1 virus was first transmitted from chickens to humans in 1997 in Hong Kong (de Jong et al., 1997). It is unusual for avian viruses to infect humans and also human viruses do not infect birds. Pigs are permissive to infection by both human and avian strains, thus may act as a "mixing vessel" and play an important role in the emergence of pandemic viruses. Alternatively, a direct jump from avian to humans may occur as a result of accumulation of adaptive

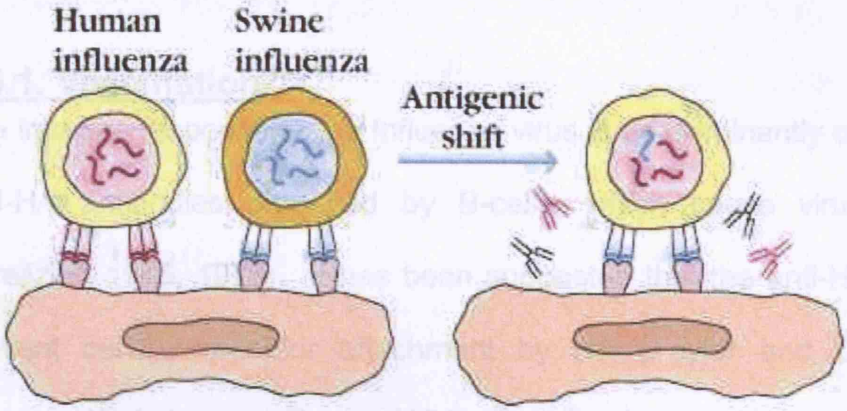

Antigenic Shift

- Major change, new subtype
- Exchange of gene segments or critical point mutations leading to new subtype
- Occur in A subtypes only
- May cause pandemics
- Example: H3N2 replaced H2N2 in 1968

Figure 1.4: A perceived mechanism by which antigenic shift occurs (simultaneous infection with a swine and human virus in an intermediate host followed by reassortment). In the case of the 1918 "Spanish" flu a straight jump from birds to humans occurred.

mutations in various genes as appears to have given rise to the 1918 H1N1 virus (Tumpey *et al.*, 2005).

1.5: Vaccination and Antivirals

1.5.1. Vaccination

The immune response to the Influenza virus is predominantly composed of IgG anti-HA antibodies produced by B-cells, which cause virus neutralisation (Virelizier, 1975, 1976). It has been suggested that the anti-HA antibody may prevent cellular receptor attachment by HA (Taylor and Dimmock, 1985; Tamura, Webster and Ennis, 1991). B cells also produce anti-NA antibodies which attenuate viral replication and budding due to inhibition of NA-mediated sialic acid cleavage (Schulman *et al.*, 1968; Johansson *et al.*, 1989). Vaccines against influenza virus primarily stimulate humoral protective immunity. The rapid evolution of the virus surface proteins gives rise to new antigenic strains and the vaccine formula needs to be updated regularly.

The World Health Organisation (WHO) coordinates a global influenza surveillance network. Routine characterization of the antigenic, genetic and epidemiological properties of currently circulating strains is performed in order to produce informed advice for vaccine strain selection. Current vaccines are based on inactivated whole virus (formalin-inactivated), split-product vaccines (disrupted) or purified surface antigens using standardised quantities of immunoreactive HA (and NA). Split and subunit vaccines induce fewer side effects in immunised individuals than whole virus vaccine and are the most widely used vaccines today.

The vaccine generally includes one type B virus and two type A subtype strains based on recent circulating strains. Inactivated vaccines are safe, immunogenic and effective, preventing illness in 70-90 % of healthy young adults. However, the need to update the vaccine on an annual basis is a limitation and novel strategies are being pursued to generate longer-lasting vaccines with improved immunogenicity (Kemble and Greenberg, 2003).

1.5.2 Antivirals

Due to the absence of a vaccine providing long-term protection there is an unmet clinical need for the development of anti-influenza chemotherapeutic agents. Currently, the drugs available include the tricyclic amine amantadine (1-aminoadamantane hydrochloride) and its structural analogue rimantadine (1-Adamantylethylamine hydrochloride) that inhibit M2, and the neuraminidase inhibitors zanamivir and oseltamivir (Figure 1.5).

Amantadine was discovered in the early 1960's and is administered to patients prophylactically during the early onset of infection and symptoms and acts to shorten the timespan of the disease. Amantadine has been licensed in the USA and UK but its use has been somewhat limited due to neurological side-effects while rimantadine, which has less of these, has been used heavily in Russia and the former Soviet States (Zlydnikov *et al.,* 1981). A major disadvantage to the use of these compounds against annual epidemics of flu is that they are only effective against Influenza A virus infections. Also, resistance to these compounds develops rapidly and therefore their prolonged use combined with side-effects is undesirable (Appleyard, 1977; Hayden *et al.,* 1989). Analysis of resistance mutations has shown that they map to the transmembrane domain of

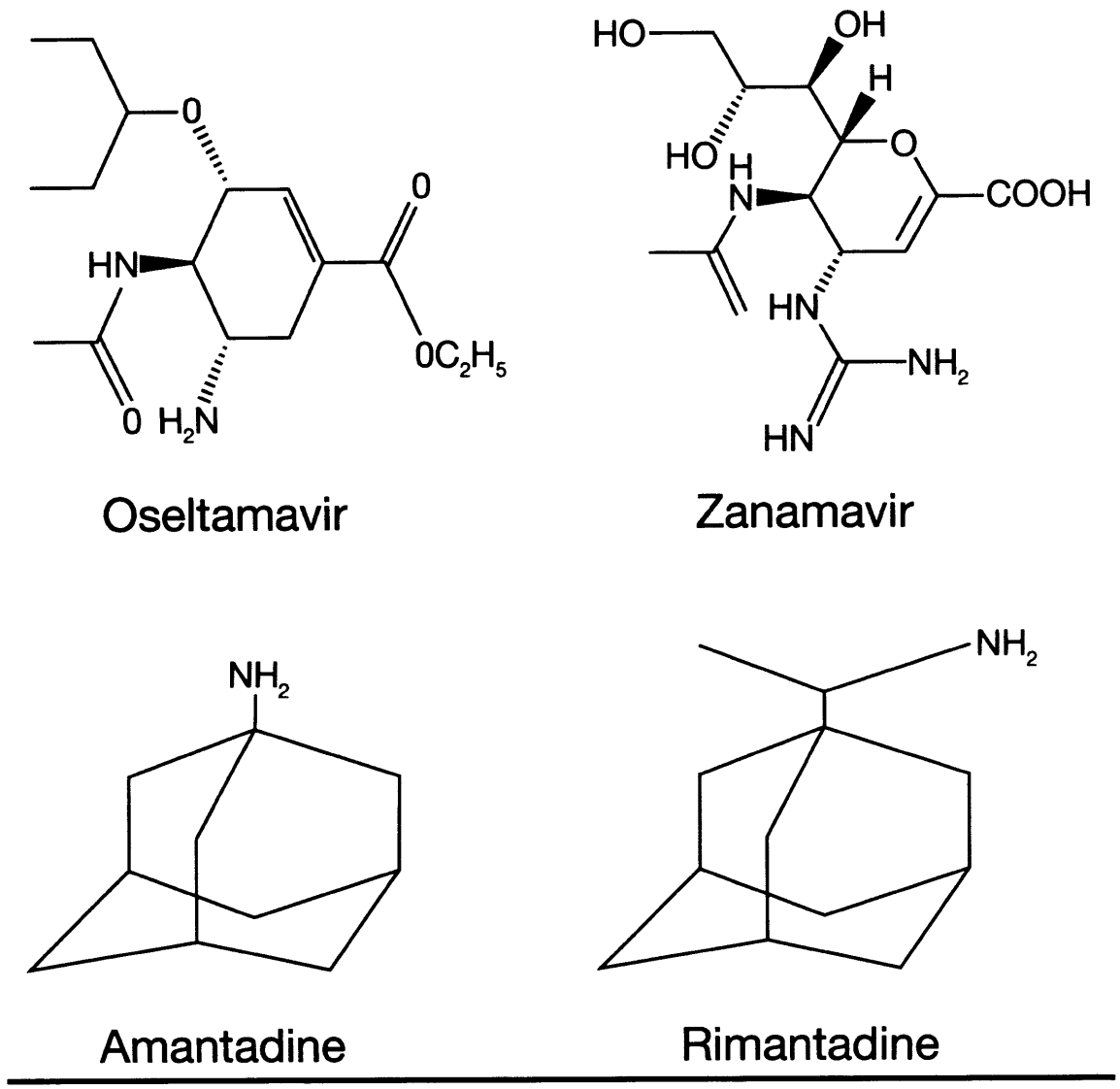

Figure 1.5: The neuraminidase inhibitors, Oseltamavir, Zanamavir, and the anti-M2 inhibitors, Amantadine and Rimantadine.

the M2 protein (Hay *et al.,* 1979, 1985). M2 inhibitors are currently not recommended for treatment of H5N1 influenza infections due to the prevalence of amantadine resistance among H5N1 viruses (Hayden, 2006).

Recent approaches to anti-influenza therapy have involved computer-aided design of chemotherapeutic agents against NA. The sialic acid-binding site on NA was identified as a large pocket on the surface of each of the four subunits (Colman et al., 1983). The surrounding amino acids are invariant in both Influenza A and B. The crystal structure allowed the theoretical design of compounds to inhibit sialic acid binding to the pocket with high affinity, and also specificity for viral neuramindases. The two compounds mentioned above were synthesised and were able to inhibit influenza virus plaque formation and virus replication in ferrets (von Izstein et al., 1993). Resistance to these inhibitors has been characterised *in vitro* and resistance has been observed following clinical treatment with oseltamivir, in particular, including H5N1 human cases (Gubaneva, 2004; Le *et al.,* 2005).

1.6: The M2 Protein of Influenza A

1.6.1: The M2 Proton Channel

Before neuraminidase inhibitors the only drugs available clinically for the treatment of influenza A were amantadine and its derivative rimantadine, which were first used in the 1960s. An early study suggested that these drugs inhibited viral entry (Kato & Eggers, 1969). Sequencing of amantadine escape mutants indicated that mutations occurred in a defined area of the M gene, which coded for a minor integral membrane protein, M2 (Hay *et al.*, 1985).

Biochemical experiments suggested that the M2 protein was tetrameric and shaped in a channel like structure (Lamb, Zebedee & Richardson. 1985; Sugrue *et al.,* 1990). This was then confirmed using direct electrophysiological measurements (Pinto *et al.,* 1992, 2000; Chizhmakov *et al.,* 1996). It should be noted that amantadine has no effect on Influenza A resistant viruses, and Influenza B and C due to the fact that they lack the M2 protein, which further reinforces this as the site of action. Both of these influenza types however encode minor integral membrane proteins, which are similar in size and structure to the M2; but are produced by either different gene segments or expression mechanisms as discussed below.

1.6.1.1: The Roles of M2 within Influenza A Virus Replication

Two roles have been identified for the M2 protein in the viral replication cycle (Figure 1.6); In virus entry during endocytosis, M2 conducts protons into the virion interior, acidifying it. This low pH causes dissociation of RNP-M1 protein interactions and facilitates release of RNP's into the cytoplasm following HA mediated membrane fusion, allowing their entry into the nucleus and initiation of replication. Addition of amantadine causes retention of RNP-M1 complexes in the cytoplasm, thereby inhibiting viral replication (Bukrinskaya *et al.,* 1982; Sugrue *et al.,* 1990; Martin and Helenius., 1991; Wharton *et al.,* 1994). When M1 expressing cells were infected with virus, replication was blocked by M1 associating with RNP's (Bui *et al.,* 1996). When the cytoplasm was acidified, however, RNPs were able to enter the nucleus and replication took place. Efficient removal of M1 from RNPs of detergent solubilized virus occurs at pH below 6 in isotonic solution and is consistent with the proposed function of M2

A)

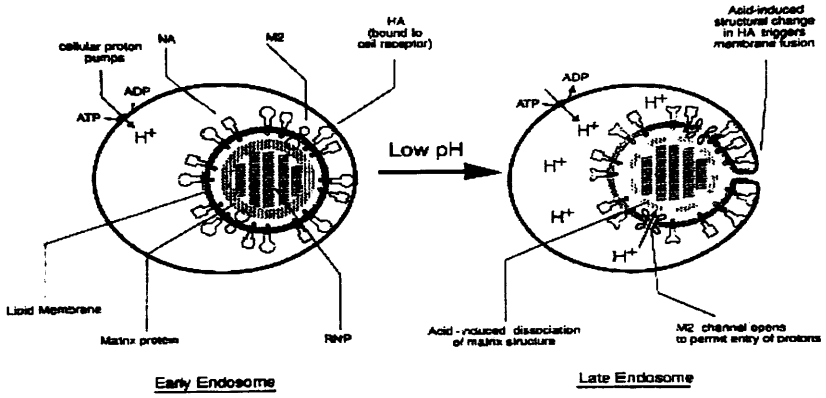

B)

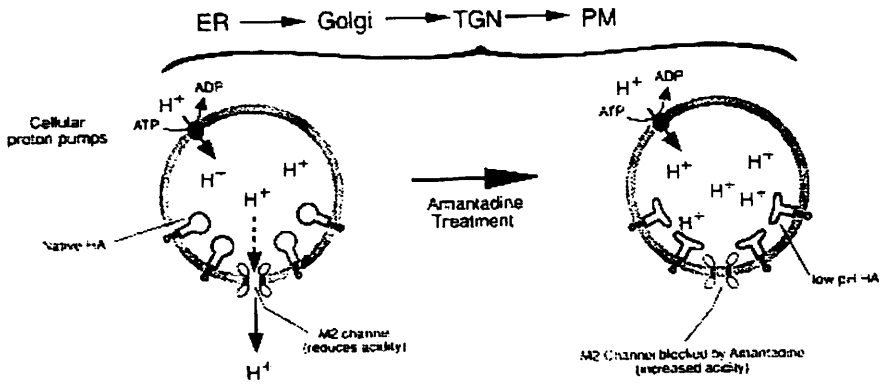

Figure 1.6: Two roles of the M2 proton channel during Influenza virus replication. A) as the Influenza virion is transported down the endosomal pathway, M2 conducts protons into the virus interior dissociating M1-RNP interactions so that free RNP's can be released and transported to the nucleus. B) M2 in the TGN acts as a proton leak channel elevating TGN pH and prevents HA conversion into its low pH form (Ciampor et al., 1992).

(Zhirnov *et al.,* 1992). During infection by pathogenic avian viruses, their HAs are proteolytically cleaved at a sequence of basic amino acids by intracellular proteases such as furin in the *Trans*-Golgi (Stieneke-Grober *et al.,* 1992).This makes them vulnerable to the low pH of the *Trans*-Golgi and irreversible structural change. Co-transport of functional M2 with HA is required to elevate the pH of the *Trans*-Golgi network, to allow passage of the native, acid-sensitive, cleaved HA1/HA2 to the plasma membrane. Inhibition of M2 by amantadine causes a reduction in pH of the *Trans Golgi* and structural change in HA thereby blocking viral replication. (Ciampor *et al.,*1992). A correlation of M2 activity and pH stability of HA is observed in pathogenic avian viruses (Grambas *et al.,* 1992).

A third role has recently been elucidated for the M2 protein. Using reverse genetics the C-terminus of the M2 protein has been shown to be important for virus morphology and production of infectious virus particles (McCown and Pekosz, 2006). Truncation of the M2 C-terminus led to a reduction in the number of infectious virus particles and budding efficiency. Also, sequences were identified that interact with the matrix protein and therefore it was concluded that M2 has a role to play in virus assembly which is distinct from that of viral uncoating and protein transport.

1.6.1.2: Ion Channel Activity of M2

The following methods have been used to measure M2 ion channel activity:

1. In oocytes of Xenopus laevis microinjected with mRNA of M2, a voltage clamp was applied across the membrane to measure electrical activity (Pinto *et al.,* 1992; Mould *et al.,* 2000).

2. Mammalian cells were stably or transiently transfected with M2 cDNA to express M2. Currents were measured using whole cell patch clamp (Figure 1.7) or pH changes measured in cells co-expressing pH-sensitive eGFP (Wang *et al.,* 1995; Chizhmakov *et al.,* 1996 Mould *et al.,* 2005).

3. Liposomes containing a pH-sensitive fluorescent dye and purified M2 channels (Schroeder *et al.,* 1994; Lin *et al.,* 2001).

4. M2 in a planar lipid bilayer system (Vijayvergiya *et al.,* 2004)

The combination of mouse erythroleukameia (MEL) cells and whole cell patch clamp allows control of the internal as well as the external medium and provides a much more precise system than oocytes to study M2 currents (Figure 1.7). M2 expressed in these cells formed proton channels with high selectivity for protons and relatively low permeability for other physiological ions (Chizhmakov *et al.,* 1996). Selectivity for protons was 10^7 times greater than that for Na^+. The flow of protons through the channel was small at neutral or alkaline pH due to low proton concentration and increased as external pH was reduced, due to the increase in the electrochemical gradient, reaching saturation at around pH 4.

The apparent dissociation constant (K_d) for interaction of protons with residues in M2 during permeation through the channel was approximately 1μM (pH 6) and is consistent with its function in endosomes and the *trans* Golgi of virus-infected cells (Grambas *et al.,* 1992). Activation of the channel was proton dependent and occurred on reduction of pH from 8 to 6.5, with an apparent K_d for protons of 0.1 μM (pH 7) (Chizhmakov *et al.,* 1996). Amino acid changes within the transmembrane domain can cause differences in channel activation and

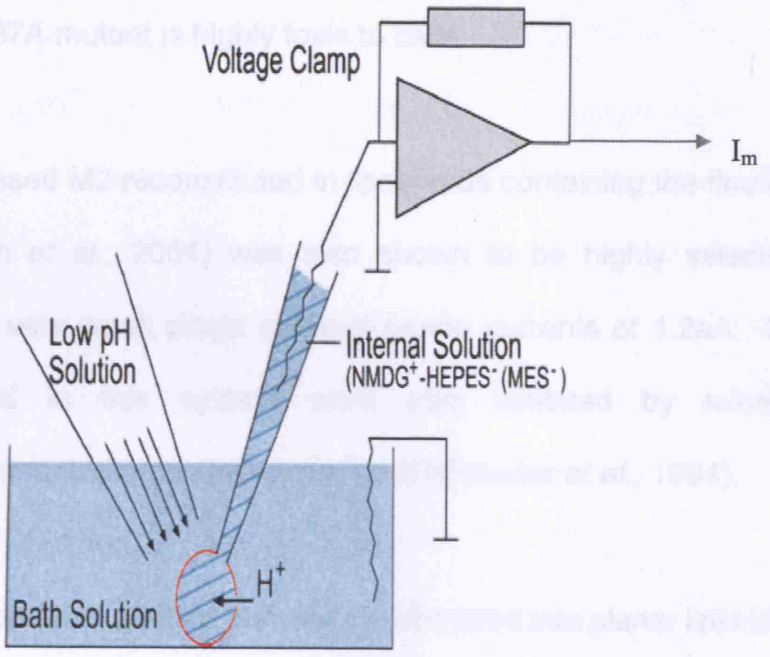

Figure 1.7: An illustration of whole cell patch clamp of MEL cells which was used to demonstrate proton selectivity of M2. MEL Cells containing M2 were voltage clamped with the whole-cell patch clamp configuration (Hamill et al., 1981). A negative feedback loop in the apparatus setup was used to control the membrane potential and set a "holding voltage" which was varied according to experimental requirements.

permeation (Chizhmakov *et al.,* 2003). An H37A substitution causes an increase in permeability of M2 to other cations but not anions, indicating that this amino acid residue is important in determining the proton selectivity of the channel (N. Mulrine and A. Hay, unpublished observations). Also the activation characteristics of the channel are destroyed and amantadine binding became reversible. The H37A mutant is highly toxic to cells.

Baculovirus expressed M2 reconstituted in liposomes containing the fluorescent dye pyranine, (Lin *et al.,* 2001) was also shown to be highly selective for protons and gave very small single channel proton currents of 1.2aA. Proton currents produced in this system were also inhibited by micromolar concentrations of amantadine and rimantadine (Schroeder *et al.,* 1994).

When bacterial expressed purified M2 was incorporated into planar lipid bilayers (Vijayvergiya *et al.,* 2004) high proton selectivity was also observed; however the proton currents were significantly larger than those observed in liposomes. These large currents were obtained at low pH values (<4) so the size of the currents may well reflect a denaturing effect upon the protein. It is also important to note that only an 80% block of channel currents was seen at pH 3 with 300μM amantadine, although amantadine affinity with trans-membrane peptide has been shown to be reduced at below pH 7 (Salom *et al.,* 2000). M2 peptide comprising mainly of the transmembrane domain (amino acids 22-46) has also been shown to form amantadine-sensitive proton channels in planar lipid bilayers (Duff and Ashley, 1992), therefore, this forms a minimal proton channel.

Despite differences in interpretation of data obtained for M2 expressed in *Xenopus* oocytes, in MEL cells and artificial systems such as liposomes and planar lipid bilayers, the M2 channel is clearly capable of pH-activated proton conduction which is blockable by M2 inhibitors such as amantadine and has properties consistent with its role in modifying virion and *trans* Goli pH during virus infection. The mechanisms of channel activation, proton conduction and block by amantadine (and related compounds) are not well understood. Inhibition by amantadine is specific and the reversibility of binding uncharacterised on the timescale of electrophysiological experiments. The kinetics of inhibition, are consistent with one tetrameric channel binding one inhibitor molecule. The available data does not indicate a simple non-competitive block as seen in other ion channels, but indicates that the block is the result of a drug-induced allosteric change in the channel (Wang *et al.*, 1993; Chizhmakov *et al.*, 1996).

1.6.1.3: Structure of the M2 Protein

The M2 protein consists of 97 amino acid subunits, translated from a spliced mRNA of the M gene (Lamb *et al.*, 1981). The M2 channel is a homotetramer of subunits comprising a 24 residue N-terminal external domain, a 19 amino acid (hydrophobic) membrane-spanning domain and a 54 residue cytoplasmic domain (Sugrue and Hay, 1991; Holsinger & Lamb, 1991; Sakagachi *et al.*, 1997). Several techniques have been used to gain an insight into the 3D structure of M2 by obtaining low resolution structures of the M2-TM peptide and full length protein.

CD measurements of a 25 amino acid peptide corresponding to the transmembrane domain of M2 showed it to be highly α-helical in various environments including lipid vesicles, SDS micelles and trifluoroethanol. Addition of amantadine did not seem to alter the structure of the M2-TM peptide (Duff *et al.*,1992; Okada *et al.*, 2001); however Salom *et al.* showed that amantadine binding of M2-TM peptide in DPC micelles caused a change in the α-helical nature of the peptide bundle at 223nm (Salom *et al.*, 2000). CD experiments of chemically synthesized M2 ligated at cysteine 50 and also bacterially expressed M2 have given α-helical content of between 60-70% although this varied with the presence of detergent (Kochendoerfer *et al.*, 1999; Tian *et al.*, 2002).

Fourier transform infrared (FTIR) spectroscopy is a technique used to study peptides in dried, flat lipid bilayers on reflective crystals by monitoring vibrations of chemical bonds. Using isotopic labeling, particular chemical bond signals such as $^{18}O=^{13}C$ can be resolved. Differences in absorption spectra from different orientations of plane polarized light can be used to determine the orientations of chemical bonds and therefore the peptide in respect to the bilayer. This technique has been applied to studies of M2 structure. Using energy minimization the M2-TM was shown to form a tetrameric α-helical bundle with a tilt between 32-35° (Kukol *et al.*, 1999; Torres *et al.*, 2000).

Solid-state nuclear magnetic resonance (ssNMR) is a technique where the chemical shift is measured for types of atomic nuclei that possess a magnetic spin in a bilayer system rather than in solution. The chemical shift of a particular nucleus depends on the chemical bond (it is part of) and on changes

in the local environment.^{15}N-^{1}H dipolar, ^{15}N chemical spectra in stacked lipid bilayers have been obtained for M2-TM and full-length M2 using PISEMA. The data produce information on the angle of the N-H bond in respect to the magnetic axis. Angles for M2-TM tilt in respect to the bilayer normal were roughly 37-38° depending on lipid used (Figure 1.8). Another experiment done with ^{15}N labeled peptide was in agreement with earlier CD observations in showing no change in the α-helical bundle upon amantadine binding (Song *et al.,* 2000). Solid state NMR measurements of full length M2 protein reconstituted into DMPC/DMPG liposomes demonstrated a stable tetrameric structure. Using a variety of ^{15}N labeling strategies in proteoliposomes, uniformly aligned solid-state NMR samples for $^{(15)}$N-$^{(1)}$H dipolar/$^{(15)}$N chemical shift correlation experiments showed a transmembrane helix in the M2 protein having a tilt angle of approximate 25°. In addition, the spectra suggest that the tetrameric protein forms a symmetric or at least pseudosymmetric bundle (Tian *et al.,* 2002).

Further ssNMR experiments indicated that the C-terminus contains amphipathic helices and is resistant to trypsin digestion indicating it may well play a role in stabilizing the tetrameric assembly of the M2 channel (Tian *et al.,* 2003; Kochendoerfer *et al.,* 1999). The pore-lining residues of the channel have been identified as 27, 30, 34, 37, and 41 with the use of cysteine scanning mutagenesis (Pinto *et al.,* 1997; Bauer *et al.,* 1999).

1.6.1.4: Proton Conduction through the M2 Channel

The major residue involved in activation and permeation of the full length M2 channel is histidine 37 (Ghandi *et al.,* 1999). Two models have been proposed

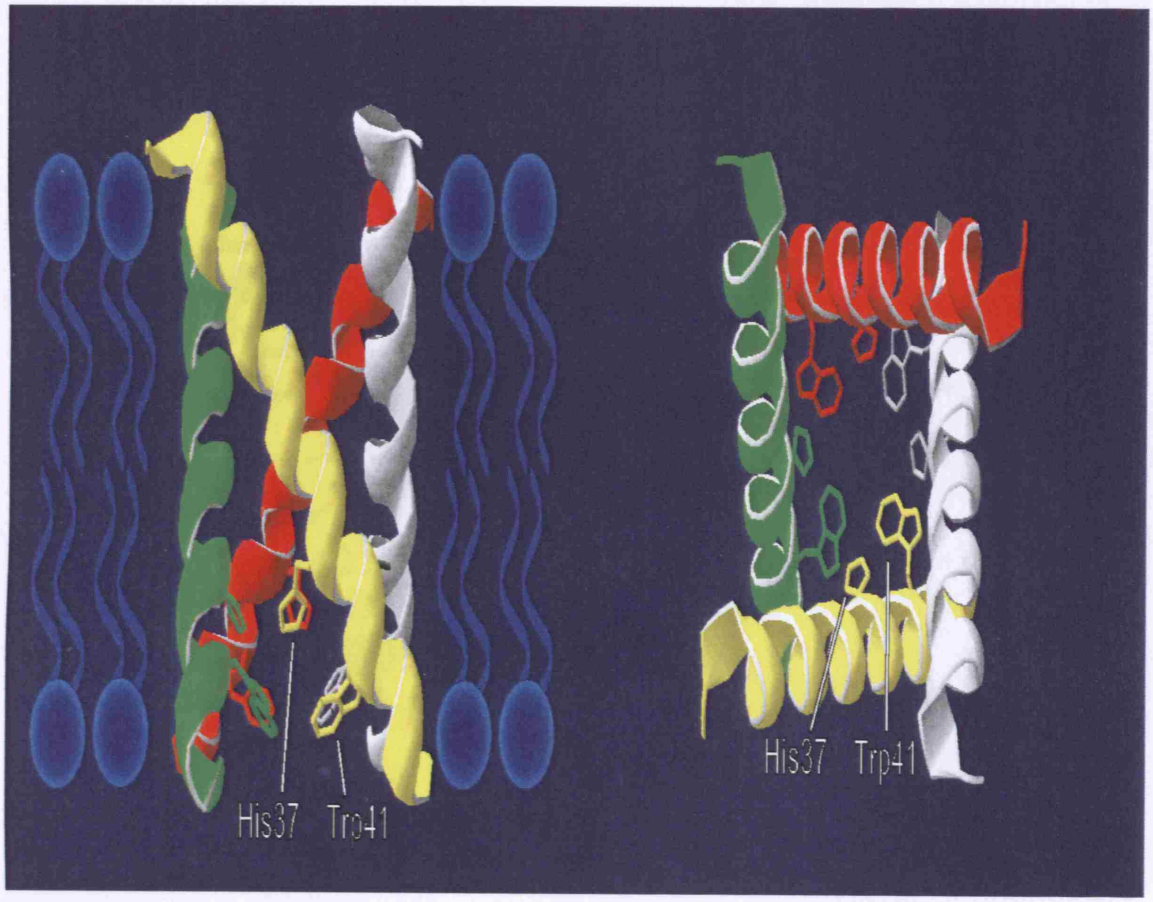

Figure 1.8: Structure of the pore of the M2 proton channel with the histidine 37 and tryptophan 41 side-chains indicated (based on ssNMR coordinates 1NYJ from Nishimura et al., 2002)

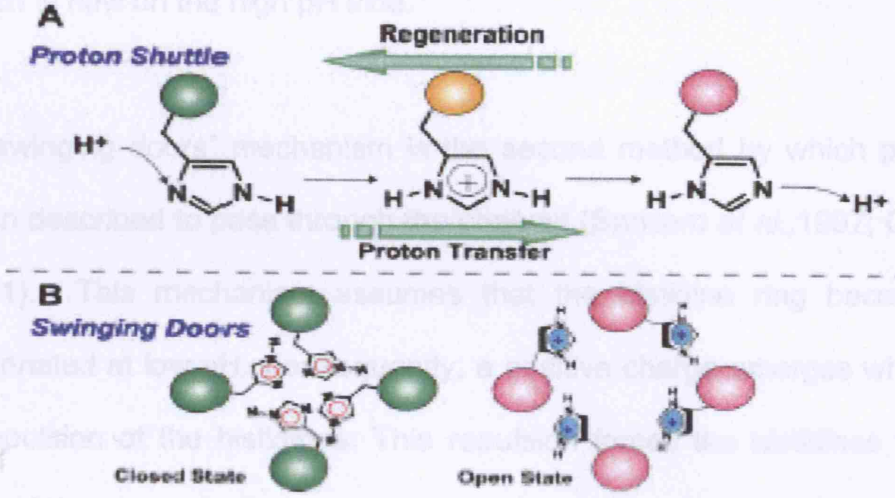

Figure 1.9: The proposed proton "shuttle" A) and "swinging doors" B) mechanisms for proton conduction of the Influenza A M2 ion channel.

for the mechanism of proton conduction through the M2 channel (Figure 1.9). A "shuttle" model proposes that the imidazole ring of His37 is located in the lumen of the M2 pore allowing protons to hop on and off the ring (Pinto *et al.,* 1997). One of the two nitrogens in the imidazole ring is protonated by the low pH and consequently the side-chain flips around the Cα–Cβ bond due to the energetic state of the two nitrogens. Additional extracellular protons attach to the unprotonated nitrogen allowing release of the proton from the other nitrogen, which is now on the high pH side.

A "swinging doors" mechanism is the second method by which protons have been described to pass through the channel (Sansom *et al.,*1997; Okada *et al.,* 2001). This mechanism assumes that the histidine ring becomes doubly protonated at low pH. Consequently, a positive charge emerges which leads to a repulsion of the histidines. This repulsion forces the histidines towards the side of the channel allowing a short-lived water wire to conduct protons. It has been speculated that, since the pKa of histidine is near the M2 activation pH, His37 is also involved with channel activation and/or proton conductance.

Solid-State NMR measurements showed that both histidine and tryptophan side chains project into channel pore (Nishimura *et al.,* 2002). Histidine 37 has been implicated in both the ion selectivity and proton conduction of the channel by mutagenesis experiments, inhibition of channel conductance by Cu^{2+} and chemical rescue of channel proton selectivity with free imidazole in solution (Wang *et al.,* 1995; Pinto *et al.,* 1997; Gandhi *et al.,* 1999; Venkataraman *et al.,* 2005).

Proton NMR has been used to show that protonation of the peptide monomer, corresponding to protonation of the first histidine of the tetramer, occurs near neutral pH, possibly associated with channel activation (Salom *et al.,* 2000).

However, an elegant ssNMR pH titration of His37 using M2 transmembrane peptide has suggested that two initial protonation events occur at pH 8.2, suggesting cooperative H^+ binding causing the His-tetrad to form hydrogen-bonded dimers. These dimers lead to a distribution of the pair of charges over the four imidazole rings to minimize charge repulsion and the channel is closed, occluded by the presence of low-barrier hydrogen bonds. When a third protonation event occurs of an imidazole ring (pKa 6.3) the channel becomes activated and is able to conduct protons (Hu *et al.*, 2006).

Raman spectroscopy of histidine protonation has inferred a pKa of 5.7, closer to the value for channel permeation. When the channel is closed all histidines exist as a cyclic hydrogen bonded network. Once protonation occurs at 5.7 all four histidine residues in the channel pore become protonated and form a pH-dependent cation-π electron interaction with tryptophan 41 which stabilizes the protonated imidazole rings and hence the open channel form (Okada et al 2001). Modelling has suggested this mechanism would involve movement of the His37 and Trp 41 side chains.

Fluorescence studies with purified recombinant full length M2 have shown two pH-dependent changes related to channel function: 1. An increase in Trp fluorescence from pH 8 to 6, possibly associated with activation due to Trp15 within the N-terminus. 2. A reduction in fluorescence from Trp41 due to

protonation of His37 associated with proton permeation of the channel (Czabotar *et al.,* 2004). Trp41 has been also been suggested as the putative "gate" of the M2 channel. When Trp41 was mutated to residues with reduced side-chain length outward proton conductance was permitted and internal access of Cu^{2+} to histidine inhibited channel currents (Tang *et al.*, 2002). Further information from chemical selectivity studies has suggested that the proton selectivity involves only His37 and that Trp41 is only involved in activation and proton conduction of the channel, therefore confirming its role as the gate of the M2 (Venkataraman *et al.,* 2005). Despite the large amount information available, the exact mechanism of proton conduction by M2 remains undefined and the precise roles of the two principal side chains His37 and Trp41 are poorly understood.

1.6.1.5: Amantadine Binding to M2

The anti-influenza A drugs amantadine and rimantadine and the inhibitor BL-1743 (not a licensed drug) block the functions of M2 and inhibit pH sensitive currents (Hay *et al.,* 1985; Pinto *et al.,* 1992; Wang *et al.,* 1993). These drugs along with their derivatives have strain-dependent activities in inhibitor sensitivity at low concentrations (5μM or less) and interact with the hydrophobic transmembrane domain of M2 (Hay *et al.,* 1985). Inhibition of M2 also occurs with very slow on- and off-rates that could not be measured during the lifetime of the experiments therefore cause difficulty in determination of equilibrium constants (Wang *et al.,* 1993).

Mutations conferring resistance to amantadine inhibition are found at positions 26, 27, 30, 31 and 34 within the transmembrane domain (L26F, V27A, A30T, S31N and G34E) (Hay *et al.,* 1985). These mutations map to one face of the

helix with most recent data suggesting lining the channel lumen. Many of the amantadine-resistance mutations induce substitution of hydrophobic channel-lining residues by longer polar residues, indicating that the adamantyl group may interact with the channel residues via van der Waals interactions (Hay *et al.,* 1985). Amantadine resistance mutations conferred resistance to BL-1743. Another partially-resistant mutant was identified for this compound, changing isoleucine at 35 to threonine which gave a more pronounced reversible binding for amantadine to this mutant indicating these two compounds have differential modes of interaction with the M2 protein (Tu *et al.,* 1996). Molecular modeling suggests that the luminal space between Leu26 and His37 is complementary in its shape, hydrophobicity, and polarity to M2 inhibitors, thereby allowing it to accommodate an amantadine molecule (Pinto *et al.,* 1997; Nishimura *et al.,* 2002).

Neutron diffraction experiments with M2 peptide in the presence of amantadine showed that amantadine interacts with M2 at specific sites within the lipid bilayer. Amantadine was found around 5Å from the centre of the bilayer. This suggests an interaction site around valine 27 and serine 31 (Duff *el al.,* 1994). Amantadine inhibition is thought to be pH dependent with drug binding tightly at neutral pH stabilizing the tetrameric structure (Wang *et al.,* 1993; Salom *et al.,* 2000); therefore it is concluded that amantadine binds the closed form of the channel. On the one hand, it is thought that the adamantyl cage interacts with valine 27 through Van der Waals interactions, while the amine group interacts with Serine 31 (Sansom and Kerr., 1993). On the other hand Pinto *et al.* 1997 proposed another model: that amantadine binds deeper in the channel and its

ammonium group hydrogen bonds with the His37 side chains (Gandhi *et al.*, 1999), acting as a surrogate proton donor.

1.7: Small Integral Membrane Proteins Of Influenza B and C Viruses

1.7.1: Influenza B

As for influenza A, dissociation of the influenza B matrix-RNP is facilitated at acid pH (Zhirnov, 1992). It would thus seem that the virus requires a channel capable of acidification of the virion interior during viral entry. The NB and BM2 proteins have been suggested as possible candidates for this role based on structural similarities to M2 with BM2 shown as both the structural and functional homologue of M2 (Figure 1.10).

1.7.1.1: The NB Protein

The NB protein (100 amino acids) is encoded within the neuraminidase (NA) gene of influenza B and is translated from the first initiation codon of the mRNA, four nucleotides before the AUG codon, which initiates translation of the NA (Shaw *et al.*, 1983). Like M2 it is synthesized in virus-infected cells in amounts comparable with the amounts of other structural components, but is incorporated into virus particles in relatively small amounts (Betakova *et al.*, 1996; Brassard *et al.*, 1996).

NB forms dimers, but its multimeric nature has yet to be established. Recently, it has been shown that knocking out NB has no obvious effect on virus replication in cell culture and only inhibits viral replication *in vivo* (Hatta and Kawaoka, 2003). This is in contrast to the effect of knocking out M2 or BM2

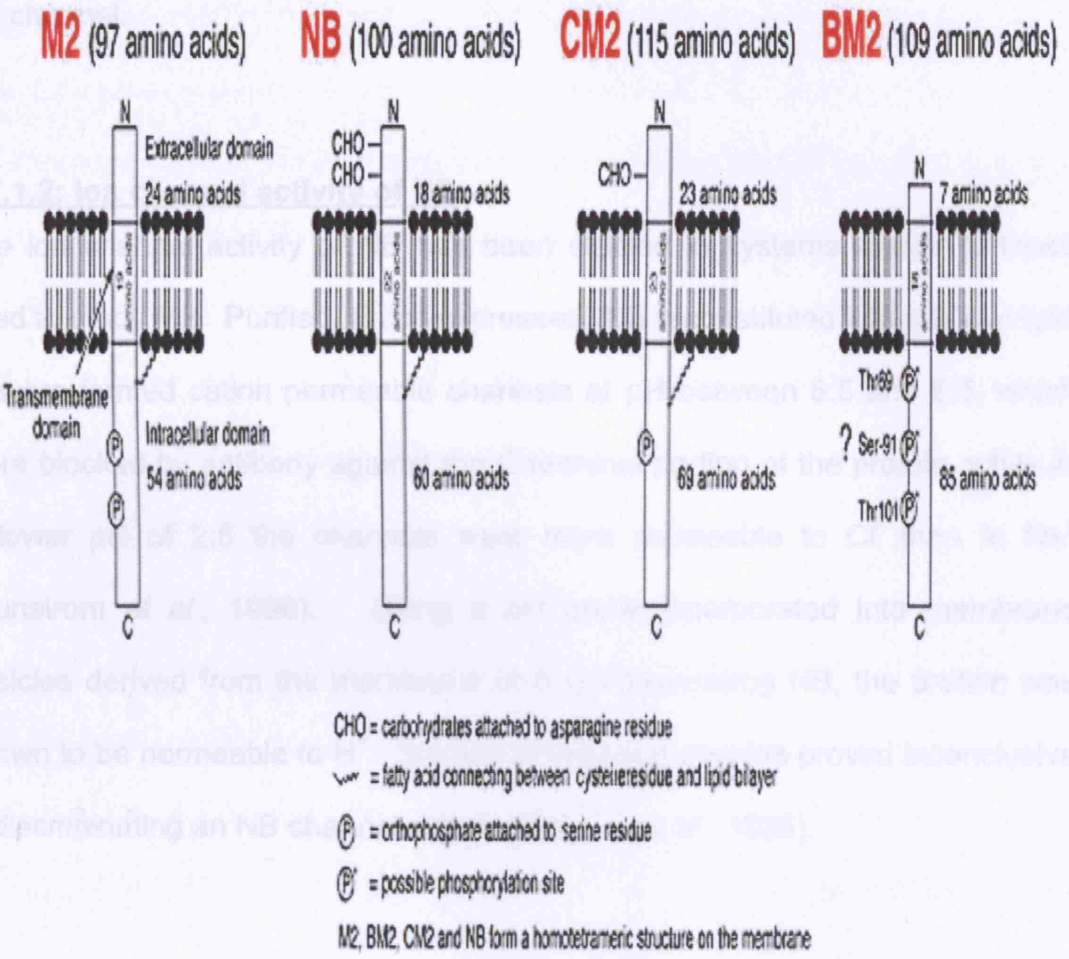

Figure 1.10: Description of the small integral membrane proteins of Influenza viruses with their post-translational modifications (Diagram courtesy of Alan Hay).

from influenza A and indicates that NB has a different role to M2 in the viral life cycle. However, as described below, there is evidence that NB can act as an ion channel.

1.7.1.2: Ion channel activity of NB

The ion channel activity of NB has been studied in systems similar to those used to study M2. Purified, *E.coli*-expressed, NB reconstituted into artificial lipid bilayers formed cation permeable channels at pH between 5.5 and 6.5, which were blocked by antibody against the C-terminal portion of the protein, while at a lower pH of 2.5 the channels were more permeable to Cl^- than to Na^+ (Sunstrom *et al.,* 1996). Using a pH probe incorporated into membrane vesicles derived from the membrane of *E.coli* expressing NB, the protein was shown to be permeable to H^+. Studies in *Xenopus* oocytes proved inconclusive in discriminating an NB channel activity (Shimbo *et al.,* 1995).

MEL cells expressing NB were used to directly compare the ion channel properties of NB with those of M2. Although there are similarities in proton permeability of the two proteins there are some notable differences in channel activity (Chizhmakov *et al.*, 1998). The activation of the NB proton channel requires Na^+ (at concentrations greater than 5mM); no H^+ current flowed through NB in response to a large pH gradient when measurements were done in the presence of only the impermeable ions NMDG and HEPES/MES, conditions which elicited full activity of M2. Secondly, external pH below 5.5 activated a Cl^- permeability. The two activities were studied separately, proton currents in chloride-free, sodium glutamate solutions and chloride currents in sodium-free NMDG chloride. NB proton currents were similar to M2 proton

currents in their response to changes in pH gradient, their dependence on membrane potential, and saturation at high external H^+ concentrations (the apparent dissociation constant for H^+ of 1μM (pH 6) was similar to that of M2). The Cl^- currents activated slowly in response to a drop in pH below 5.5 and exhibited very strong outward rectification i.e. outward current (corresponding to an inward flow of negative chloride ions) was much greater than inward current. In normal physiological solutions (below pH 5.5) NB is permeable to both H^+ and Cl^-; it is not yet clear, however, whether a single NB channel is permeable to both ions or whether two different molecular entities account for separate permeabilities to H^+ and Cl^-.

There is evidence that peptides corresponding to the transmembrane domain of NB conduct current when inserted into lipid bilayers (Fischer *et al.*, 2000). Intriguingly, these currents are sensitive to amantadine, albeit at concentrations higher (≈1mM) than that observed for M2-TM peptides inserted in bilayers (Fischer *et al.*, 2001). As described above, there is no evidence that amantadine has a specific effect on influenza B viral replication.

1.7.1.3: The BM2 Protein

In addition to the matrix protein, RNA segment 7 of influenza B encodes a second short membrane protein, denoted BM2. However, unlike Influenza A M2, it is translated from a bicistronic mRNA in an open reading frame that is +2 nucleotides to that of the M1 coding sequence (Horvath *et al.*, 1990). The BM2 protein is present in infected cells and virus particles (Odagiri *et al.*, 1999) and, has many similarities to M2. It is a 109 residue integral membrane protein with the ectodomain being located at the N-terminus. It assembles into oligomers,

possibly tetramers, and the proposed transmembrane domain contains a histidine and a tryptophan at similar positions to that found in M2 (Paterson *et al.,* 2003). It has been confirmed that BM2 has ion channel activity (Mould *et al.,* 2003) and, thus, acts in an analogous role to that of M2 in influenza A.

1.7.2: Influenza C

RNA segment 6 (M gene) of *Influenza C* virus is 1,180 nucleotides in length and contains a single open reading frame (ORF) coding for a 374-amino-acid protein (p42) (Hongo *et al.,* 1994). The CM2 protein is generated from the primary gene product p42 by a signal peptidase cleavage (Hongo *et al.,* 1998).

1.7.2.1: The CM2 Protein

CM2 consists of a 27-amino-acid N-terminal extracellular domain, a 32-amino-acid transmembrane domain, and a 56-amino-acid C-terminal cytoplasmic domain (Figure 1.10) (Hongo *et al.,* 1997). This protein forms disulfide-linked dimers and tetramers, and is post-translationally modified by palmitoylation through a thioester linkage and by phosphorylation (Hongo *et al.,* 1997; Li et al., 2001). Furthermore, a small amount of the CM2 protein was shown to be incorporated into progeny virus particles. Thus, CM2 shares many biochemical properties with Influenza A virus M2 and Influenza B virus BM2. It has been reported that CM2 has intrinsic ion channel activity and is permeable to chloride ions (Hongo *et al.,* 2004); however, due to the apparent lack of requirement for acid pH for dissociation of the influenza C matrix-RNP interaction, the case for CM2 having an ion channel role is less compelling (Zhirnov, 1992).

1.8: Optical Spectroscopy

1.8.1: Fluorescence

Fluorescence is a category of luminescence that occurs when absorption of a photon leads to emission of another photon. This process is illustrated in the Jablonski diagram in Figure 1.11 (Jablonski, 1935). As light is absorbed by a particular fluorophore, electrons from the lowest vibrational energy level of the ground state are excited to one of the vibrational levels of either S_1 and S_2. Following internal conversion (IC) the electron relaxes to the lowest state of S_1 and therefore is thermally equilibrated. Return to the ground state usually occurs to a lower vibrational energy level with emission of a photon allowing fluorescence to occur (Lackowicz, 1999). There are two other important characteristics, which should be considered. These are quantum yield of a particular fluorophore (Q), which is the ratio of the number of photons emitted to the number absorbed, and the fluorescence lifetime of a fluorophore, which is defined as the average time it spends in the excited state prior to return to the ground state (Strickler and Berg, 1962). Photon emission by a fluorophore is controlled by two rate constants, the emissive rate of the fluorophore (Γ) and the rate of non-radiative decay (k_{nr}) (Birks, 1973). Both of these processes lead to a reduction of the excited state. The quantum yield is defined by equation 1.1.

$$(1.1) \quad Q = \frac{\Gamma}{\Gamma + k_{nr}}$$

Fluorescence emission is a random process and therefore most fluorophores do not emit their photons at precisely the fluorescence lifetime. The fluorescence lifetime is defined by equation 1.2.

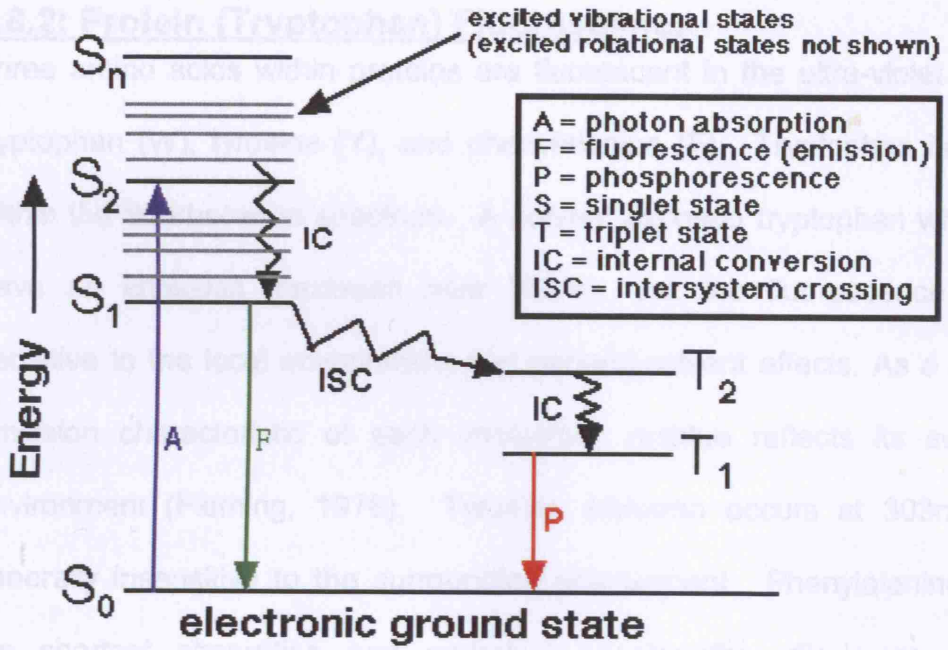

Figure 1.11: A Jablonski diagram showing the various processes which can occur upon fluorescence excitation. S_0 symbolises the ground state while S_1 and S_2 denote the first and second excited electronic states, respectively. The intermediate vibrational energy levels are shown as grey lines. Vertical lines indicate the transitions between states due to their instantaneous nature.

(1.2) $\tau_n = 1/\Gamma$

Where the fluorescence lifetime is (τ_n) is equal to 1 divided by the emissive decay rate.

1.8.2: Protein (Tryptophan) Fluorescence

Three amino acids within proteins are fluorescent in the ultra-violet spectrum, tryptophan (W), tyrosine (Y), and phenylalanine (F). Tryptophan is dominant within the fluorescence spectrum. A solvent exposed tryptophan will normally have an emission maximum near 355nm, but the fluorescence is highly sensitive to the local environment and general solvent effects. As a result, the emission characteristic of each tryptophan residue reflects its surrounding environment (Fleming, 1978). Tyrosine emission occurs at 303nm and is generally insensitive to the surrounding environment. Phenylalanine displays the shortest absorption and emission wavelengths, displaying structured emission near 282nm. With a quantum yield of 0.03 and because wavelengths longer than 280nm are used in protein fluorescence experiments phenylalanine fluorescence is very rarely seen (Permyakov *et al.,* 1993).

Tryptophan and other indole derivatives within their long-wavelength absorption contain two overlapping electronic transitions ^1L_a and ^1L_b. These states have similar energies and, depending on the environment, either state can have the lowest energy (Eftink, 1991). These transitions have different absorption dipole moments. This makes the photophysics of tryptophan very complex, especially because the different states respond differently to solvent polarity (Albinsson, 1989). However tryptophan's unique sensitivity to its environment can be

understood in terms of these two transitions. For example, in cyclohexane, in the absence of hydrogen bonding, the emission of tryptophan is structured and represents the ^1L_b transition, while in 100% ethanol when hydrogen bonding occurs structured emission is lost and is indicative of the ^1L_a transition (Gryczynski, 1988). Although it is likely that on both occasions some dual emission may occur, ^1L_a seems to be more solvent sensitive due to the involvement of the polar nitrogen atom of the indole (Strickland *et al.*,1972).

1.8.3: Fluorescence Quenching

Fluorescence intensity can be reduced by a wide variety of processes. A decrease in fluorescence intensity is called quenching. Quenching of fluorescence occurs when a fluorophore within the excited state is deactivated by contact with another molecule in solution (Knibbe, 1968). Many molecules can act as collisional quenchers such as oxygen, amines and electron deficient molecules such as acrylamide (Kautsky, 1939; Eftink and Ghiron, 1981). The effect of the quencher on fluorescence intensity is described by the Stern-Volmer equation (equation 1.3).

$$(1.3)\quad \frac{F_o}{F} = 1 + K[Q] = 1 + k_q \tau_o [Q]$$

In this expression (K), is the Stern-Volmer constant (this defines the accessibility of fluorescent residues to a particular quencher, and is equal to the biomolecular quenching constant times the unquenched lifetime of the fluorophore), (k_q) the biomolecular quenching constant, (τ_o) is the unquenched lifetime and [Q] is the quencher concentration. It should be noted that there is no chemical modification of either molecule during the quenching process. The mechanism of quenching between tryptophan and acrylamide is likely to be due

to electron transfer from the indole ring to the acrylamide that would not occur in the ground state (Eftink, 1991). The other main type of quenching is static quenching which occurs from non-fluorescent complexes of fluorophore and quencher and does not rely on diffusion and molecular collisions (Seidel, 1996).

Molecular information can be derived from collisional quenching, such as the accessibility of a probe to a quencher like iodide or acrylamide and therefore its location in a particular protein polypeptide chain. Collisional quenching of proteins can be used to determine the extent of exposure of tryptophan to the aqueous phase (Eftink and Ghiron, 1981). If a tryptophan is highly buried inside a protein the extent of quenching will be less than if the tryptophan residue is at the surface. Water-soluble quenchers do not readily penetrate the hydrophobic regions of a protein and therefore correlation between emission maximum and quenching constant is significant (Petrich *et al.*, 1987).

Most blue shifted tryptophans are essentially inaccessible to quenching by acrylamide while red shifted residues are nearly always accessible (Eftink, 1991). Collisional quenching can also be used to resolve the contributions of surface and buried tryptophans to the total fluorescence of the protein. If some residues in a multi-tryptophan protein are inaccessible to quenching, then a downward curvature will be seen in the Stern-Volmer plot (Avigliano, 1984). The fraction of accessible quenching can be obtained from plotting F_0/F versus the reciprocal quencher concentration where the *y*-intercept represents infinite quencher concentration.

It has previously been observed that protonation of histidine residues results in changes in the photophysics of adjacent tryptophan residues in proteins. Solution studies have shown that the protonated form of histidine is a more efficient quencher of tryptophan in solution than the neutral form (Loewenthal *et al.*, 1991). The most extensive study of a tryptophan residue near a histidine has been carried out in the enzyme barnase. Protonation of His18 of barnase caused a 3-fold decrease in quantum yield and a 2-fold decrease in the fluorescent lifetime of the adjacent Trp94. The pK_a of His18 of barnase was determined to be 7.75 (Shinitzky *et al.*, 1967). The exact mechanism by which enhanced quenching by protonated histidine takes place is not fully understood. Shinitzky and co-workers suggested that the histidine forms a B charge complex in the ground electronic state between its imidazole ring and the ring of tryptophan with the complex resulting in fluorescence quenching. Burstein *et al.* (1974) determined that the protonated form of histidine is a more efficient form of collisional quencher than its neutral state while Willaert *et al.* (1992) concluded that the ground state is important too but that His^+ is several times more efficient at quenching Trp fluorescence than neutral His (Bushueva *et al.*, 1974).

1.8.4: Fluorescence Polarisation

If a fluorophore absorption dipole moment is aligned in a defined orientation with respect to the fluorophore molecular axis, photons with the same electric vector as the absorption dipole moment will be preferentially absorbed (Lakowicz *et al.*, 1993). This is called polarisation. If fluorophores within a solution are randomly orientated then excitation with polarised light will lead to a selectively excited population of fluorophores whose absorption dipole moment

is orientated parallel to the electric vector of excitation (Spencer *et al.*,1970). Emission occurs parallel to the emission dipole moment axis. The angle between these moments determines the maximum measured anisotropy. Fluorescence polarisation (P) is defined by equation 1.4:

$$(1.4) \quad P = \frac{I_{\Pi} - I_{\perp}}{I_{\Pi} + I_{\perp}}$$

where I_{Π} (vertical) and $I_{\perp}$ (horizontal) are the fluorescence intensities of the polarised emissions, respectively. Several effects are capable of decreasing the observed anisotropy, the most common being rotational diffusion which occurs during the lifetime of the excited state and reorients the emission dipole of the fluorophore.

In solution most small fluorophores rotate on a picosecond timescale so that many rotations can occur in the nanosecond lifetime of a fluorophore in the excited state. Therefore, in non-viscous solution polarisation for a small, rapidly rotating fluorophore will be near to zero. The polarisation of a fluorophore attributed to a large slowly rotating protein molecule will be larger. Energy transfer between fluorophores may also decrease anisotropy (Weber, 1966). Polarisation can be used to measure the size, shape and molecular weight of proteins due to the effects these characteristics have on the rotational correlation time, i.e. larger proteins will rotate more slowly giving increased anisotropy. Within membrane proteins contained in a lipid bilayer, anisotropy can give information on the viscosity and local motion of amino acid side chains such as tryptophan or information on the lipid bilayer itself.

1.8.5: Resonance Energy Transfer

Resonance energy transfer (RET) provides information on distances between sites in macromolecules. The process of RET occurs whenever the emission spectrum of a fluorophore called the donor, overlaps with the absorption spectrum of another molecule called the acceptor (Förster 1948). RET is described by equation 1.5:

$$(1.5)\quad k_T(r) = \frac{1}{\tau_D}\left(\frac{R_0}{r}\right)^6$$

In this equation, r is the distance between the donor (D) and acceptor (A) RET molecules, τ_D is the lifetime of the donor, R_o the Förster distance and $k_T(r)$ the rate of energy transfer. The extent of RET is determined by the distance between the donor and acceptor and the spectral overlap which is described in the terms of the Förster distance (R_o) (the distance at which energy transfer is 50% efficient). The efficiency of energy transfer is give by equation 1.6

$$(1.6)\quad E_T = \left(\frac{R_0}{r + R_0}\right)^6$$

Förster distances are typically in the range of 15-60A, which is comparable to the thickness of a biological membrane.

1.8.6: Circular Dichroism Spectroscopy

Circular dichroism (CD) is the experimentally measured difference in absorbance between left and right circularly polarised light. CD is an absorption phenomenon; therefore the chromophores that contribute to a CD spectrum are the same as those which contribute to an absorption spectrum (Trp, Tyr, Phe, Cys and the peptide bond). A near UV-CD spectrum (260-350nm), derived from

the afore-mentioned amino acids, gives information on the tertiary and quaternary structure of the protein, while a far UV-CD spectrum (190-260nm), mainly derived from the peptide bond absorption, reflects secondary structure content of the protein (α-helix, β-sheet and random coil). CD spectroscopy, although it provides low resolution structural information, is extremely sensitive to conformational changes and a large range of conditions can be utilised to study this. Also, relatively low amounts of material are required. CD has been used for: estimation of protein secondary structure content, detection of conformational changes in proteins; monitoring of protein denaturation by either temperature or addition of chemical denaturants, and studying ligand-protein interactions and kinetics of binding.

1.8.7: M2 Tryptophan Fluorescence Project Aims

Work by Czabotar et al. (2004) used tryptophan fluorescence to identify two pH-related structural changes that occurred in the M2 channel. These are described in section 1.6.1.4. The aims of this project were two fold. Firstly to use tryptophan fluorescence and associated techniques to probe the structural changes that occur in the M2 channel and gain further insight into the mechanism of M2 activation and permeation by protons. Secondly, to use Trp fluorescence to study inhibition of the M2 channel by anti-M2 inhibitors like amantadine and rimantadine, thereby trying to understand both the inhibition and resistance mechanisms in M2, to produce superior inhibitors.

1.9: Green Fluorescent Protein

The green fluorescent protein of the jellyfish *Aequorea Victoria* (GFP) is a naturally occurring bioluminescent protein. No other substrates or cofactors are

required for fluorescence. The cloning of cDNA encoding gfp10 from *Aequorea Victoria* (Prasher *et al.,* 1992) has allowed expression of functional GFPs heterologously in diverse cell types such as bacteria, plants and mammalian cells (Chalfie *et al.* 1994; Inouye *et al.,* 1997). GFP has now been utilized for a substantial number of novel and useful biological applications such as reporters of gene expression (Chalfie *et al.,* 1994), fusion tags to monitor protein intracellular location or protein trafficking (Wang and Hazzelrigg, 1994) and markers of cell lineage (Cubitt *et al.,* 1995).

The structure of wild-type GFP is shown in figure 1.12 (Yang *et al.,* 1996). GFP consists of a unique 11 β-sheet barrel-like structure with a diameter of 24Å and a vertical measurement of 42 Å. The barrel contains a diagonal α-helix running through the centre that links the chromophore to the β-sheet barrel. The surrounding amino acids are confirmed as a cyclised hexapeptide formed from residues Phe64-Ser-Tyr-Gly-Val-Gln69 of GFP (Cody *et al.,* 1993). The spectral properties of wild-type GFP give absorption peaks at 398nm and 475nm and emissions at 508nm and 503nm, respectively (Ward, 1982; Heim *et al.,* 1994).

Protonation events within the GFP chromophore produce these differential absorption peaks. At 398nm the peak is attributed to the non-protonated form of the chromophore while the absorption peak at 475nm is attributed to an anionic form (Niwa *et al.,* 2006). However due to the phenolic oxygen of Tyr66 being more acidic in the excited form than the ground state, excitation of either species produces similar spectra. Studies have suggested 7 classifications of GFP based upon the spectral properties of the wild-type protein and its mutants.

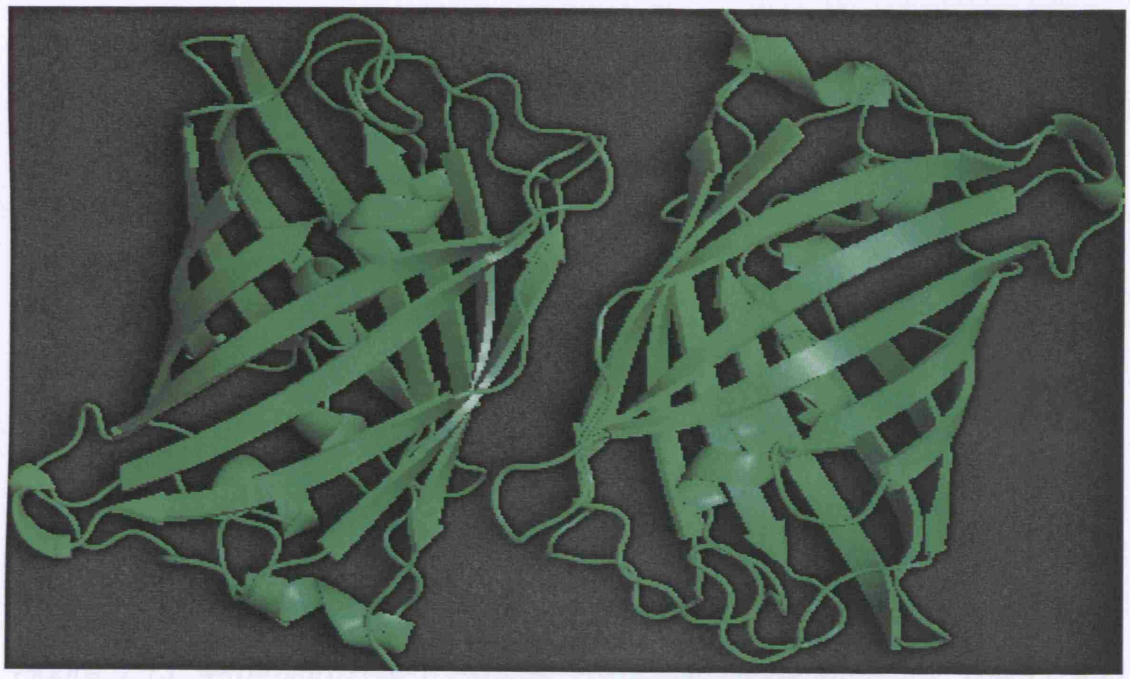

Figure 1.12 Solid-state structure of GFP as a dimer. The 11-sheet β-barrel surrounds the chromophore, which is located in the centre. The majority of GFP and its mutants have been crystallized as dimers. It should be noted that GFP is not an obligate dimer and its functional unit is monomeric. Dimer formation is due to crystal growth conditions. (Coordinates for figure were obtained from PDB, code 1GFL).

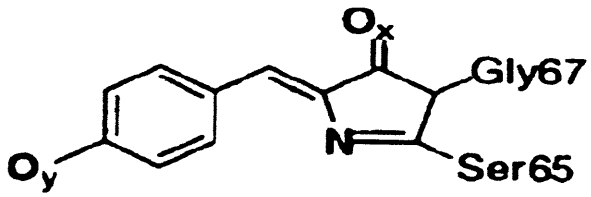

Figure 1.13: 4-(p-hydroxybenzylidene) imidazolid-5-one structure. The O_y and O_x and the N atoms are shown in bold as possible protonation sites (Adapted from Zimmer 2002).

Short α-helical sections at each end of the barrel enclose the chromophore thereby protecting it from quenching by molecular oxygen and hydronium ions.

The surrounding amino acids form a hydrogen-bonded network that surrounds the chromophore. Initially the GFP chromophore was isolated from a small peptide fragment of a papain digest of heat-denatured GFP (Sakurai *et al.,* 1979). To identify the chemical components which allow the GFP to fluoresce small model compounds were synthesised for comparison of spectral properties to the GFP chromophore and 4-(ρ-hydroxybenzylidene) imidazolid-5-one was proposed as the structure (Figure 1.13).

These mutants have provided insight into the mechanics of the GFP chromophore, which is thought to be in equilibrium between the phenol and phenolate forms hence the two excitation spectra. Based on spectral and structural information a mechanism for production of fluorescence by GFP has been surmised (Figure 1.14) (Van Thor *et al.,* 1998; Heim *et al.,* 1994; Liu *et al.,* 1997).

The chromophore exists initially in a neutral state producing the 398nm spectrum. The chromophore is capable however of undergoing a protonation step, which leads to the formation of an intermediate state. This state itself is not responsible for any fluorescence output. Protonated Tyr66 is then shuttled through the surrounding hydrogen-bonded network compiling the chromophore. This leads to a conformational change, which produces the anionic form of the chromophore producing fluorescence. The mechanism above has been partially validated by the absorption and Stark spectra of the wild type and

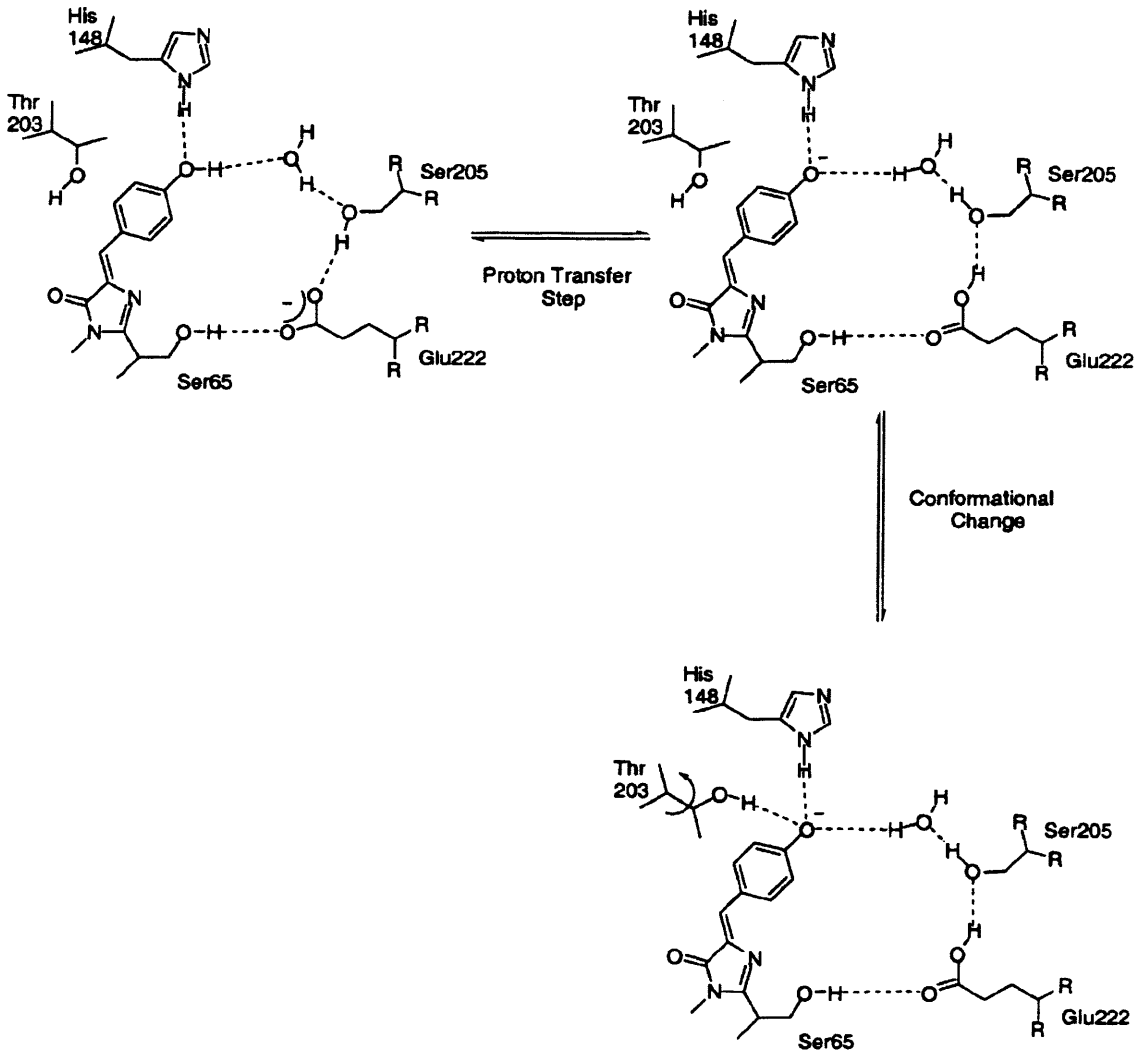

Figure 1.14: Proposed model for fluorescence production of wild-type GFP. An anionic form of the chromophore is produced from the neutral state after a proton transfer step which induces a conformational change shuttling protonated Tyr66 through the hydrogen-bonded network via an intermediate state (Reproduced from Zimmer 2002).

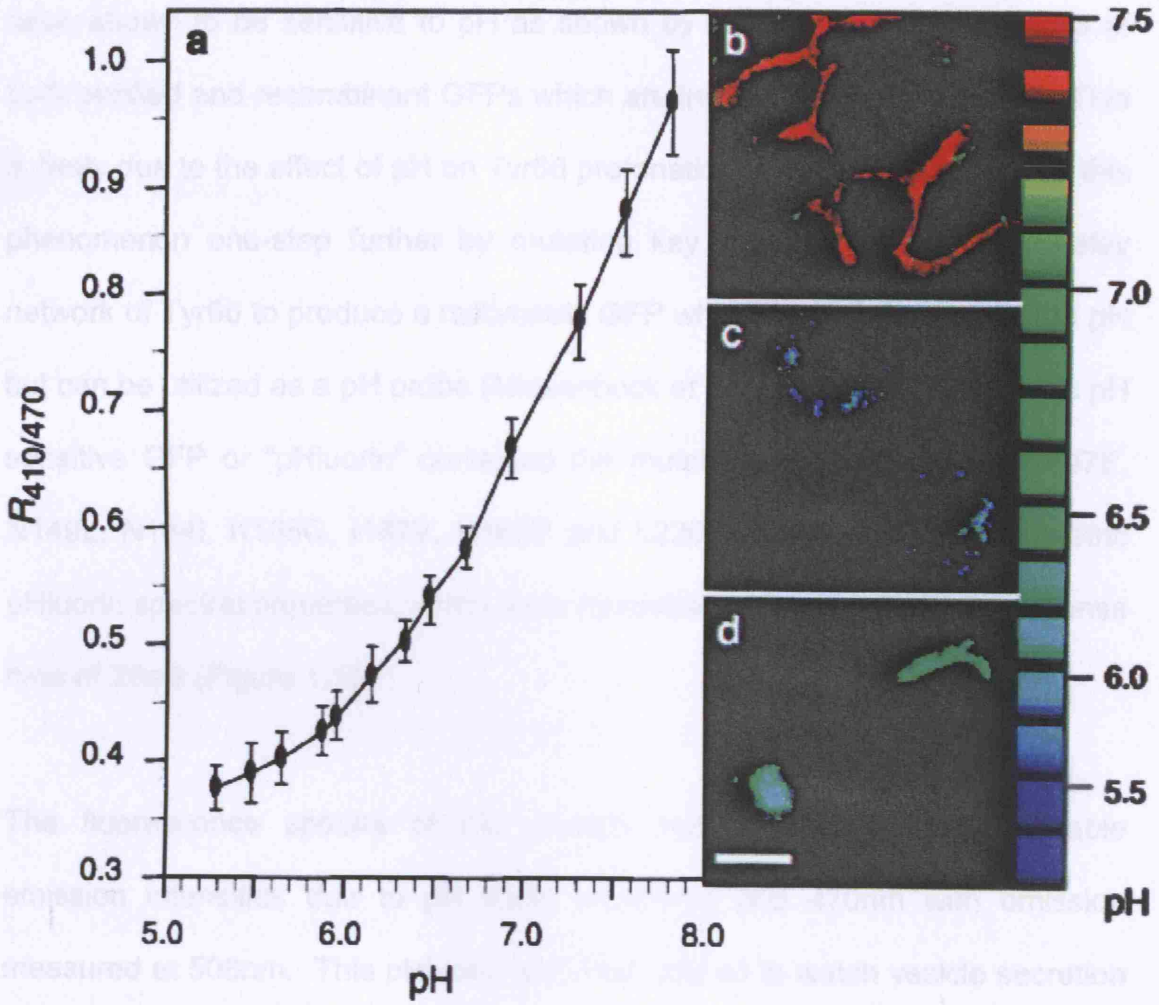

Figure 1.15: pH measurements with ratiometric pHluorin in HeLa cells. Calibration of $R_{410/r470}$ ratio with pH in cells expressing glycosyl-phosphatidylinositol (GPI) anchored ratiometric pHlourin at their surface. Adapted from Miesenbock et al 1998.

associated mutants (Chattoraj *et al.,* 1996). This mechanism, if correct, has been shown to be sensitive to pH as shown by the spectral characteristics of both purified and recombinant GFPs which are influenced by ambient pH. This is likely due to the effect of pH on Tyr66 protonation. Miesenbock et al took this phenomenon one-step further by mutating key residues in the proton-relay network of Tyr66 to produce a ratiometric GFP which is not only sensitive to pH but can be utilized as a pH probe (Miesenbock *et al.,* 1998). The ratiometric pH sensitive GFP or "pHluorin" contained the mutations S202H, E132D, S147E, N149L, N164I, K166Q, I167V, R168H and L220F. This gave the ratiometric pHluorin spectral properties, which were reversible from pH 8-5 with a response time of 20ms (Figure 1.15).

The fluorescence spectra of this mutant were characterized by variable emission intensities due to pH shifts at 410nm and 470nm with emission measured at 508nm. This pHluorin was then utilized to watch vesicle secretion in synaptic transmission (Miesenbock *et al.,* 1998).

1.9.1: M2-GFP Project Aims

The M2-GFP construct created gave rimantadine-blockable activity measured in a HA protection assay that was comparable to wild-type M2. The goal of our project was to see if the pH-sensitive GFP attached to the M2 C-terminus could be used to measure rimantadine-blockable M2 activity in the form of either channel currents or local pH changes in the vicinity of the plasma membrane. This could then be used as an assay for structure-function studies of channel mutants with sensitivity to inhibitors of M2.

Chapter 2: Materials and Methods

2.1: Materials

2.1.1: Cell Lines

Mouse Erythroleukemia (MEL) Cells

The cells were erythroid progenitor cells arrested at the proerythroblast stage. They were derived from the spleens of susceptible mice infected with Friend leukemia virus and can be maintained in cell culture indefinitely. Treatment with compounds such as dimethyl sulphoxide cause MEL cells to undergo erythroid differentiation causing synthesis of haemoglobin (Hb). This synthesis of Hb has led to MEL cell utilization as an erythroid expression system.

2.1.2: Bacterial Strains

***Escherichia coli* DH5α (Promega)**

Genotype:supE44ΔlacU169(ϕ80lacZΔM15)HsdR17recA1endA1gyrA96thi-1relA1

This strain was used for recombinant DNA work.

***Escherichia coli* BL21 C41 (DE3)** (A gift from Katrin Rittinger)

Genotype: F^- ompT $hsdS_B(r_B^-m_B^-)$ gal dcm (C41, DE3)

This strain was used for expression of recombinant M2 protein. C41 is a mutant of host BL21 (DE3) strain selected for its ability to produce elevated levels of toxic membrane proteins at high saturation density (Miroux and Walker 1996).

2.1.3: Vectors

pEV3 vector (Needham *et al.*, 1992)

This vector contains the human/β-globin promoter and human globin locus control region (LCR) to allow independent expression of the desired protein upon Hb production by MEL cells induced by DMSO (Figure 2.1). This produces a LCR/MEL expression system for high level expression of heterologous proteins.

pPROEX Hta (Gibco BRL)

This vector was used for high-level expression of His-tagged membrane proteins in BL21 cells by induction with IPTG (Figure 2.4).

2.1.4: PCR Primers

Table 2.1 lists the primers that were used in the experiments detailed in the Methods and Results. Please refer to appropriate sections regarding usage of a particular set.

2.1.5: Molecular Biology Reagents

Agarose (Biorad)

Big Dye Terminator Sequencing Kit (Used as per manufacturers protocols)

DNAeasy Tissue Extraction Kit (Qiagen) (Used as per manufacturer's protocols)

DpnI restriction enzyme

Pfu Turbo polymerase (Stratagene)

Purelink Quick Plasmid Miniprep Kit (Invitrogen) (Used as per manufacturers protocols)

Set 1	Forward Primer 5'-3'
	AGTCTTCTAACCGAGGTCGAAACGCC
	Reverse Primer 5'-3'
	TTATTTGTATAGTTCATCCATGCCATGTGTAATCCC
Set 2	Forward Primer 5'-3'
	CCTACCAGAAACGGATTCGAATGCAGCTGCAGCG
	Reverse Primer 5'-3'
	CGCTGCAGCTGCATTCGAATCCGTTTCTGGTAGG
Set 3	Forward Primer 5'-3'
	CATTGGGATCTTGCACTTTATATTGTTCATTCTTGATCGTCTTTTCTTC
	Reverse Primer 5'-3'
	CATTGGGATCTTGCACTTTATATTGTTCATTCTTGATCGTCTTTTCTTC
Set 4	Forward Primer 5'-3'
	GTAGAAGGCCCTCTTTTCAAA
	Reverse Primer 5'-3'
	GATTCAAGTGATCCTCTCGTT

Table 2.1: Primers used for sequencing of M2-GFP and M2 constructs (Sets 1 and 4 respectively) and primer sets for creation of W15F and W41F M2 mutants (Sets 2 and 3 respectively).

Quickchange Site-directed Mutagenesis Kit (Stratagene) (Used as per manufacturer's protocols)

T_4 DNA ligase (Promega)

10X TBE buffer (108 g/L Tris base, 55 g/L Boric acid and 9.3g/L Na_4EDTA)

2.1.6: Antibodies

2.1.6.1: Primary Antibody

R68 or N94: anti-M2 rabbit serum raised against peptide either for the first 24 N-terminal amino acids or a C-terminal peptide (SAVDVDDGHFVNIELE). For Western-Blot working concentration was 1:1000.

2.1.6.2: Secondary Antibody

Anti-Rabbit IgG Horseradish peroxidase (HRP) (Biorad). For Western-Blot the working concentration was 1:2000.

2.1.7:Chemicals (Suppliers)

αMEM media

Acrylamide powder (Sigma)

Acryamide/Bisacrylamide solution (Biorad)

Amantadine (Sigma)

Ammonium Persulphate (Sigma)

Ampicillin (Sigma)

Aprotinin (Sigma)

APTS (Sigma)

Biuret Reagent (Sigma)

Blotting paper (In-house Stores)

Bovine Serum Albumin (BSA)

Bromophenol Blue (BDH Chemicals)

Calcium Chloride (Sigma)

Cellulose Dialysis Tubing 4-12Kda cutoff (Biorad)

Citric Acid (In-house Stores)

SeeBlue 2 Protein MW markers (Invitrogen)

Dithiothreitol (Sigma)

Σ-Caproic acid (Sigma)

ECL Kit (Invitrogen)

EDTA (Sigma)

EDTA-free protease inhibitor tabs per 100ml (Roche)

Ethanol (In-house Stores)

Fetal Calf Serum (Homemade)

Gey's medium (123mM NaCl, 5 to 100mM KCl, 0.86mM $Na_2HPO_4.12H_20$, 0.18mM KH_2PO_4, 5.7mM Glucose, 1.3mM $MgCl_2.6H_2O$, 1.46mM $CaCl_2.2H_2O$, pH 8-5)

G418 (Geniticin) (In-house Stores)

Gelcode Blue Coomassie Stain (Pierce)

Glucose (In-house Stores)

Glycine (In-house Stores)

HEPES (Fluka)

Imidazole (Fluka)

Isopropyl β-D-thiogalactopyranoside (IPTG)

Liquid broth (bacto tryptone 10g/L, yeast extract 5g/L, NaCl 10g/L, maltose 2g/L, 100μg/ml ampicillin, pH7) or an agar equivalent. (In-house Stores)

Magnesium Chloride (Sigma)

MES (Sigma)

Methanol (In-house Stores)

N,N-Dimethyldodecylamine-N-oxide (LDAO) (30%) (Fluka)

Phenylmethylsulfonyl fluoride (PMSF)

Phosphate Buffered Saline (PBS) Tween 20

Potassium Chloride (Sigma)

Potassium Phosphate (Monobasic) (Sigma)

PVDF membrane (Biorad)

Rimantadine (Sigma)

Running Buffer, Laemmeli (25mM Tris-HCl pH 7.2, 200mM glycine and 0.1% SDS)

Sample Buffer, Laemmeli (125mM Tris-HCl pH6.8, 4% SDS, 20% glycerol, 100mM dithiothreitol (DTT) and 0.002% bromophenol blue)

20% SDS (Biorad)

Sodium Chloride (Biorad)

Sodium Phosphate (Dibasic)

Soya bean trypsin inhibitor (Biorad)

Streptomycin and penicillin (GIBCO BRL)

Tris Base (Sigma)

Tween 20 (Fluka)

2.2: M2-GFP Experiments

2.2.1: M2-GFP Cloning

A cDNA copy of a ratiometric pH-sensitive GFP (Miesenbock *et al.*, 1998) was fused through a double repeat serine-glycine linker to the C-terminus of a cDNA

copy of M2 mRNA of A/Chicken/Germany/27 (H7N7, Weybridge strain). A cDNA copy of the M2-GFP fusion protein was then cloned into the BglI site of plasmid pEV3 (Figure 2.1) and the vector was electroporated into MEL C88 cells and transfected as previously described (Needham *et al.,* 1992). MEL C88 clones expressing M2-GFP and Weybridge M2 were a gift from Dr Tanya Betakova. Sequencing was performed using primer set 1 from section 2.1.4.; Table 2.1) A clone, M2-GFP 127-2 (Figure 2.2) expressing high levels of M2 fusion protein upon induction, was selected for study.

2.2.2: DNA Sequencing

DNA sequencing of the M2-GFP construct was performed using primer set 1 from section 2.1.4; Table 2.1 and the Big Dye sequencing terminator kit as per manufacturer's instructions. This technology is based on the dideoxy termination method (Sanger *et al.,* 1977). Sequencing reactions were performed on a PTC-100 programmable thermal controller (MJ Research Inc). The resultant products are cleaned with ABI 300 PCR cleaning columns and sequenced 5'-3' and 3'-5' using an AB 377 automated sequencer (according to the manufacturer's instructions).

2.2.3: Cell Culture

Mouse erythroleukaemia (MEL) cells expressing the "Weybridge" M2 (WM2) and clone 127-2 expressing the M2-GFP fusion proteins were maintained at 37°C (3-5% CO_2) in α minimal essential media (αMEM) supplemented with 10% FCS, streptomycin and penicillin (GIBCO BRL) and G418 (10μM) for positive selection of clones. Cells were grown in suspension; however C88 cells are semi-

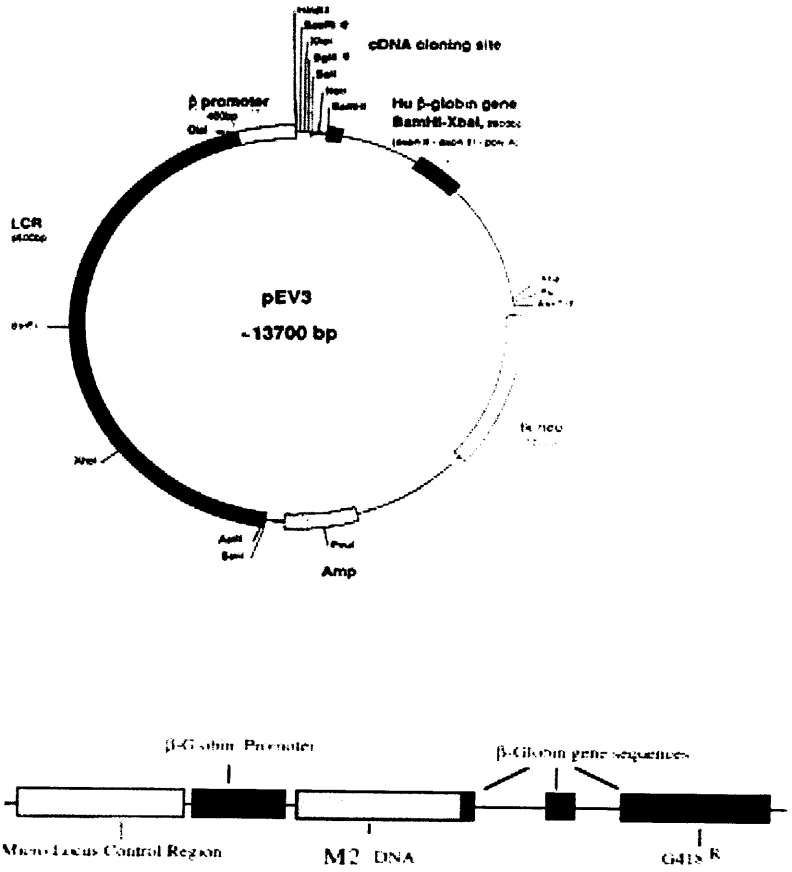

Figure 2.1: Maps of pEV3 vector (Needham et al., 1992).

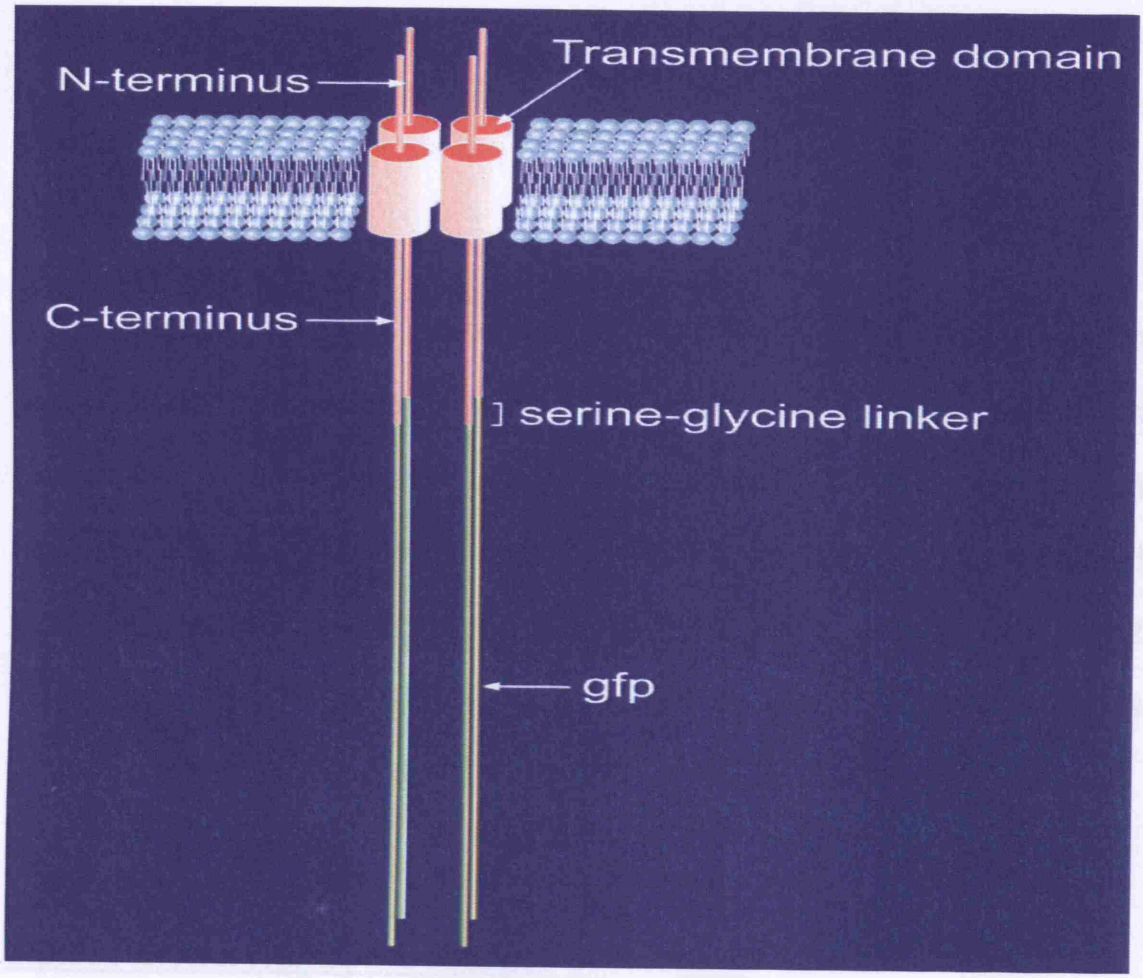

Figure 2.2: A diagrammatic representation of the M2-GFP fusion protein inserted in the plasma membrane. The GFP was fused to the C-terminus of M2 by a double repeat serine-glycine linker attached to the N-terminus of GFP. Localisation of fluorescence from MEL cells indicated this construct was expressed in the plasma membrane.

adherent so before subculturing a sharp tap of the culture flask was performed to dislodge any adherent cells. MEL cells grew rapidly dividing approximately every 12-24 hours. When cell density reached $2x10^6$ cells/ml the flask was sub-cultured to $5x10^4$ cells/ml. Cell counting was performed using a hemocytometer under a light microscope.

2.2.4: M2 and M2-GFP Protein Expression

MEL cells transfected with either WM2 or M2-GFP construct were seeded in six-well plates at approximately $1x10^6$ cells/ml concentration. Protein expression was induced by the addition of 2% dimethylsulphoxide (DMSO). This caused MEL cell erythroid differentiation and Hb production, which in-turn induced protein expression. 24 hours post-induction cell growth ceased due to M2 expression. Protein expression was analyzed by SDS-PAGE with samples taken from days 0-4 post induction.

2.2.5: Polyacrylamide Gel Electrophoresis

SDS polyacrylamide gel electrophoresis was performed as per the Laemmli method (Laemmli., 1970) and was used to analyse MEL cell expression of the M2 and M2-GFP proteins.

2.2.5.1: Preparation of SDS Gels and Sample Preparation

Gels consisted of a 1cm 4% acrylamide stacking gel (0.5M Tris-HCl pH 6.8, 20% w/v SDS, 30%/0.8% w/v acrylamide/bisacrylamide, 10% ammonium persulphate (APS) and Tetramethylethylenediamine (TEMED)) and a 12% 5-7cm separating gel (0.5M Tris-HCl pH 8.8, 20% w/v SDS, 30%/0.8% w/v acrylamide/bisacrylamide, 10% Ammonium persulphate (APS) and TEMED).

An overlay of propanol was placed over the gel until polymerization was complete and then removed. MEL cells were washed with PBS and extracted on ice for 15 minutes with 0.1ml extraction buffer (1% NP-40, 150mM NaCl, 2mM $MgCl_2$, 1mM EDTA, 0.2% soya bean trypsin inhibitor, 10μg/ml aprotinin, 1mM phenylmethylsulfonyl fluoride (PMSF), 20mM Tris-HCl, pH 7.5) and the extracts spun at 13200rpm for 5 minutes. Aliquots were mixed with an equal volume of 2x sample buffer (125mM Tris-HCl pH 6.8, 4% SDS, 20% glycerol, with or without 100mM dithiothreitol (DTT) and 0.002% bromophenol blue) and heated at 100°C for 5 minutes. 20μl samples were analyzed by SDS-PAGE using See blue 2 markers (Invitrogen).

2.2.5.2: Electrophoresis and PVDF Electroblotting

Gels were run in 1X running buffer (25mM Tris-HCl, 200mM glycine and 0.1% SDS) at 100-200V. Upon removal of the gel from running buffer, blotting paper cut to the size of the gel was put in 3 solutions, Anode 1 (90.75g Tris 500ml Methanol 2L H_2O), Anode 2 (7.56g Tris 500ml Methanol 2L H_2O) and cathode solution (7.87 Tris, 13.2 Σ-Caproic acid and 500ml methanol). The gel was placed on an Immobilon-P PVDF membrane and electroblotting was performed at 15-20V for 1 hour. Post-blotting the membrane was washed with PBS containing 0.02% TWEEN 20.

2.2.5.3: Western Blotting

The membrane was blocked by incubation at room temperature in 5% powdered milk with 0.02% Tween 20 in PBS for 1hr and then incubated in the same solution with anti-M2 rabbit serum (R68) raised against peptide corresponding to the first N terminal 24 amino acids (at a dilution of 1:1000). The membrane was then washed in PBS-Tween 20 solution and incubated with

1:2000 protein A conjugated to horse-radish peroxidase for 1hr (BIORAD). Following further washing steps in PBS Tween, the blot was then developed with ECL solution (Invitrogen) for 1 minute. The blot was then exposed to autoradiograph in film in a dark room for 1-5 seconds.

2.2.6: Fluorescence Microscopy

For fluorescence microscopy, cells were washed twice (4000rpm, 3 minutes) and resuspended in PBS (~$1x10^7$ cells). 0.2ml of cell suspension was added to 40mm coverslips (Chance Propper Ltd) previously treated with 2% APTS (Sigma) and left for 5 minutes at room temperature for a monolayer to form. MEL cells attached to coverslips were placed in a homemade sealed perfusion chamber on a deltavision fluorescence microscope and perfused with Gey's medium (123mM NaCl, 5 or 100mM KCl (high KCl), 0.86mM $Na_2HPO_4.12H_20$, 0.18mM KH_2PO_4, 5.7mM glucose, 1.3mM $MgCl_2.6H_2O$, 1.46mM $CaCl_2.2H_2O$) buffered by 120mM HEPES or MES to variable pH values (pH 8 to 5) with and without 50μM rimantadine. The chamber had an inlet and outlet which, were attached to a gravity based perfusion system and waste bottle respectively. Images were collected on a deltavision microscope using either a x40 or x100 objective. Solution changes were performed at timed intervals with the gravity based perfusion system using manual valves. Excitation wavelengths of 410nm and 470nm with exposure times of 50-200ms for each image were used with emission spectra collected at 508nm. All measurements were normalized with respect to the ratio at pH 8, taken as 1. A ratio of the fluorescence values was obtained for images of the surface of individual cells plasma membranes, using the program imageJ with which pixel counting was performed. Ratio values were calculated using the following formula:

$$(2.1)\quad Ratio = \frac{(R_{410} - Bk_{410})}{(R_{470} - Bk_{470})}$$

with R_{410} and R_{470} being the fluorescence emission intensities at these excitation wavelengths of 410 and 470, respectively, and Bk_{410} and Bk_{470} being the corresponding background measurements from the surrounding medium. These ratio values were then converted to pH values with the aid of a calibration curve. For WM2 expressing MEL cells a different procedure was used for loading of SNARF-1-AM and spectroscopic analysis. Please refer to C.Thompson PhD thesis (1994).

2.3: M2 Production in Bacteria

2.3.1: M2 Protein and Mutants

A Weybridge M2 protein with His-tag and linker, a truncated mutant lacking amino acids 1-19, a V27A rimantadine-resistant mutant, and an H37A mutant (Figure 2.3) were all gifts from Peter Czabotar. All constructs were contained in the pPROEX HTa vector (Figure 2.4). Using the M2 protein sequence site-directed mutagenesis was used to create single tryptophan mutants of M2 (W15F and W41F) to study the individual functions of the Trps in this protein. Attempts were made to express all these proteins in the *E. coli* strain C41 (DE3) and then purify the proteins for biophysical studies.

2.3.2: Cloning

2.3.2.1: Competent Cells and Transformation

E.coli cells were made competent using the $CaCl_2$ method and transformed using the methods described by Sambrook *et al* (Sambrook *et al.*, 1989).

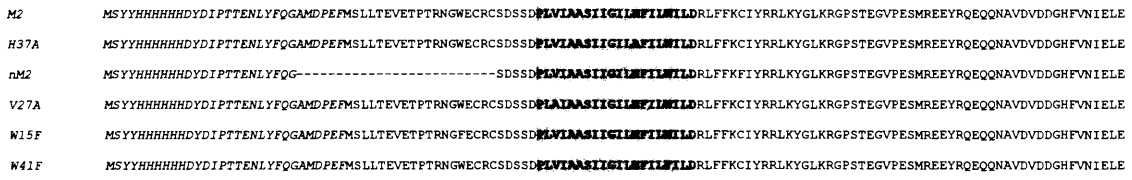

Figure 2.3: Sequences of wild type and mutant M2 proteins. Non-M2 sequences derived from the expression vector (containing the six His tag) are in italics. The transmembrane domain is shaded grey. The deleted region of nM2, displayed as a dashed line, includes 6 amino acids from the vector sequence in addition to amino acids 1-19 of M2.

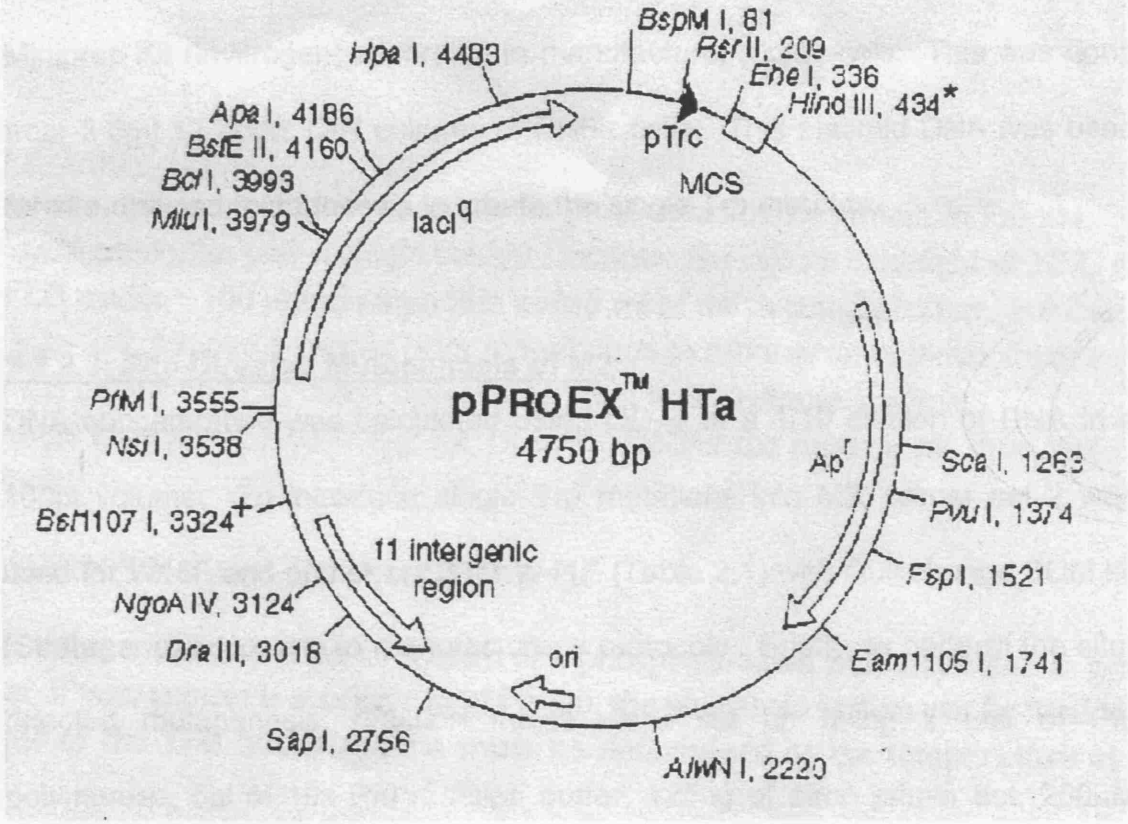

Figure 2.4: Map of pPROEX Hta vector (Gibco BRL)

Briefly, DNA was added to competent bacterial cells and incubated on ice for 30 minutes. Cells were then incubated for 2 minutes at 42°C to induce heat shock within the bacterial cells. Immediately after, cells were placed on ice for a further 2 minutes. Cells were plated onto agar plates with 100μg/ml ampicillin to select transformed cells.

2.3.2.2: Isolation of Plasmid DNA from *E.coli*

Plasmid DNA for M2 in pPROEX Hta was isolated using Purelink Quick Plasmid Miniprep Kit (Invitrogen) according to manufacturer's protocols. This was done from 3-5ml 12 hours O/N cultures of DH5α cells. This plasmid DNA was used for site-directed mutagenesis to create the single Trp mutants.

2.3.2.3: Site-Directed Mutagenesis of M2

DNA concentration was calculated using OD_{260} of a 1/10 dilution of DNA in a 100μl volume. To introduce single Trp mutations into M2, primer set 2 was used for W15F and primer set 3 for W41F (Table 2.1) with Quikchange SDM kit (Stratagene) according to manufacturer's protocols. Briefly, to perform the site-directed mutagenesis, reaction mixes were set up using 1 unit of Pfu polymerase, 5μl of 10x Pfu reaction buffer, 125ng of each primer set, 250μM dNTP's, 10-30ng of M2 pPROEX DNA and the volume made up to 50μl with MiliQ H_2O. Both positive and negative controls were set up with each reaction. PCR tubes containing reaction mix were then placed in a PTC-100 programmable thermal controller (MJ Research Inc) and cycled using the following steps:

1. 25°C for 30 seconds
2. 95°C for 30 seconds; 55°C for 1 minute

4. 68°C for 12 minutes

This cycle was repeated 20 times and then PCR samples were left overnight at 4°C. The PCR reaction template which had become methylated during the SDM procedure was digested using enzyme *DpnI* (Stratagene) according to manufacturer's protocols and then transformed using the heat shock method into competent *E.coli* DH5α cells, prepared by the calcium chloride method, as mentioned in 2.3.2.1. Transformed *E.coli* cells were streaked onto LB agar plates containing 100μg/ml ampicillin (Sigma) and the plates incubated overnight at 37°C. Single colonies were then picked and grown; DNA was extracted, as described previously and sequencing of W15F and W41F M2 mutant DNA was performed, as per method used in section 2.2.2, using primer set 4 (Table 2.1) to confirm the introduction of the correct mutations.

2.3.3: Recombinant M2 Purification Procedure

2.3.3.1: Induction of Protein Expression

E.coli cells expressing WM2 (BL21 C41 (DE3)) were grown in 500ml liquid broth (LB) (bacto tryptone 10g/L, Yeast extract 5g/L, NaCl 10g/L, Maltose 2g/L, 100μg/ml ampicillin, pH7) O/N at 30°C in an incubator. The low temperature made sure that all *E.coli* cells were still growing by the morning. All cultures were inoculated from a single colony grown on LB agar streaked from glycerol stocks. The 500ml overnight culture was then used to inoculate a total volume of 20L LB in a New Brunswick Scientific Bioflo 4500 fermenter, using 500rpm rotor speed and 30cu.ft./min aeration at 37°C. Cells were grown for approximately 2-4 hours with constant aeration to an optical density of 1-1.2 before induction of protein expression with 0.2mM isopropyl β-D-

thiogalactopyranoside (IPTG). Cells were harvested after 2 hours and frozen as a pellet, which was kept at -20°C.

2.3.3.2: Protein Extraction

Approximately 10-15g of the above pelleted *E.coli* cells were thawed at 4°C and resuspended in 100ml of lysis buffer (20mM Tris-HCl pH 8, 200mM NaCl, 1% N, N-dimethyldodecylamine-N-oxide (LDAO), 10mM imidazole, 0.5mM PMSF, 3 EDTA-free protease inhibitor tabs per 100ml (Roche)). The presence of PMSF and EDTA-free protease inhibitor was especially important to avoid proteolytic cleavage of the M2 protein. The sample was then placed in a beaker contained in ice water and sonicated at maximum intensity in 10 second bursts with 20 second rest periods for 10 minutes. If the temperature went above 30°C sonication was stopped for a period of 5 minutes and then resumed. This caused lysis of the *E.coli* cells releasing the expressed M2 into the supernatant. To remove all non-particulate cellular components the lysed supernatant was centrifuged at 17000rpm for 30 minutes at 4°C. Supernatant was then passed through a 0.22μm steritop filter (Fisher Scientific) to remove precipitates.

2.3.3.3: Nickel-Chelation Chromatography

A column of 25ml nickel Ni-CAM HC Resin column (SIGMA) was prepared by packing resin followed by washing with double distilled H_2O and the FPLC buffer (20mM Tris-HCl pH 8, 200mM NaCl, 1% LDAO, 10mM imidazole, 0.5mM PMSF) to equilibrate column. The clarified supernatant was applied to the nickel resin at a rate of 1ml/min with use of a fisher scientific pump. Flow-through was collected to aid in analysis of protein purification procedure. The column with His-tagged M2 bound, was washed with 100ml FPLC buffer to elute any non-

specifically bound protein followed by the application of more washing buffer (20mM Tris-HCl pH 8, 1M NaCl, 1% LDAO, 20mM imidazole) to elute any ionically bound protein. Buffer (100ml) was then applied once more but containing 0.1% LDAO to lower detergent concentration for biophysical studies. Finally, M2 protein was eluted with elution buffer over an imidazole gradient (20mM Tris-HCl pH 8, 200mM NaCl, 0.1% LDAO, 20-300mM imidazole); 10ml fractions which were then collected and analysed on SDS-PAGE gels.

2.3.3.4: SDS-PAGE Gel Staining

SDS-PAGE gels were run as per section 2.2.4, but gels were stained instead of western-blotting, in order to observe which fractions from the nickel column contained M2 protein. Polyacrylamide gels were stained using gelcode blue (a coomassie based product). Briefly, a gel was removed from the electrophoresis chamber, washed 3x5 minutes in ultra-pure water and then placed in gelcode stain for at least 1 hour. After the 1 hour, the gel was washed in ultra-pure water once more to destain and enhance band visibility. Gels were then scanned using a Kodak scanner and software.

2.3.3.5: Dialysis and Size Exclusion Chromatography

Fractions which were identified as containing M2 protein were pooled and placed in a cellulose dialysis bag with a 4-12 Kda cutoff and dialyzed O/N in 1L of basic FPLC buffer (20mM Tris-HCl pH 8, 1M NaCl, 0.1% LDAO) to remove imidazole. The next day, protein concentration was calculated from the OD_{280} of a 100µl sample. The protein sample was placed in a centricon with 40Kda cutoff and spun at 4000rpm for 1 hour to concentrate sample to a 1ml volume. This was then filtered and applied over a superdex 200 gel filtration column (Amersham Biosciences) again precharged in FPLC buffer (20mM Tris-HCl pH

8, 200mM NaCl, 0.1% LDAO). Passage through the column was monitored by OD_{280} and 0.5ml fractions were collected and samples were analysed SDS-PAGE gels stained with gelcode blue to confirm protein presence. Identity of WM2 was confirmed by western-blot described in section 2.2.4.4. All protein concentrations were determined spectrophotometrically at 280nm using the following extinction coefficients: 20700 M^{-1} cm^{-1} for M2 and H37A and 12102 $M^{-1}cm^{-1}$ for nM2, which were calculated based on aromatic residue content.

2.4: Fluorescence Spectroscopy

Tryptophan fluorescence emission spectra were recorded using a SPEX FluoroMax fluorimeter with excitation at 290 nm (bandwidth 0.2 nm) and emission scanned from 300 to 450 nm (bandwidth 1.5 nm). Spectra were recorded at 20°C in UV-transmitting plastic cuvettes. Solutions consisted of 0.33μM M2 tetramer in FPLC buffer (0.1% LDAO, 100mM NaCl and 10mM Tris pH 8). The pH was lowered by addition of small amounts of 150mM citrate pH3.5, 0.1% LDAO and 100mM NaCl. Amantadine, rimantadine and other M2 inhibitors were made up in the above buffers. All drugs were soluble in buffer below pH 7. Data processing and analysis were performed using the Specpro software package. Spectral shifts were determined by calculating the first derivative from the smoothed emission spectra, using the above software package. The emission maximum was where the first derivative of the fluorescence spectrum crossed the X axis at zero. Emission maximum measurements were then fitted to a ligand protonation profile with two protonation events, for activation and permeation respectively, using the following scheme:

$L + H \leftrightarrow HL$ where K_{HL}=[HL]/([L][H])

and pK_{HL}=Log{[HL]/([L][H])}

$HL + H \leftrightarrow H_2L$ where K_{H2L}=[H_2L]/([HL][H])

and pK_{H2L}=Log{[H_2L]/([HL][H])}

The optical signal is therefore calculated as:

Signal=ε(H_2L)[H_2L]+ε(HL)[HL]+ε(L)[L]

Acrylamide quenching studies were performed by adding small aliquots of 2M acrylamide to protein or protein/rimantadine adjusted to different pH values with citrate buffer. The excitation wavelength for fluorescence quenching was 295nm in order to avoid inner filter effects from the absorption of acrylamide. The results were analyzed using the modified Stern-Volmer equation (2.2) (Eftink & Ghiron, 1981):

(2.2) $F_0/F = (1 + K_{SV}[Q])e^{V[Q]}$

where F_0 and F are the fluorescence in the absence and presence of acrylamide, respectively, [Q] is the concentration of acrylamide, K_{SV} is the Stern-Volmer constant for collisional quenching, and V is the static quenching constant. Polarization values were calculated from the equation (2.3) (Lakowicz, 1999):

(2.3) $$p = \frac{I_{VV} - GI_{VH}}{I_{VV} + GI_{VH}}.$$

where I_{VV} and I_{VH} are the measured fluorescence intensities (after appropriate background subtraction) with the excitation polarizer vertically oriented and emission polarizer vertically and horizontally oriented, respectively. *G* is the grating correction factor and is the ratio of the efficiencies of the detection system for vertically and horizontally polarized light, and is equal to I_{HV}/I_{HH}.

Red-edge excitation shift (REES) measurements were made in quartz cuvettes using the same conditions, except that the excitation wavelength was varied by 2.5nm between 280-300nm. Above 300nm Trp fluorescence was too weak to be observed.

2.4.1: Kinetic Drug Binding Measurements

Kinetic drug binding measurements were made under pseudo first-order conditions (with drug in excess over protein) using time-resolved emission intensities at single wavelengths. Excitation was performed at 290nm and emission was recorded at the λ_{max}. In the case of M2 this was 337/341nm depending on pH. The increase in fluorescence intensity was recorded and analyzed as an exponential decay using an in house software program called Curfit (a non-linear least-squares fitting program). The optical signal for kinetic experiments was fitted to the following equation:

(2.4) Signal $=S_\infty - (S_\infty - S_0)\, e^{-t.\, kobs}$

Where S_0 and S_∞ are the signals at time zero and time infinity respectively and e is the exponential raised to the power of time and k_{obs}. The kinetic mechanism used to calculate k_{obs} is described by the formula 2.5:

(2.5) $k_{obs} = k_{on}[drug] + k_{off}$

where the observed binding rate (k_{obs}) is a function of the on rate (k_{on}) which is drug concentration dependent, plus the off rate (k_{off}). The k_{on} and k_{off} rate were calculated from the slope of the curve and y-intercept of the graph respectively.

2.4.2: Equilibrium Binding Measurements

For equilibrium measurements, a protein concentration of 0.33μM was kept constant while increasing amounts of M2 inhibitors were added until drug saturation. As in kinetic measurements, the λ_{max} of emission spectra was used to measure the observed fluorescence intensity change. Data was processed using the program Specpro. Dissociation constant values (K_d) were determined using Curfit with the assumption that a simple 1:1 complex was formed. The reaction is described by the formula 2.5:

(2.6) $M2 + D \Leftrightarrow M2D$

where M2 is one tetramer and D is one M2 inhibitor molecule.

The data were fitted to the following equation:

(2.7) Signal =εm[M]+εmd[MD]

Where εm and εmd are the specific optical properties of M and MD respectively. A value for the dissociation constant (K_d) was obtained by a non-linear least squares fit of this equation to the data with concentrations calculated by solving;

(2.8) $[MD]^2-(K_d+M_t+D_t)[MD]+M_tD_t=0$

Where the subscript t denotes total concentration.

2.5: Circular Dichroism Spectroscopy

The CD spectra of the M2 tetramers and M2/amantadine complexes were recorded on a Jasco J-715 spectropolarimeter at 20°C in 20mM Tris-HCl pH 8, 100mM NaCl plus 0.1% LDAO. Intensities are reported as differential absorption (ΔA) or as the circular dichroism extinction coefficient ($\Delta\varepsilon_M$) calculated using the molar concentration of peptide or protein. Values of $\Delta\varepsilon_{MRW}$ (the mean residual CD extinction coefficient) may be calculated as $\Delta\varepsilon_{MRW} = \Delta\varepsilon_M/N$, where N is the appropriate number of peptide bonds. Secondary structure

content was calculated from CD spectra using the method from Sreerama and Woody, 2000.

Chapter 3: Results

3.1: The Use of a M2 Fusion Protein to Measure M2 Activity

The aim of this project was to investigate the use of a pH-sensitive GFP (pHlourin) fused to the C-terminus of the M2 protein to measure its proton channel activity, in particular in an attempt to detect proton flux through the channel (Figures 2.1 and 2.2).

Initial studies by Dr. Tania Betakova conducted with the M2-GFP construct in a vaccinia/HeLa cell co-expression system using an HA protection assay (see Betakova *et al.* 2005 for a detailed description of the HA protection assay) had shown that the pH modulating activity of the M2-GFP fusion protein to be comparable to that of the wild-type M2 (personal communication), therefore providing the basis for further investigation.

This section describes fluorescence studies of the M2-GFP fusion protein expressed in a MEL cell expression system. Its localisation, functional capacity and the ability of the fused pHluorin to detect and measure the pH changes of the M2 channel in the vicinity of the plasma membrane were investigated.

3.1.1: Expression of the M2-GFP Fusion Protein

The GFP moiety was attached to M2 with a 1:1 stoichometry, consequently four GFP monomers were present in each channel tetramer. Expression of the M2-GFP fusion protein and the parental wild type Weybridge M2 protein (WM2), are compared following induction by 2% DMSO in stably transfected in MEL cells.

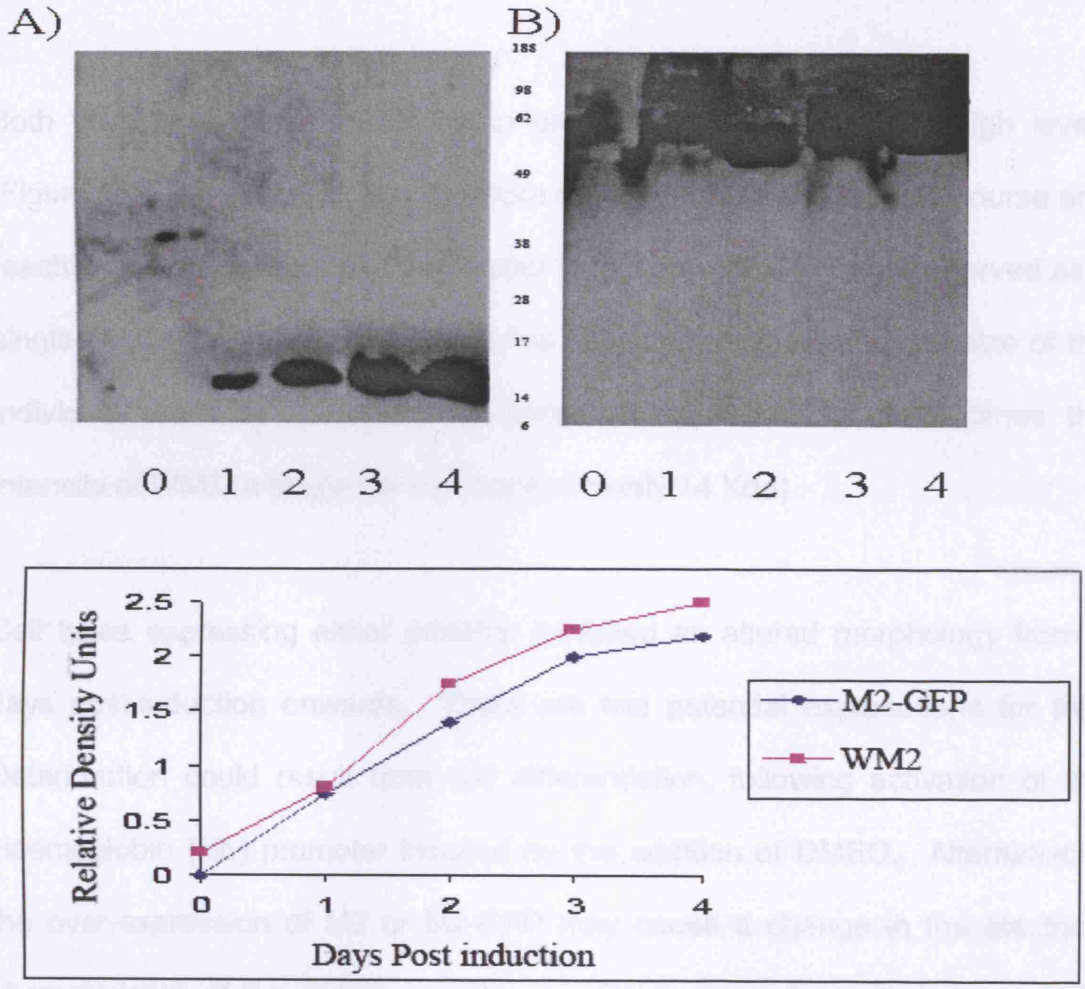

Figure 3.1: Expression profiles by Western Blot of WM2 (A) and M2-GFP (B) in MEL cells from days 0 to 4 post-induction. Band intensity was quantified as arbitary units using the program ImageJ (see methods section 2.25).

Cell lysates were taken over a 4-day period post-induction and expression levels were determined by Western-blotting, using an anti-M2 antibody, as described in section 2.24. The Western-blot was viewed by autoradiography and the relative density of bands was calculated using the imaging program ImageJ.

Both WM2 and the M2 GFP fusion proteins were expressed at high levels (Figure 3.1), increasing in intensity from days 0-3 with a similar time course and reaching a maximum around day 4 after induction. M2-GFP was observed as a single band of approximately 55Kda (as expected for the combined size of the individual proteins) and were expressed at approximately three times the intensity of WM2 (a single band of approximately 14 Kda).

Cell types expressing either proteins exhibited an altered morphology from 4 days post-induction onwards. There are two potential explanations for this. Deterioration could result from cell differentiation, following activation of the Haemoglobin (Hb) promoter induced by the addition of DMSO. Alternatively, the over-expression of M2 or M2-GFP may cause a change in the electrical characteristics of the cellular membrane. Previous studies with induced MEL cells have indicated that prolonged expression of M2 in MEL cells for longer than 4 days compromises integrity of the cell (Carol Thompson, PhD Thesis 1994). Cells were therefore used 3-4 days post infection.

3.1.2: Cellular Localisation of M2-GFP and Calibration of Fluorescence

The cellular localization of the M2-GFP protein was determined using GFP fluorescence. M2-GFP MEL cells were visualized at 4 days post-induction using

a Leica microscope equipped with a Deltavision imaging system. Fluorescent images were recorded at 508nm using excitation wavelengths of 410nm and 470nm. Both sets of images are over-layed in Figure 3.2. Fluorescence signals of intact MEL cells were observed to be strongest at these wavelengths, as described by Miesenbock *et al.,* 1998, suggesting the fluorescent properties of the M2-GFP fusion protein were consistent with those previously published for other GFP fusion proteins (Miesenbock *et al.,* 1998). Furthermore, the image in Figure 3.2 shows fluorescence emanating predominantly from the plasma membrane. M2 as an integral membrane protein is predominantly localized to the plasma membrane of cells (Leser and Lamb, 2005). Consequently, the fluorescence pattern observed indicated that the M2-GFP fusion protein was transported to the plasma membrane and did not accumulate in intracellular compartments.

To establish if the pHluorin retained its pH sensitivity after fusion to M2, fluorescence was measured in a homemade chamber in a deltavision microscope, MEL cells expressing M2-GFP were contained in the chamber and perfused with high KCl (115mM) Gey's medium buffered at known pH values and containing 10mM nigericin. Nigericin is an antibiotic from *Streptomyces hygroscopicus.* It is most commonly used as an antiporter of H^+ and K^+ and can transport various ions across membranes such that intracellular and extracellular K^+ is equilibrated and also intracellular and extracellular pH. Images were recorded, and the ratio of emission at 410 and 470nm excitation, normalized to pH 8 and plotted against the corresponding pH values (Figure 3.3). Measurements were performed in the vicinity of the plasma membrane. The calibration curve of the M2-GFP probe shows a ratiometric response from 1

to 0.35 when pH was changed from 8 to 5 through various intervals. The pH dependence is similar to that reported by Miesenbock *et al. 1998,* with GPI anchored GFP (Miesenbock *et al.,* 1998). The greatest pH response observed was between 8 and 6 and comprised almost 85% of the fluorescence change in the vicinity of the plasma membrane, in the GFP fluorophore between pH 8 and 5. The GFP probe therefore, is most sensitive in this pH range. The low response between pH 6 and 5 would make pH estimates within this range relatively inaccurate, and require multiple measurements to reduce the standard error. This calibration curve was used to estimate pH in the vicinity of M2-GFP expressed in MEL cells.

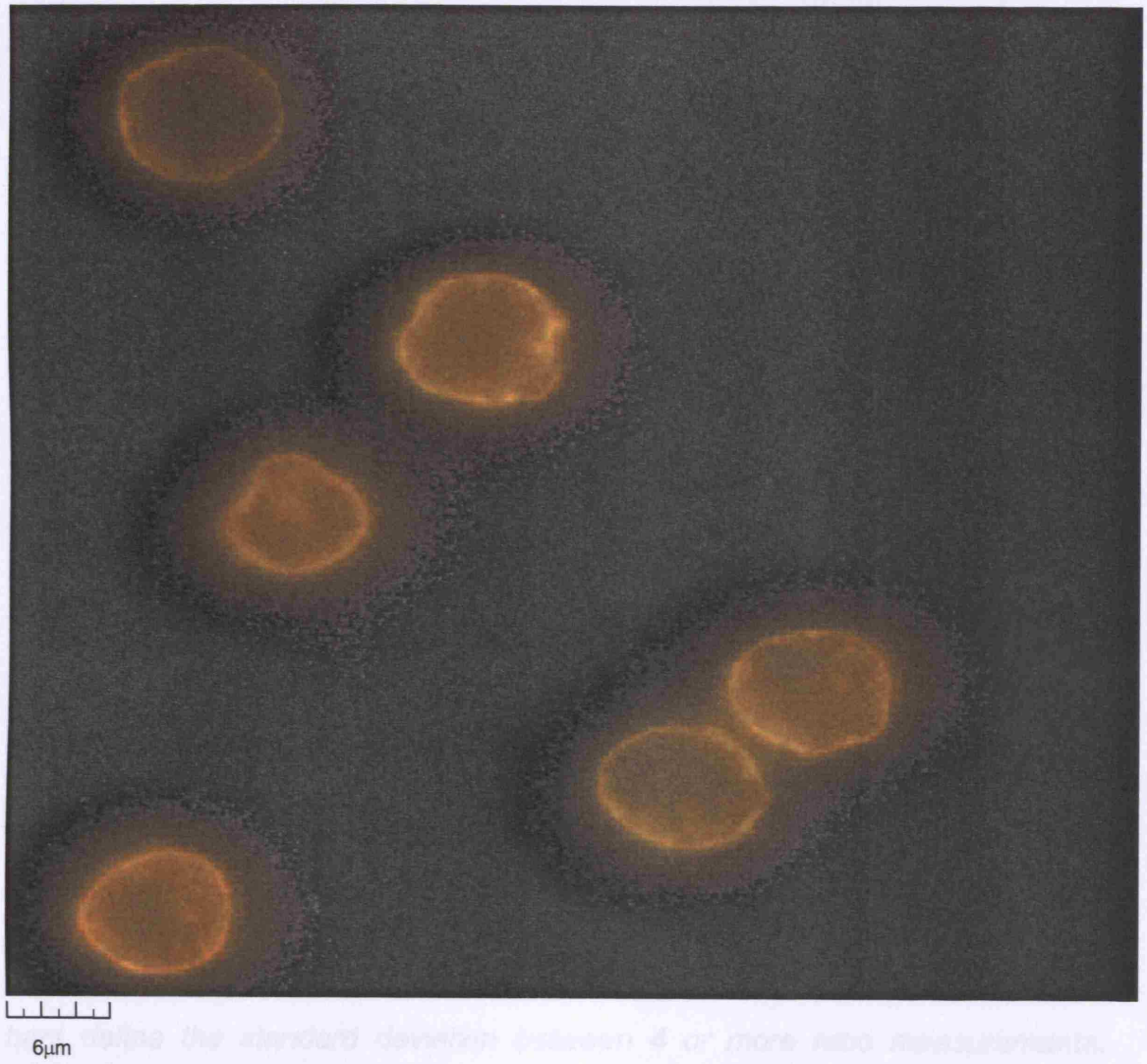

Figure 3.2: Fluorescent image of M2-GFP protein expressing MEL cells perfused with high KCl Gey's medium, pH 8. Images at 510nm (excitation wavelengths of 410nm and 470nm were over-layed) revealed that the predominant localization of fluorescence is close to the plasma membrane.

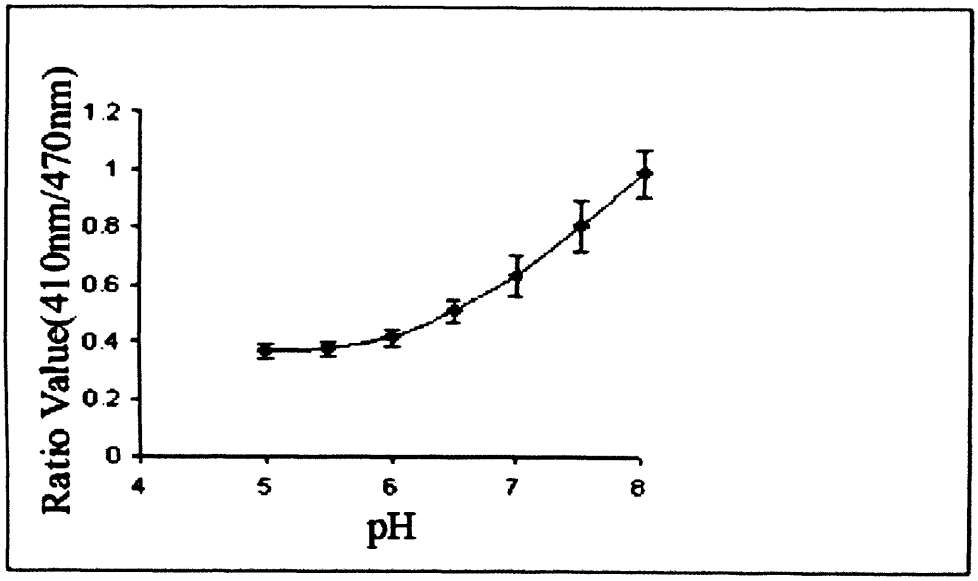

Figure 3.3: Calibration curve of the M2-GFP protein. M2-GFP cells were perfused with Gey's medium of defined pH containing 100mM KCl and 10mM nigericin. Fluorescence emission was measured at 510nm and excited at 410 and 470nm wavelengths. Data was fitted to a polynomial function using Microsoft Excel. Ratios were calculated and plotted against pH values. Error bars define the standard deviation between 4 or more ratio measurements.

3.1.3: Ability of M2-GFP to Detect M2-Specific pH Changes

Measurements of cells were taken at numerous time points at either pH 8, 7, 6 or 5 post-induction to establish whether the amount of M2-GFP influenced the pH in the expressing cells (Figure 3.4). These were compared in Figure 3.4 with measurements of the effect of WM2 on cytoplasmic pH of MEL cells, previously determined by Carol Thompson using the pH indicator SNARF1-AM. WM2 caused a gradual decrease of approximately 0.3 pH units in cytoplasmic pH over 4 days of induction, which was inhibited by rimantadine, at approximately neutral pH. The M2-GFP fusion protein demonstrated a smaller reduction in pH of approximately 0.05 units over 4 days, some 5-fold less than that determined for WM2. There was relatively little change in the pH of cells treated with rimantadine. The results of these experiments suggest that the M2-GFP fusion protein may have a lower ability than WM2 to change the pH in the vicinity of the probe, close to the plasma membrane, although this may not reflect intracellular pH as a whole.

The pH modulating activity of the M2-GFP fusion channel was further examined in the presence of the ionophore nigericin to investigate the contribution of M2-GFP to determining the pH gradient across the plasma membrane (Figure 3.5). The external solution was continuously changed resulting in a graduated lowering of pH from 8 to 5 (see Methods 2.2.5).

As shown in Figure 3.5, above pH 7.2 equilibration of intracellular pH with extracellular pH by nigericin increased the pH above that in untreated cells. This difference is due to the plasma membrane. Below pH 7.2 nigericin caused a decrease in the pH detected by GFP. These data

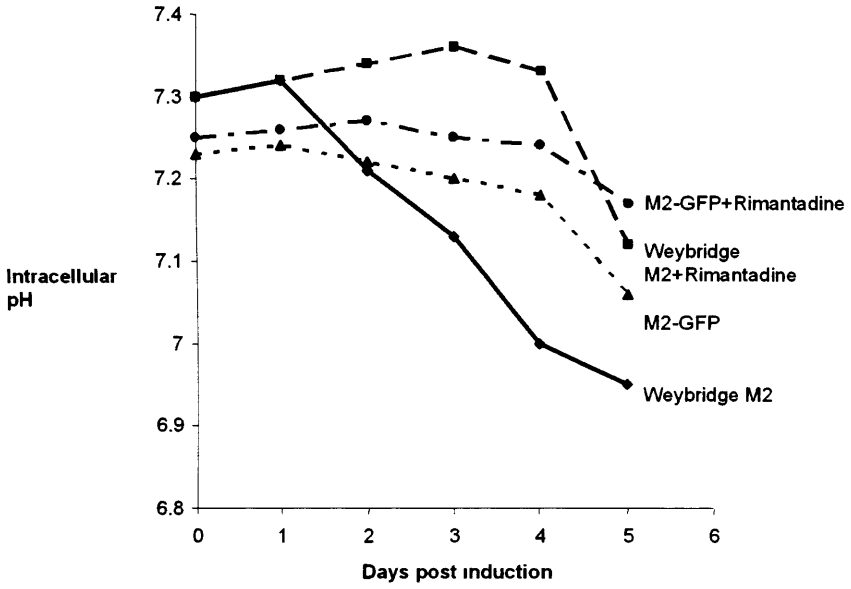

Figure 3.4: Comparison of changes in pH with time post induction in MEL cells either expressing WM2, labeled with SNARF-1-AM to measure cytoplasmic pH (data taken from C. Thompson PhD Thesis 1994) or M2-GFP (determined in this study) in high KCl buffer. Rimantadine (50μM) was added at the time of induction.

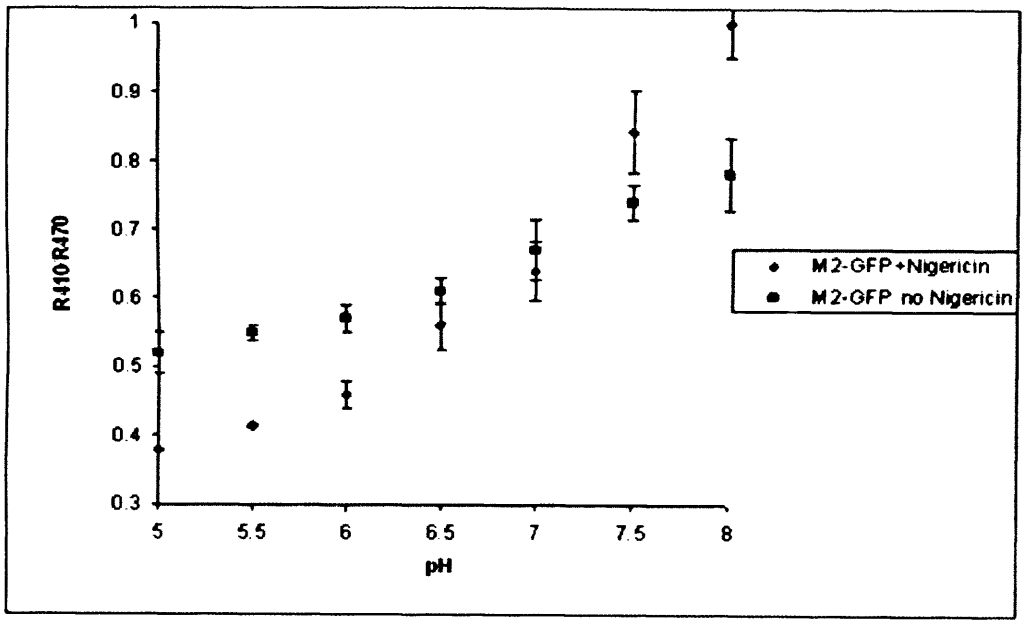

Figure 3.5: Experiment of M2-GFP MEL cells exposed to 0.5 pH unit intervals in buffered, high KCl Gey's medium with and without Nigericin (10μM). Emission at 510nm was recorded at excitation wavelengths of 410nm and 470nm and the ratio calculated. Error bars define the standard deviation between 4 or more ratio measurements.

are similar to those obtained using SNARF-1 as a probe for cytoplasmic pH of MEL cells by C.Thompson (PhD Thesis, 1994). Further experiments conducted with and without rimantadine were inconclusive, but did not reveal any significant influence of the channel of the M2-GFP fusion protein in reducing the pH gradient across the plasma membrane, as was observed for the M2 channel WM2-expressing MEL cells (C. Thompson, PhD Thesis 1994).

Although apparent that M2-GFP did not affect significantly the steady-state pH gradient across the cell membrane, further experiments were conducted to determine if the probe could detect proton flux or changes in proton flux, induced in response to changes in external pH (Figure 3.6). Several variations in the experimental setup were used: Firstly, fluorescence was measured following single pH steps from 8 to 7, 6 or 5, in a single solution change, in an attempt to observe local pH changes, in a temporal manner, in response to increase in proton flux through M2-GFP. Rimantadine addition experiments were also performed to determine the effect of switching off M2-dependent proton flux on the local pH. Lastly, the effects of valinomycin-induced pH gradient changes were investigated. Nigericin was used in the first two types of experiment to investigate the response of the pHluorin to equilibration of the internal and external pH, as a positive control to mimic the presence of a highly active proton channel.

When the external pH was lowered from 8 to 7, 6 or 5 the intracellular pH of M2-GFP cells decreased gradually to 7.21, 6.62 and 6.32, respectively (Figure 3.6). There was however, no abrupt change to reflect proton flux through the channel and measurements were conducted in the presence of rimantadine to detect

any small influence of blocking. Following change to pH 6 the reduction in pH was more gradual in the presence of rimantadine, the "steady-state" level was 0.1 pH units higher and the increase following the shift back to pH 8 was less marked. Following a shift to pH 5, the presence of rimantadine caused a slight elevation of 0.05 pH units in the steady-state pH. Rimantadine treated cells that underwent the same pH changes gave internal pH values of 7.25, 6.72 and 6.37. In contrast, in the presence of nigericin the drop in intracellular pH was more prominent following the pH shift down and recovery was faster following the shift up. There was no indication therefore that the pHluorin was detecting major changes in local pH as a result of proton flux through M2-GFP. Endogenous ion channels in most cell types help passage ions across the plasma membrane; however, MEL cells are known to have a minimal endogenous channels, hence their choice for electrophysiological studies of M2. Experiments by Carol Thompson revealed that M2 could abolish this in/out pH gradient near neutral pH. This effect is not seen in Figure 3.6. When external pH was lowered from 8 to 7, 6 or 5 the intracellular pH changed to 6.95, 5.90 and 5.30, respectively. The changes observed in nigericin treated cells indicated that the membrane and the intracellular contents of the cell are acting to buffer against the pH change in order to maintain the function of the cell, as seen in Figure 3.6.

These results showed that when external pH is lowered some M2, rimantadine-blockable, pH-modulating activity could be observed. Changes were small however and no rapid transient changes were detected. One possible explanation for this is that the pH changes may have been too large to detect more subtle effects of M2-GFP in pH modulating activity. After demonstrating

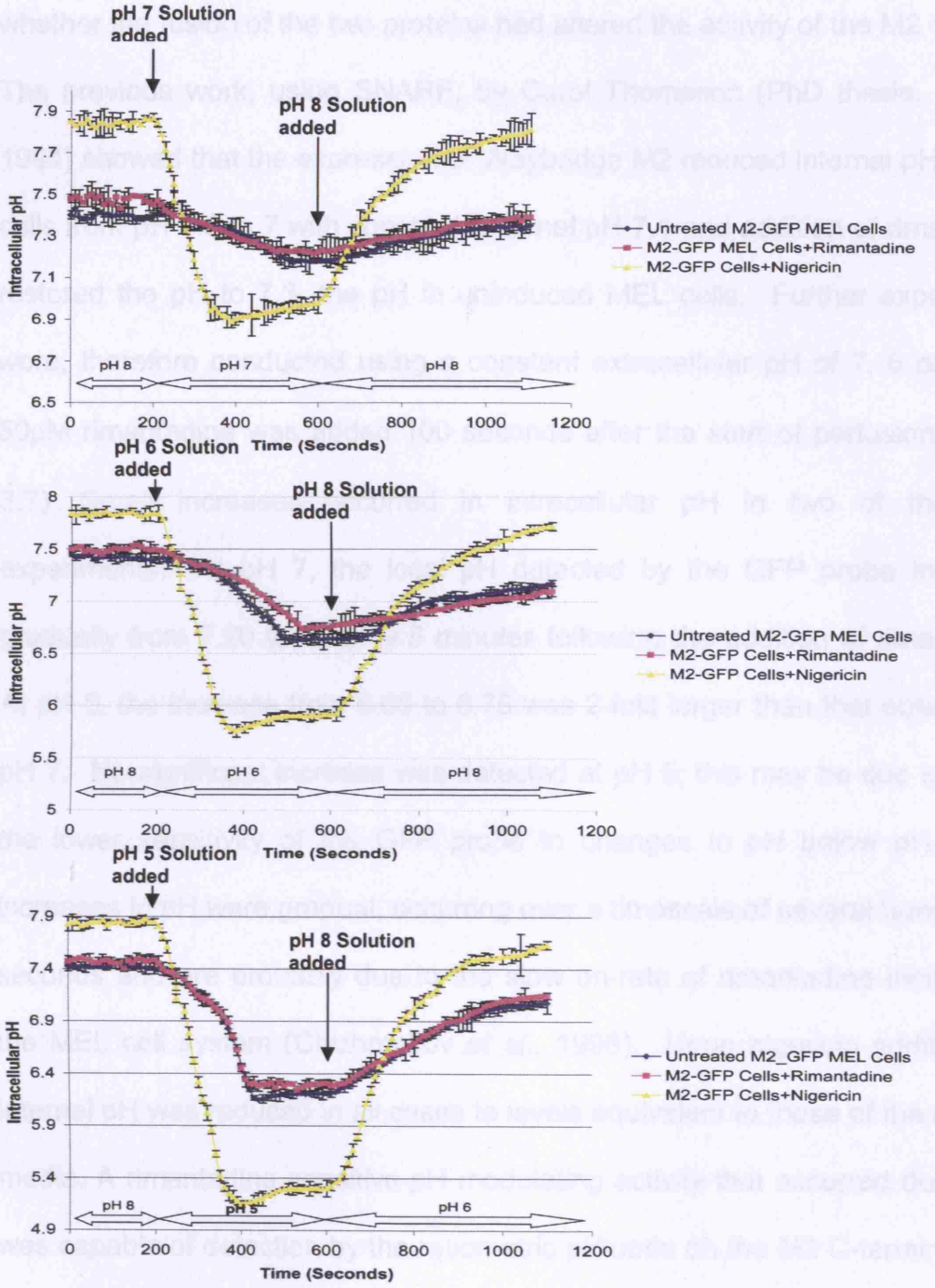

Figure 3.6: pH titration studies with M2-GFP expressing MEL cells. Cells were either untreated or treated with 50μM rimantadine or 10μM nigericin 5 minutes prior to measurements. Perfusion was performed by a gravity based perfusion system with pre-made buffers (refer to Method 2.2.5). Error bars define the standard deviation between 4 or more ratio measurements.

the pH sensitivity of the GFP combined to M2 it was necessary to examine whether the fusion of the two proteins had altered the activity of the M2 channel. The previous work, using SNARF, by Carol Thompson (PhD thesis, January 1994) showed that the expression of Weybridge M2 reduced internal pH of MEL cells from pH 7.3 to 7 with constant external pH 7.1 and addition of rimantadine restored the pH to 7.3, the pH in uninduced MEL cells. Further experiments were, therefore conducted using a constant extracellular pH of 7, 6 or 5, and 50μM rimantadine was added 100 seconds after the start of perfusion (Figure 3.7). Small increases occurred in intracellular pH in two of the three experiments. At pH 7, the local pH detected by the GFP probe increased gradually from 7.20 to 7.25 by 5 minutes following the addition of rimantadine. At pH 6, the increase from 6.65 to 6.75 was 2-fold larger than that observed at pH 7. No significant increase was detected at pH 5; this may be due in part to the lower sensitivity of the GFP probe to changes in pH below pH 6. The increases in pH were gradual, occurring over a timescale of several hundreds of seconds and are probably due to the slow on-rate of rimantadine inhibition in the MEL cell system (Chizhmakov *et al.,* 1996). Upon nigericin addition, the internal pH was reduced in all cases to levels equivalent to those of the external media. A rimantadine sensitive pH modulating activity that occurred due to M2 was capable of detection by the ratiometric pHluorin on the M2 C-terminus. It is apparent, however that the channel has relatively little influence on the transmembrane gradient and that effect was more readily observed at pH 6 than 7, which may reflect the activation of M2 below pH 7.

To further probe M2-GFP activity by another method, valinomycin-induced pH gradients were investigated as a sensitive way to detect M2-GFP dependent pH

changes (Figure 3.8). Valinomycin is a K^+ ionophore which shifts K^+ along the concentration gradient from the inside to the outside of the cell. For example, if valinomycin is added to liposomes with a 100 fold K^+ concentration gradient from inside to outside it results in a flux of K^+ out of the liposome. In response, protons are then conducted into the liposome down the electrochemical gradient if proton channels are present. If a proportion of this current were subject to inhibition by rimantadine, this would indicate that M2 contributes to the process. This method has previously been used to confirm the functionality of M2TM (Hu *et al.,* 2006).

The ratio of K^+ concentration between the inside and outside of cells was kept at ≈100 fold with 100mM K^+ inside and 1mM outside in the perfusion buffer. The pH was kept constant at 7 and measurements were taken for 100 seconds, prior to the addition of valinomycin. After 300 seconds carbonyl cyanide *m*-chlorophenyl-hydrazone (CCCP), a proton ionophore was added to allow proton flow into MEL cells to reduce the electrochemical gradient. This also confirmed GFP probe functionality and verified the structural integrity of the cells. After approximately 400 seconds, back titrations were performed with HCl (1 mM) to provide a calibration for the titration at a known pH. Upon Valinomycin addition intracellular pH decreased by approximately 0.07 pH units from 7.24 to 7.17 (Figure 3.8); this inward conduction of protons was blocked upon addition of 50μM rimantadine. The M2-GFP protein did not cause an abrupt change in response to the valinomycin-induced electrochemical change in cellular membrane potential but a gradual decrease in pH over approximately 120 seconds and only a fraction of that caused by CCCP. These measurements

indicated once again that the M2-GFP protein forms proton channels but that the effects on pH detected by the pHluorin probe are small.

Following completion of the fluorescence experiments, electrophysiological measurements by Dr Sergi Tokar compared rimantadine-sensitive current densities for WM2 cells and M2-GFP MEL cells gave values of 2.6 and 0.75 pA/pF respectively indicating that M2-GFP cells have approximately 3X less M2 channel activity than wild-type WM2 cells when the proteins are expressed in similar amounts in MEL cells(Figure 3.9).

The reason for this reduction in M2 channel activity could be due to several reasons. It may be due to either improper folding of the M2 channel or improper formation of tetrameric M2 due to steric hindrance. Both of these scenarios could lead to an altered conformation of the channel, or more specifically the key His37 and Trp41 side chains and their interaction. This may be reflected in reduced specific activity in the M2-GFP protein compared with wild-type Weybridge M2 or a reduction in the number of active channels.

In the various experiments the apparent activity of M2-GFP was either very small, or at least 3-5 fold less when compared with wild-type M2 protein. The GFP probe was clearly sensitive to pH and able to measure gross changes in pH, especially in the range of 8-6, where it was most sensitive. However, despite the reduced activity of the M2 fusion protein, increased buffering in the vicinity of the protein, close to the membrane, may have reduced the M2-induced changes in local pH in comparison with the previously measured cytoplasmic pH using SNARF-1. Future experiments might investigate

increasing the length of the linker between the GFP and M2 protein to avoid steric hindrance; however it is apparent from the experiments conducted that the GFP is unlikely to provide a measure of changes in proton flux through the fused M2 channel. Alternatively M2 and GFP could be co-transfected into the same cell to measure the activity of M2 by its effect on *Trans-Golgi* pH.

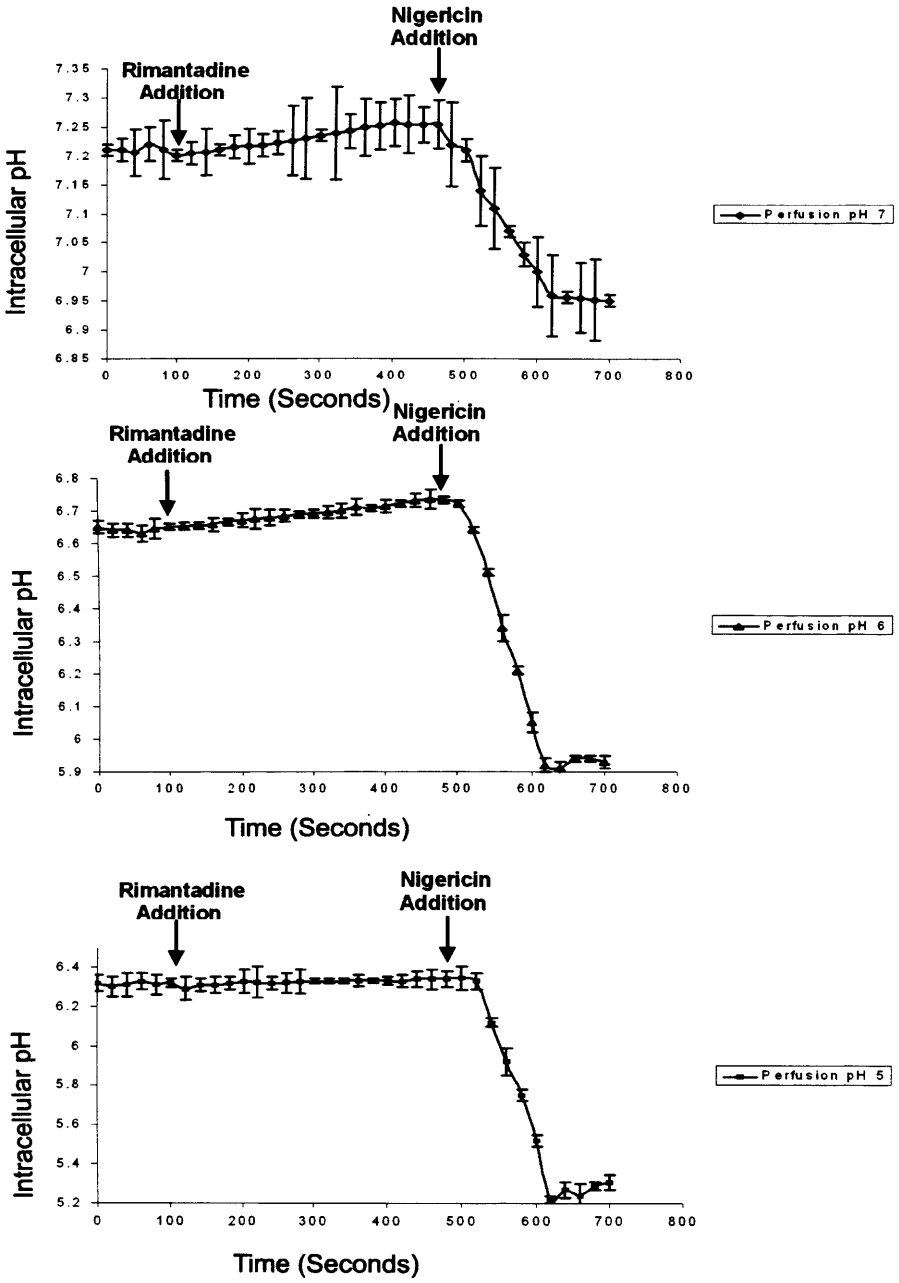

Figure 3.7: The effect of rimantadine on M2-GFP determined in transfected MEL cells in high KCl buffer (115mM). M2-GFP MEL cells were kept at constant pH 7, 6 or 5 while fluorescence was measured. 50μM rimantadine was added after 100 seconds and 10μM Nigericin after 500 seconds. pH values were estimated from the calibration curve in figure 3.3. Error bars define the standard deviation between 4 or more ratio measurements.

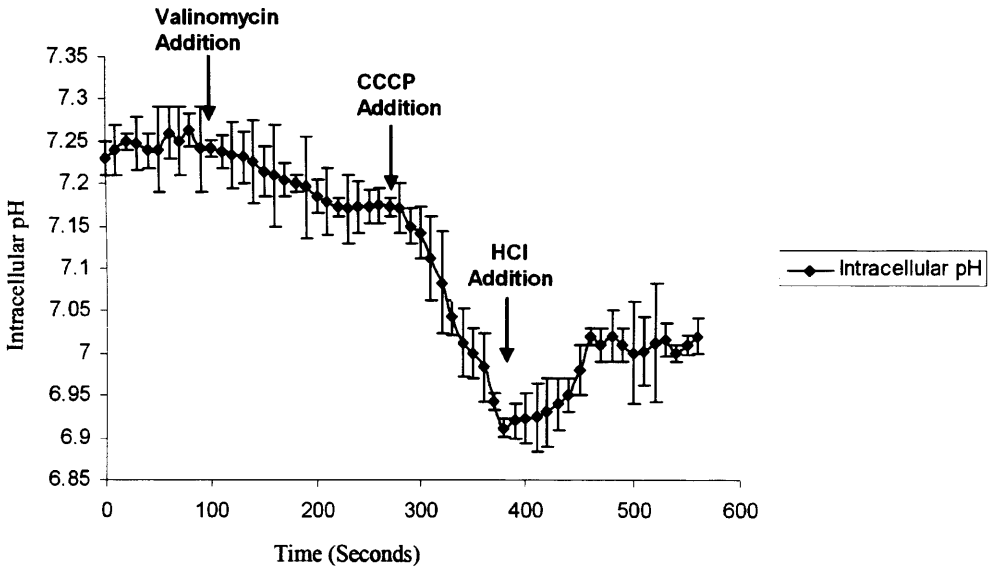

Figure 3.8: Valinomycin-induced gradient studies with M2-GFP MEL cells. Upon valinomycin addition in low K^+ buffer, an electrochemical gradient was produced that drives H^+ uptake by the MEL cells. Carbonyl cyanide m-chlorophenylhydrazone (CCCP) was added to allow proton transfer to reduce the electrochemical gradient. Error bars define the standard deviation between 4 or more ratio measurements.

A)

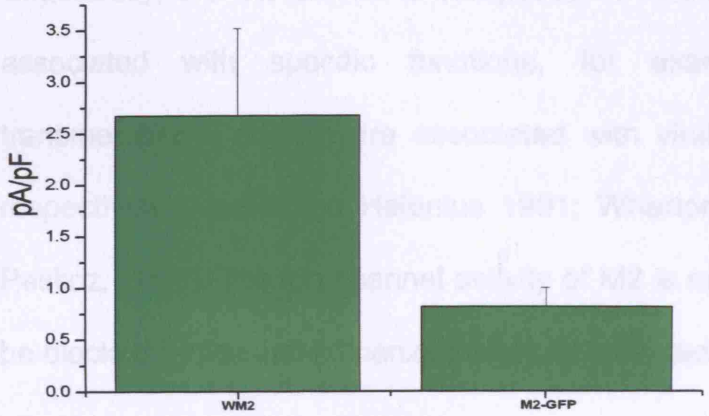

B)

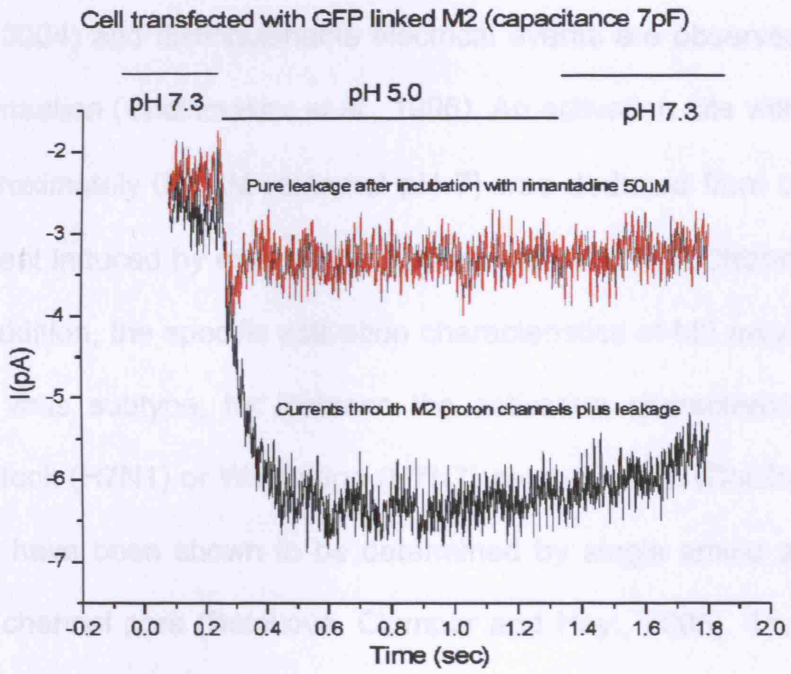

Figure 3.9: A) Current density comparisons of M2-GFP MEL cells and Weybridge M2-expressing cells (n=4). B) Measurements of currents within M2-GFP cells with and without rimantadine. 50μM Rimantadine was added to cells after approx 2 seconds to inhibit M2 and determine the rimantadine-sensitive current. Currents were measured as described in Chizhmakov et al. 1996.

3.2: Spectroscopic Studies of Recombinant Influenza A M2 Protein and Mutants

Structurally, the M2 protein is composed of defined regions; such regions are associated with specific functions, for example the C-terminus and transmembrane domain are associated with viral budding and cellular entry, respectively (Martin and Helenius 1991; Wharton *et al.*, 1994; McCown and Peskoz, 2006). The ion channel activity of M2 is essential to viral entry and can be blocked by the anti-influenza inhibitors amantadine and rimantadine.

The M2 channel is highly selective for protons, has low permeability for other physiological ions (Chizhmakov *et al.,* 1996; Mould *et al.,* 2000; Vijayvergiya *et al.,* 2004) and distinguishable electrical events are observed for activation and permeation (Chizhmakov *et al.,* 1996). An activation site with an apparent K_a of approximately 0.1 μM (external pH 7) was deduced from changes in outward current induced by external pH between 8.5 and 6.5 (Chizhmakov *et al.,* 1996). In addition, the specific activation characteristics of M2 may vary depending on the virus subtype; for instance the activation characteristics of the M2's of Rostock (H7N1) or Weybridge (H7N7) avian strains, (Chizhmakov *et al.,* 2003) and have been shown to be determined by single amino acid changes within the channel pore (Betakova, Ciampor and Hay., 2005). Thus proton activation and proton permeation of the channel are controlled by different amino acids in M2 and therefore have distinct genetic bases (Betakova, Ciampor and Hay, 2005). Proton permeation of the M2 channel fits a single site binding model with dissociation constant, K_p, of between 1 and 10μM.

This section describes the use of intrinsic protein fluorescence to investigate pH-dependent structural changes in the M2 channel pore related to channel

activation and proton conduction and in particular, the roles of His37 and Trp41 residues. A number of fluorescence techniques were used to study purified recombinant M2 protein and mutants expressed in *E.coli*. The use of fluorescence-based techniques permitted further investigation of the nature of the pH-dependent interaction between the His37 and Trp41 residues and provided insights into the environment of the channel pore and the possible mechanisms of proton conduction.

3.2.1: Expression and Purification of Influenza A M2 Protein and Mutants

3.2.1.1: Expression of M2 and Mutant Proteins

The M2 protein of A/chicken/Germany/27 (H7N7, Weybridge strain), a truncated mutant lacking amino acids 1-19, nM2, a rimantadine-resistant mutant M2V27A and an M2H37A mutant lacking His37 were expressed in the *E. coli* strain C41 (DE3) using the expression vector pPROEX Hta (Gibco BRL) (Miroux and Walker, 1996; Czabotar *et al.,* 2004). The M2 construct consisted of a His-tag, linker and the M2 protein sequence (Figure 2.3; Czabotar *et al.,* 2004); SDS-PAGE and Western-blotting were used to ascertain the levels of their expression and oligomeric form.

An anti-M2 polyclonal antibody raised against the conserved C-terminus of the protein was used to compare the relative expression levels of all three mutants over time. Prior to performing SDS-PAGE, the disulphide bridges in the protein were reduced by the addition of 100mM DTT to the sample buffer. When reduced, the M2 proteins gave bands of monomers or monomers plus dimers,

the relative proportions of which depended on the amount of protein loaded onto the gel and varied between experiments (Figure 3.10). If more protein was loaded onto the gel less protein was dissociated to its monomer form while some remained as tetramer. The most likely cause of this is the increased amount of protein may have affected the action of DTT breaking down disulphide bonds. The increased amount of protein may have led to higher protein association leading to disulphide bridges being protected from the action of DTT.

Following induction of expression with 1mM IPTG, amounts of M2 increased with time over 3 hours. Previous work conducted by P. Czabotar (NIMR, London) had shown that 2-3 hours was the optimum time for M2 expression. Furthermore, the OD_{600} of the bacterial culture decreased significantly after 3 hours post-induction. Beyond this time bacterial cells lysed due to toxicity of the M2 channel and increased the possibility of protein degradation. Expression levels for the two mutants, nM2 and M2H37A were compared with full length M2 by densitometry using ImageJ (Figure 3.10 B and C). SDS-PAGE of M2H37A indicated the presence monomer and dimer and some tetramer as for the Wild-type M2 protein (Figure 3). The incomplete dissociation observed here complicated the quantitative analysis of protein expression. However, if all bands were included in the overall analysis of protein expression then similar quantities of H37AM2 and WM2 were produced. nM2 expression produced approximately 30% less protein than that of wild type. All nM2 protein, upon boiling in SDS sample buffer reduced to the monomeric species, due to elimination of the N-terminus which contained the disulphide linkages.

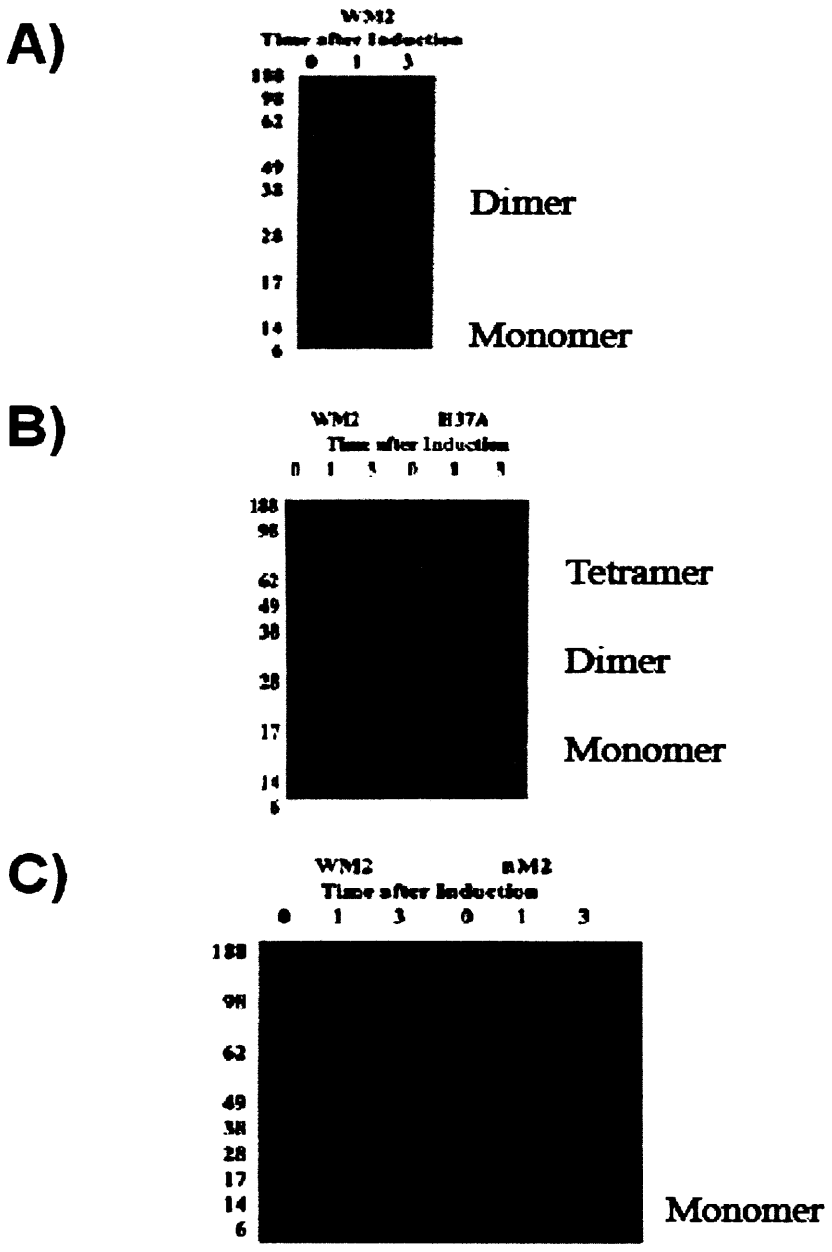

Figure 3.10: Expression of wild type and mutant M2 Proteins. Cell lysates were taken at 1 or 3 hours after induction of E.Coli cells to express WM2, M2H37A or nM2. SDS-PAGE and Western blotting, using an anti-M2 polyclonal antiserum, was used to identity the proteins (Approximately 0.1-0.5 μg of protein was reduced by addition of DTT at 100mM concentration).

Single tryptophan mutants of M2 were created by site-directed mutagenesis of either of the two tryptophans to phenylalanine. As the fluorescence spectrum of tryptophan is cumulative, elimination of either Trp residue to form the two single tryptophan mutants allows study of the individual fluorescence signals of either Trp without interference. Their expression pattern over a time course of 3 hours is shown in Figure 3.11. Substitution of either tryptophan residue resulted in a markedly reduced expression of the mutant M2 proteins; a small amount of oligomer formation at an approximate molecular weight of 98Kda, together with a small amount of what was potentially degraded M2 at 10 Kda was observed. This suggests that presence of both trp residues is important for the correct protein folding and/or expression. Alternatively, the insertion of phenylalanine may cause the reduced quantity of protein expression or may alter the protein in such a way that it is either unable to fold correctly and aggregates or degrades. The exact reason for such a pronounced change in expression and oligermisation state is not fully understood. However, both tryptophan residues are found adjacent to the membrane, or in the interfacial region of the membrane, and tryptophan residues with delocalized electron structures in this location are known to promote protein folding in the membrane and encourage structure stabilization.

Several attempts to purify both tryptophan mutants using the standard method failed to yield sufficient protein for experimentation. On the other hand, the M2 mutant containing a rimantadine resistance mutation V27A was successfully cloned and expressed; the mutation caused a reduction in expression of approx 30% compared to wild type, and yielded sufficient protein for further study (Figure 3.11).

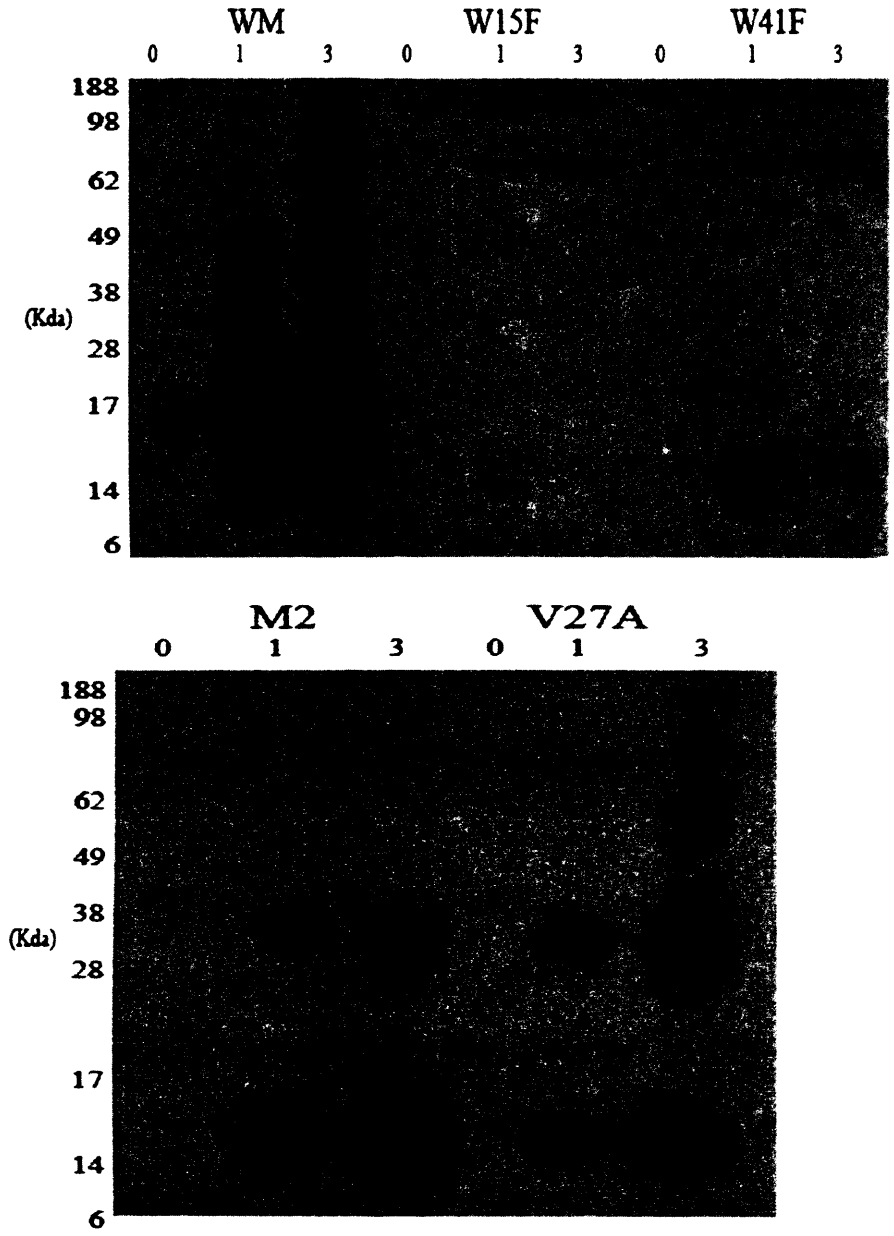

Figure 3.11: Comparison of the expression of wild-type M2, the single tryptophan mutants, W15F and W41F, and the rimantadine-resistant mutant, V27A, by Western-blot in the presence of DTT (100mM). Cell culture was performed as described in Methods. Molecular weight markers are shown to the left of each blot.

3.2.1.2: Purification of Wild Type and Mutant M2 Proteins

SDS-PAGE and Western-blot analysis were performed at various stages of the protein purification procedure, described in the Methods, in order to quantify the amount of protein recovered at each stage of the purification process and to assess its quaternary structure (Figure 3.12 A and B). Purification was performed in the presence of the detergent LDAO (N, N-Dimethyldodecylamine-N-oxide) in order to solubilise the hydrophobic segments of the protein. The purification process consisted of immobilized nickel ion affinity chromatography followed by gel filtration chromatography on a Superdex 200 column (Amersham Biosciences).

Immobilized metal ion chromatography utilizes the presence of a hexahistidine tag, engineered to either the C or N-terminus of a protein. The His tag binds specifically to the metal ions immobilized on beads; in this case a resin containing nickel ions was used, but other metals including cobalt can also be used for protein purification. Protein, attached to the column is washed, to remove any non-specifically bound proteins (refer to Methods) and then the protein of interest is eluted from the column using an imidazole gradient, with imidazole acting as a competitor for the metal ions.

Western-blot analysis revealed M2 present within the cell lysate (Figure 3.12 A). All M2 protein was bound to the nickel column, as the flow-through contained no M2. The three wash steps each clean the column of protein that might bind in a non-specific manner, in order to achieve the goal of pure M2. Wash 1 helps to clean the column of any undesired protein/debris from the cell lysate; wash 2 contains high salt to disrupt any ionic interactions with the nickel

A)

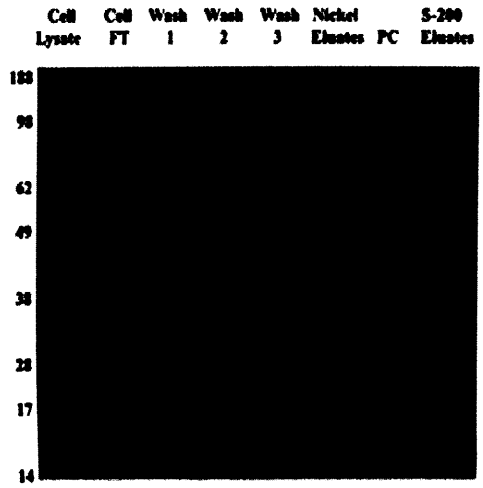

B)

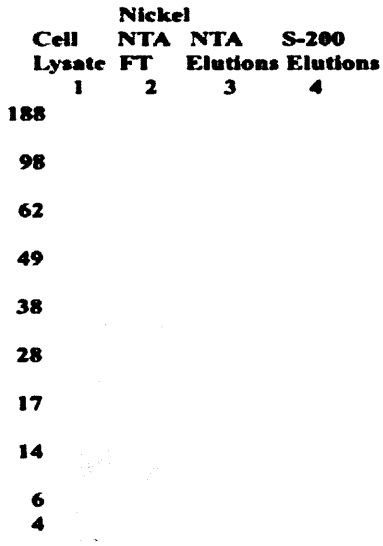

Figure 3.12: Analysis of the purification procedure of M2 by A) Western blot and B) gelcode blue stain of reducing of SDS-PAGE gels. The labels are as follows; Cell lysate= Clarified cell lysate, Wash1-3=Column washes (see text), NTA (Nickel Tag Activity) flowthrough= column flowthrough from nickel column, Nickel eluates or NTA elutions= M2 samples eluted by 20-300mM Imidazole and S200 elutions= M2 samples from superdex 200 column.

column. This leaves only the tightly bound protein linked to the column through the His-tag. Wash 3 lowers the detergent concentration just above its critical micellular concentration (CMC), a standard step in membrane protein purification, in order to make the protein suitable for biophysical studies or crystallization trials. Wash 1 and wash 2 both eluted small amounts of M2, and either non-specific or ionically bound proteins. Wash 3 also eluted a small amount of bound M2. When the imidazole concentration was increased through a gradient from 20mM to 300mM, bound M2 was removed from the nickel column suggesting that the His-tag successfully interacts with the nickel column allowing purification of the M2 protein.

Protein eluates were dialyzed overnight to remove all traces of imidazole before measuring absorption at 280nm. Protein preparations were then concentrated in a 40Kda cut-off centricon before gel filtration. No significant amounts of protein passed through the centricon suggesting that most M2 is in an oligomeric form of greater than a dimer. Size exclusion chromatography was then performed. The underlying principle is that particles of different sizes will filter through a stationary phase at different rates. This results in the separation of a solution of particles based on size. The protein in a 1ml volume was passed over a superdex 200 size exclusion column, from which fractions were taken and pooled. This acts as a further purification step to ensure that M2 tetramer is the predominant species in the S-200 fractions. Figure 3.12, shows a Coomassie stained SDS-PAGE gel shows the various protein purification stages and illustrates the different stages in the purification of M2 by immobilized Nickel ion affinity chromatography and size exclusion chromatography, and that when

reduced, M2 monomer is the predominant protein present in the final protein preparation.

The amount of purified protein obtained from the purification procedure was measured by OD_{280} using the tryptophan content of M2 (Figure 3.13). The absorption spectrum of the M2 preparation contains a peak at 280nm as expected for tryptophan absorption. The spectrum from 300 to 410nm is flat indicating no contaminating protein species are present in the M2 preparation. The concentration of the protein can then be calculated and knowledge of the extinction coefficients or the tryptophan, tyrosine and phenylalanine content of the protein.

The amount of M2 obtained from 10g of lysed bacteria was 2-3 mg, which is approximately 0.0003% of the total protein content of the cell. This was fairly constant for different protein preparations. To quantify total protein, a Biuret assay was performed upon the bacterial cell lysate (Figure 3.15). This experiment gave values of approximately 1.5mg of M2 protein for 5 grams of *E.Coli* protein Attempts to quantify the amount of M2 in relation to total protein in the *E.coli* cell lysate were done by Western-blotting the cell lysate against standard amounts of purified M2. This was unsuccessful due to radiation burn of the autoradiograph and the dependence of complete reduction of M2 to monomer on the amount of protein loaded. Variations in amount of what could be up to 1 mg. The yield of M2H37A was similar to that of M2 of approximately 1.5-2.25 mg, while both nM2 and V27A gave lower yields of approximately of 1mg. This protein yield is a reasonable amount for performing

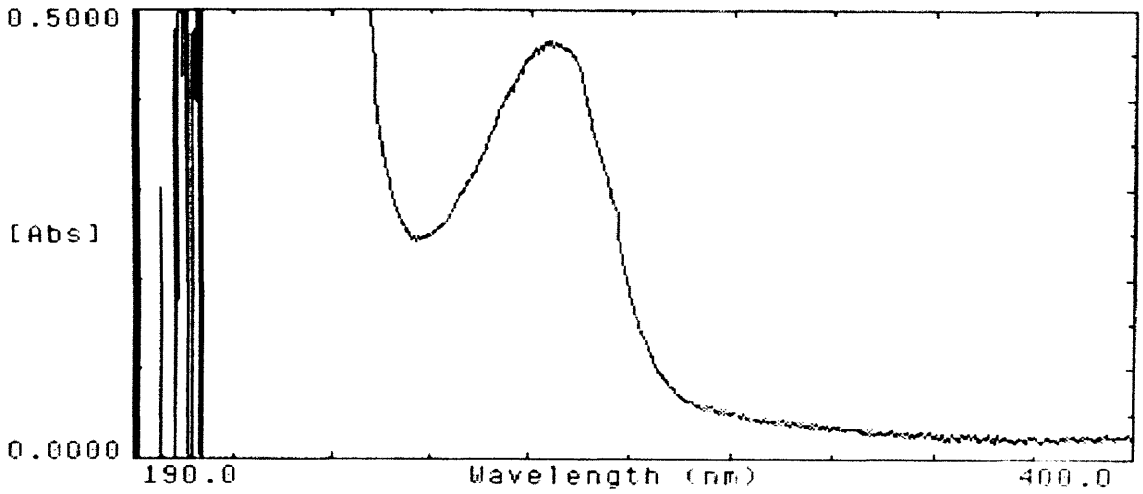

Figure 3.13: UV absorption spectrum of purified M2 in LDAO, to quantify the amount of purified protein. The observed peak is similar to that observed for pure tryptophan.

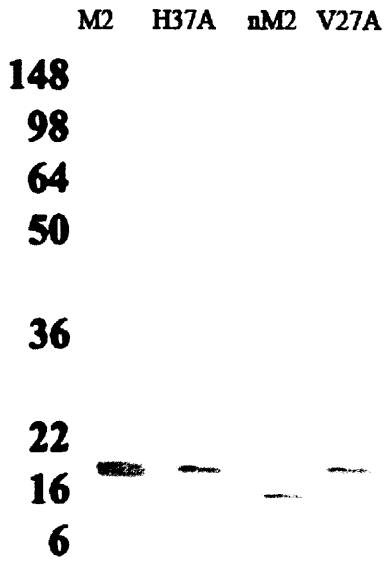

Figure 3.14: Purified M2, M2H37A, nM2 and V27A mutant proteins were resolved by SDS-PAGE gradient gels. Approximately 1-1.5 μg of protein was reduced by addition of DTT to 100mM and gels were stained with Coomassie brilliant blue.

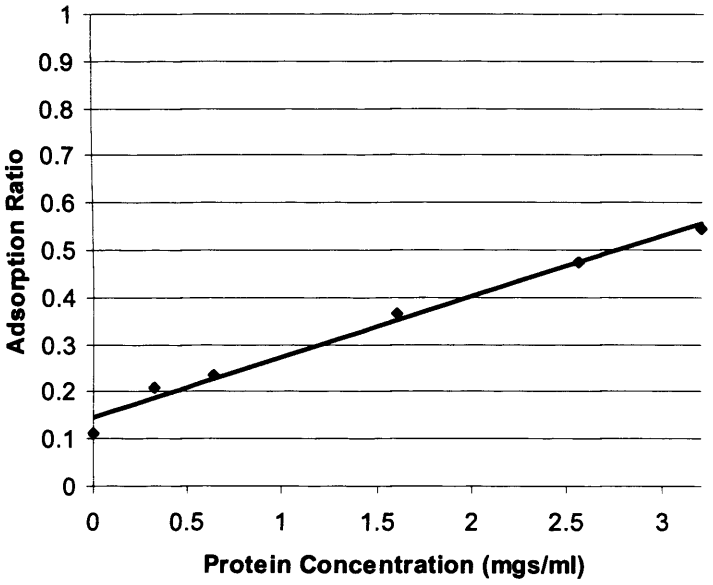

Figure 3.15: Biuret Assay standard curve to estimate total protein in bacterial cell lysate after M2 induction.

biophysical studies on a membrane protein. The presence of detergent and/or *E.coli* lipids still attached to the hydrophobic domains of M2 may affect both the appearance and ability of M2 to fully reduce to monomer on SDS-PAGE gels.

Two types of gel were used to study M2 migration by SDS-PAGE. Firstly homemade gels were used for normal Western-Blotting and Coomassie blue staining while for protein weight estimation and to check the tetrameric state, pre-cast gradient gels (Invitrogen) were used. Staining an SDS-PAGE gel with gelcode blue assessed the purity of recombinant M2 preparations. The purified wild type or mutant M2s routinely gave bands of monomer upon gelcode blue staining of reduced gradient SDS-PAGE gels (Invitrogen). Figure 3.14 shows sharp bands of monomer with no prominent contaminating species indicating pure preparations. Previous reports have suggested that M2 stains poorly with Coomassie due to the presence of the hydrophobic transmembrane domain (Lin *et al.*, 2001).

3.2.2: Characterization of Recombinant M2 Protein

To characterize these membrane proteins and their suitability for biophysical studies, a number of experiments were performed to verify the size and folding of the wild-type and mutant M2s. The oligomeric state was investigated by performing SDS-PAGE of both unreduced and reduced samples. Western blot analysis of non-reduced samples showed a number of multimeric species present, as seen in virus-infected cells (Sugrue and Hay 1991) while reduced samples gave predominantly monomeric species (Figure 3.16). Disulphide-linked tetramers were evident in the unreduced samples, illustrating that the M2 proteins purified from *E.Coli* resemble tetrameric channels. Furthermore, titrations of rimantadine inhibition gave a 1:1 stoichmetry of M2 tetramer with drug, indicating that over 99% of M2 protein was in a tetrameric form (Czabotar *et al.,* 2004; see later). On SDS-PAGE gels smearing was evident with M2 and H37A, possibly due to the continued presence of *E.coli* membrane lipids attached to the transmembrane domain of M2 or insufficient SDS content. Truncated nM2, which lacks cysteines, was not covalently linked and dissociated more readily into monomeric form; however tetramers were more evident in the unreduced sample.

CD spectroscopy was performed to analyze folding and structure content of the M2 protein and its mutants (Figure 3.17). Secondary structure assignment was elucidated using different mathematical algorithms using various sets of reference proteins with known crystallographic structure (refer to section 2.5). The measurements were analyzed after 25 scans each with 3 different methods for calculation of secondary structural content. The M2 proteins contained 50-

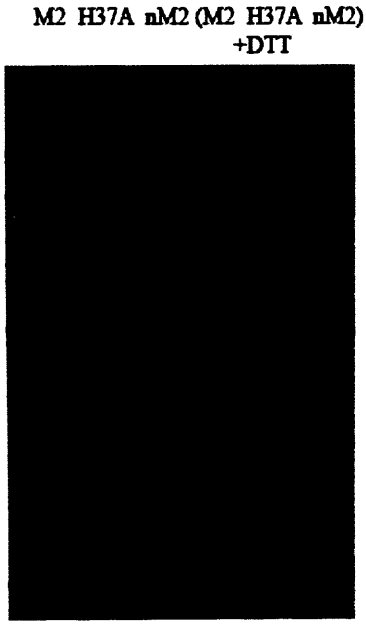

Figure 3.16: Purified M2 and mutants resolved by SDS-PAGE. Approximately 0.15μg of non-reduced and reduced (100mM DTT) protein was analyzed and detected by Western-blot using anti-M2 polyclonal sera. Molecular weight markers are defined on the left of the gel.

55% α-helical content. Previous measurements of refolded M2 from bacteria had given values of approximately 60% (Tian *et al.*, 2002).

The loss of the N-terminus did not cause any significant change in the CD spectrum; a slight increase in α-helical content could be accounted for by removal of the N-terminal 19 amino acids, suggesting the N-terminus is unstructured.

The M2H37A mutant also showed no significant differences in structure and any small deviations in the spectrum from that of wild-type M2 were well within the 5% error range for structure content determination by CD spectroscopy. The M2V27A mutant also gave a spectrum close to that of wild-type M2 and a α-helical content of 50-55%, equivalent to that of the wild-type protein (data not shown). These studies did not reveal any gross differences in structure of the wild-type and mutant proteins and provide a basis for more detailed comparison of local structural changes by fluorescence.

3.2.3: Tryptophan Fluorescence of M2 protein

The characteristic emission spectra resulting from tryptophan fluorescence can provide information relating to the environment surrounding individual tryptophan residues as well as structural information about the protein. Two major types of information can be elucidated by this technique. Firstly, the interaction of tryptophan with other residues can be studied by changes in fluorescence intensity. Secondly, the polarity of the environment surrounding the tryptophan is indicated by the emission maxima (λ_{max}); for example a tryptophan in a

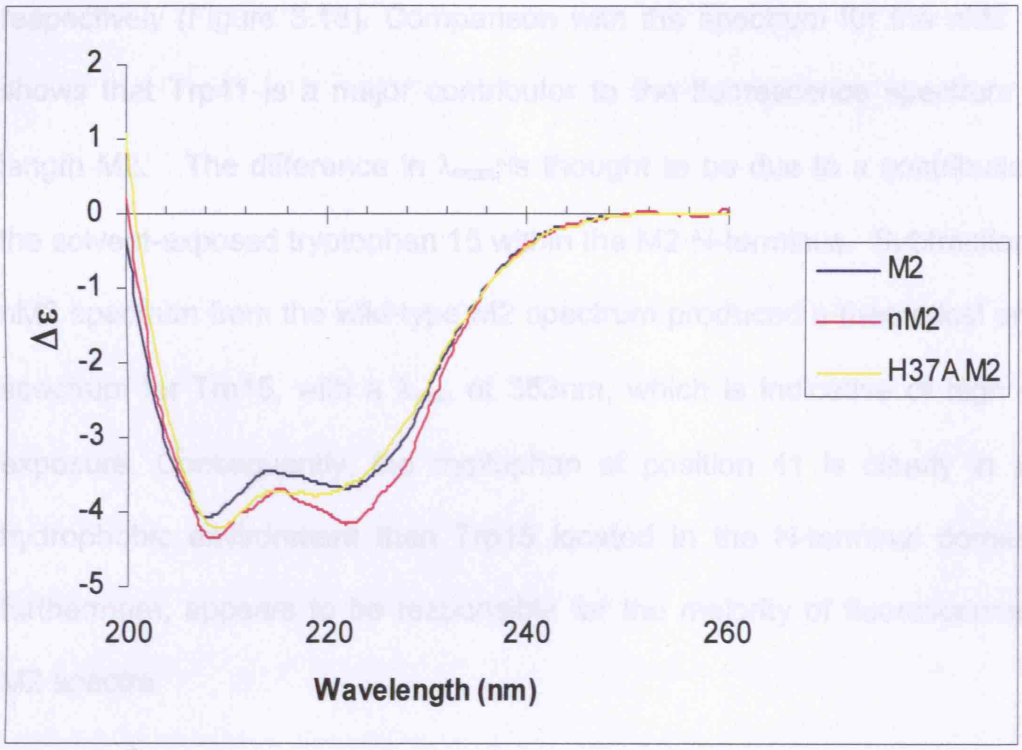

Figure 3.17: CD spectra of M2, nM2 and M2H37A proteins. The x-axis measures the wavelength at which the reading was taken. The y-axis describes the molar circular dichroism ($\Delta\varepsilon$)

hydrophobic environment gives a peak at about 330nm while one exposed to water has a peak at about 350nm. M2 and nM2 in FPLC buffer (refer to section 2.4) at pH 8 gave spectra with λ_{max} of approximately 338nm and 333nm respectively (Figure 3.18). Comparison with the spectrum for the nM2 mutant shows that Trp41 is a major contributor to the fluorescence spectrum of full-length M2. The difference in λ_{max} is thought to be due to a contribution from the solvent-exposed tryptophan 15 within the M2 N-terminus. Subtraction of the nM2 spectrum from the wild-type M2 spectrum produced a theoretical emission spectrum for Trp15, with a λ_{max} of 353nm, which is indicative of high solvent exposure. Consequently, the tryptophan at position 41 is clearly in a more hydrophobic environment than Trp15 located in the N-terminal domain, and furthermore, appears to be responsible for the majority of fluorescence in the M2 spectra.

The M2H37A mutant exhibited a slight blue shift in emission maximum to 339nm, indicating that the presence of histidine 37 in the channel pore contributes to a more hydrophobic environment for one or both tryptophans of the M2. The spectrum of V27A, shown in Figure 3.19, is similar to that of wild type M2, with a λ_{max} of 337nm.

To characterize structural changes related to functional activity, pH titrations of M2, nM2 and M2H37A fluorescence intensity were performed (Figure 3.20). The fluorescence intensity of full-length M2 increased by nearly 20% as pH was reduced from 8 to 6, similar to previously reported data (Czabotar *et al.,* 2004). Below a peak at pH 6.2, tryptophan fluorescence was quenched progressively as pH was reduced, with 75% of maximum fluorescence quenched between pH

3 and 4 f (Figures 3.21). Below pH 4, the addition of rimantadine did not fully reverse the fluorescence quenching (see later), and hence pH may have affected protein structure. Therefore, measurements below pH 4 could not be related to channel functionality and were not studied further. An approximate reduction in tryptophan fluorescence of 1/3 was observed down to pH 5 from pH 6.2 (Figure 3.20).

The N-truncated M2 mutant nM2 exhibited a gradual increase in fluorescence intensity of approximately 10% as pH was reduced from pH 8 to 7. Below pH 7 tryptophan fluorescence was quenched to 80% at pH 5 (of the level at pH 8), comparable to the result obtained with full-length M2. This result suggests that fluorescence quenching emanates from Trp41. A pKa of 6.13 was calculated for the quenching of tryptophan 41 fluorescence when data was fitted to a ligand protonation profile using the program Specpro (refer to section 2.4).

Conversely, M2H37A (Figure 3.20) exhibited a consistent increase in tryptophan fluorescence of almost 20% as pH was reduced from 8 to 5. No decrease in fluorescence intensity was observed below pH 6, illustrating that the quenching observed in previously reported data for nM2, and demonstrated that change in pH did not influence tryptophan fluorescence between pH 8 to 6. The increase seen here is less than that for M2 and also shifted to higher pH. Therefore it is difficult to understand where the fluorescence increase in nM2 originates from.

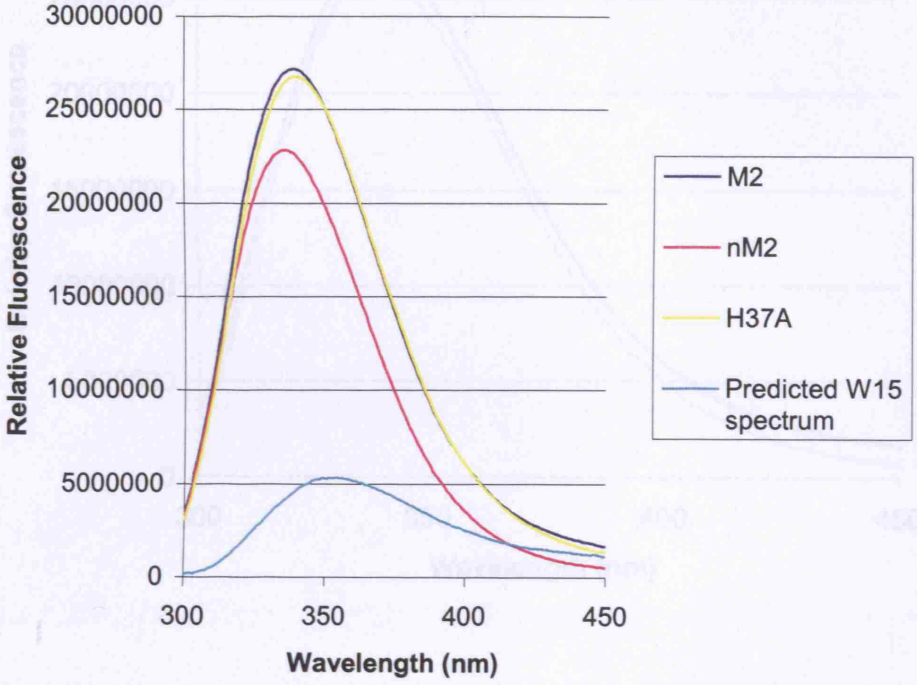

Figure 3.18: Fluorescence emission spectra of 0.33μM M2, nM2 or M2H37A in FPLC buffer (Refer to section 2.4) at pH 8 and the predicted spectrum for tryptophan 15 in M2. All protein concentrations were determined by OD_{280} and scatter analysis performed using Specpro (refer section 2.5).

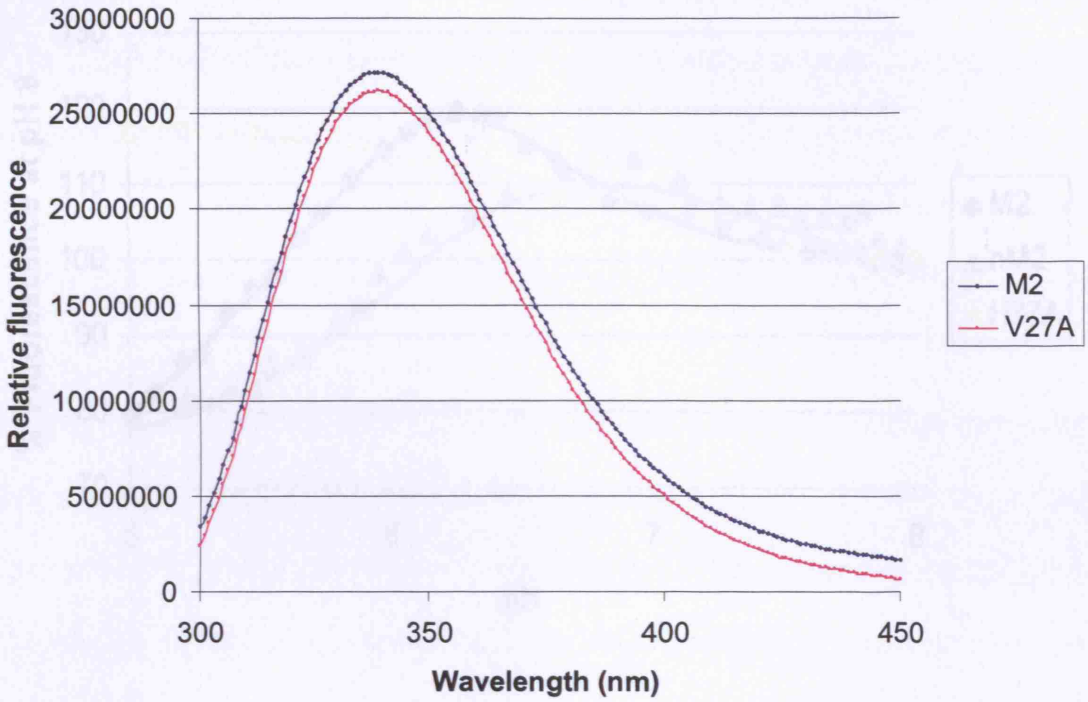

Figure 3.19: Fluorescence spectra of 0.33μM M2 and V27A mutant protein tetramer in FPLC buffer at pH 8.

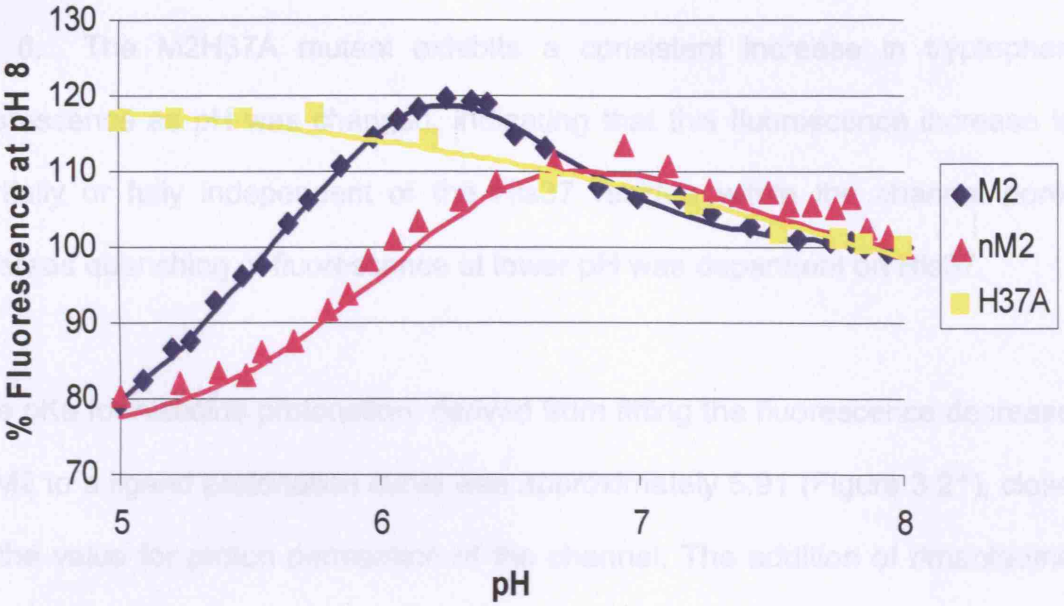

Figure 3.20: pH titrations of tryptophan fluorescence from 0.33μM protein of M2, nM2 and M2H37A. Fluorescence intensities were normalized against each protein's intensity at pH 8 to produce relative fluorescence values. All data points for the 3 proteins were then fitted using a ligand protonation profile described in section 2.4 of the methods.

The increase in fluorescence of M2 was originally attributed to Trp15 and that it was the single most important residue involved in the fluorescence increase observed between pH 8 and 6 in M2. Interestingly, the small increase in nM2 is shifted to pH 7 compared with that seen in M2, which occurs at approximately pH 6. The M2H37A mutant exhibits a consistent increase in tryptophan fluorescence as pH was changed, indicating that this fluorescence increase is partially or fully independent of the His37 residue within the channel pore, whereas quenching of fluorescence at lower pH was dependent on His37.

The pKa for histidine protonation, derived from fitting the fluorescence decrease in M2 to a ligand protonation curve was approximately 5.91 (Figure 3.21), close to the value for proton permeation of the channel. The addition of rimantadine fully reversed fluorescence quenching in both M2 and nM2 to above pH 8 levels and exerted no effect upon M2H37A, as previously described (Czabotar *et al.*, 2004).

No reversal of fluorescence quenching was seen with the amantadine-resistant mutant M2V27A showing that the effect was specifically related to M2 channel function. When pH was lowered to 5 fluorescence was quenched by 20% in the case of M2 and 15% in the case of V27A (Figure 3.22). Addition of rimantadine caused only a small increase in intensity of 2-3% in the case of V27A fluorescence while M2 fluorescence quenching was fully reversed by 35% to approximately the maximum fluorescence at pH 6.2. Therefore, rimantadine as expected exerted a minimal effect on V27A. To see the effect of rimantadine and M2 inhibitors on M2 tryptophan fluorescence post addition, pH titrations were performed with and without the presence of 50μM rimantadine.

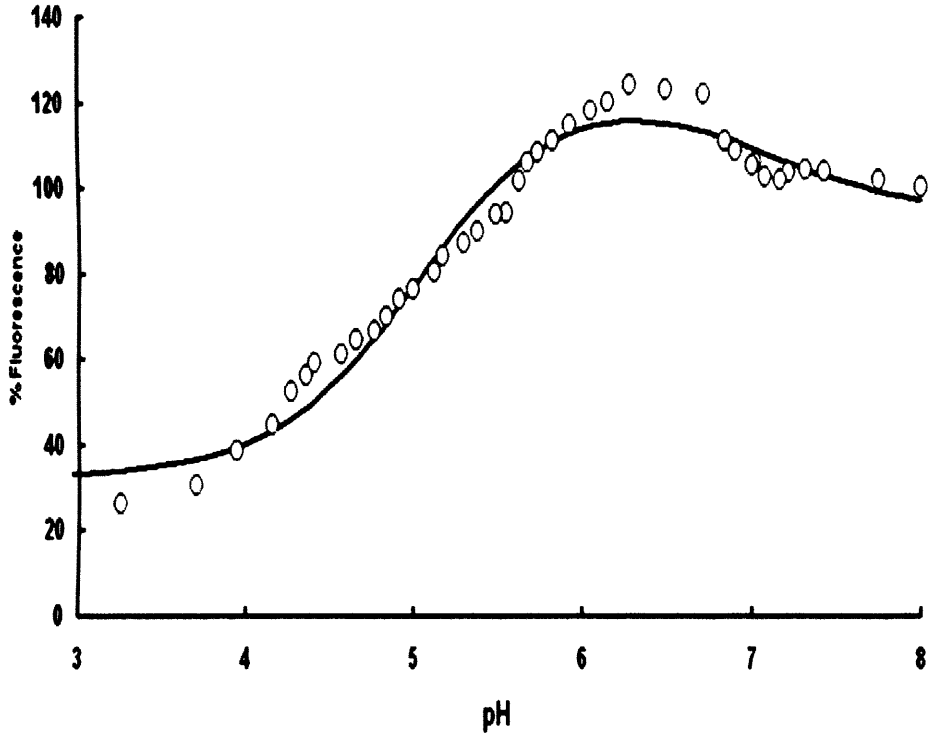

Figure 3.21: pH titration of tryptophan fluorescence of 0.33μM M2 from pH 8 to 3. Fluorescence intensities were normalized against each protein's intensity at pH 8 to produce relative fluorescence values. Data points were then fitted to a curve using a ligand protonation profile described in section 2.4 of the methods.

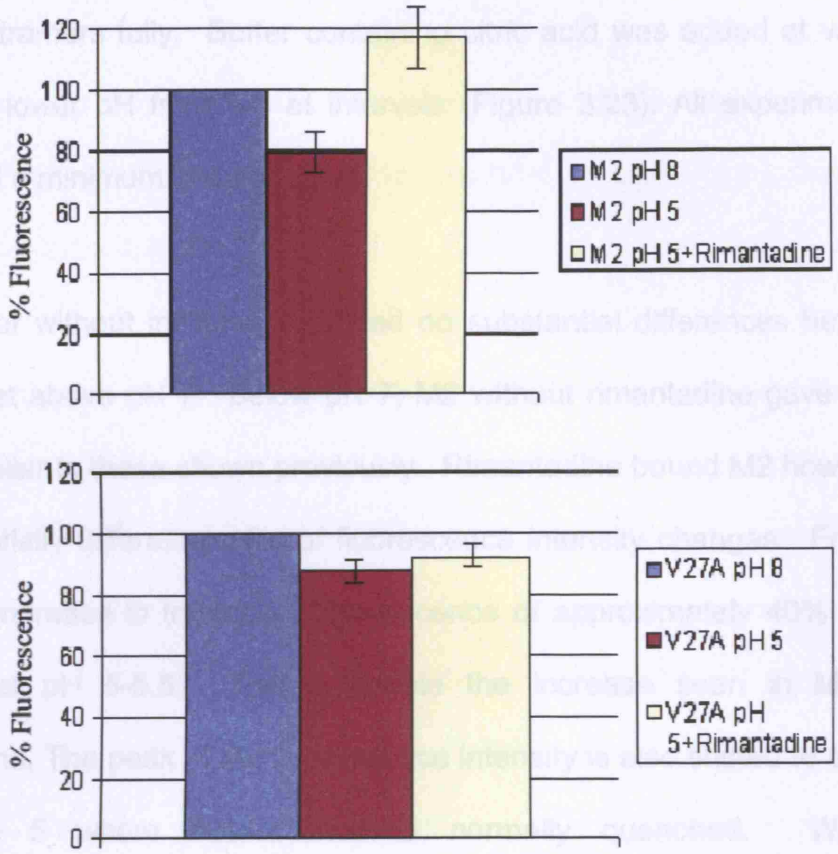

Figure 3.22: Bar charts showing fluorescent changes induced by pH 8-5 and the effect of rimantadine on M2 and the rimantadine-resistant mutant V27A. The peak seen after rimantadine addition equates to the level as seen at pH 6.2.

M2 was added to buffer at a concentration of 0.33μM at pH 8 and mixed with rimantadine and allowed to equilibrate for 5 minutes while the inhibitor bound the M2 tetramers fully. Buffer containing citric acid was added at various pH values to lower pH from 8-4 at intervals (Figure 3.23). All experiments were performed a minimum of three times.

M2, with or without inhibitor, exhibited no substantial differences between the titrations at above pH 7. Below pH 7, M2 without rimantadine gave a titration profile similar to those shown previously. Rimantadine bound M2 however gave a substantially different profile of fluorescence intensity changes. From below pH 7 an increase in tryptophan fluorescence of approximately 40% was seen peaking at pH 5-5.5. This is double the increase seen in M2 without rimantadine. The peak of the fluorescence intensity is also shifted to a lower pH closer to 5 where fluorescence is normally quenched. With these measurements it should be noted that there may be a contribution to the spectrum from Trp15 in the N-terminus; however, from previous experiments this contribution is minimal. Below approximately pH 4.9 the fluorescence intensity was reduced. For nM2 (the N-truncated form of M2) the unbound form again gave results similar to those described before. However, with 50μM rimantadine bound the different titration profile was shown. An increase of 15% in relative fluorescence from pH 8 to 5 and a similar decrease in fluorescence intensity was seen below approximately pH 4.9, comparable to that for drug-bound M2. As previously, it is apparent therefore that the reduction in fluorescence of rimantadine bound M2 is independent of Trp15. Because of the inability to characterize the fluorescent increase seen from pH 8-6 it is difficult to interpret the effect of rimantadine upon M2 and nM2 protein at this pH. It is

possible the Trp15 environment is changing and therefore reporting a global effect as rimantadine inhibits M2 hence the larger change not seen in nM2.

H37A gave a continual increase in fluorescence intensity as pH was lowered. This occurred in both unbound and rimantadine bound M2 but the increase was more pronounced in the latter by of 25%. The fluorescence intensity reached a plateau at pH 5. Thus unlike both M2 and nM2 no decrease in fluorescence intensity was seen below pH 5 suggesting that, in the case of both M2 and nM2, this decrease is dependent on His37 and may be due to protonation of His37 quenching Trp41 fluorescence. It would seem therefore that rimantadine binding may alter the pH at which tryptophan fluorescence quenching occurs by altering the pKa of the histidine. It may well achieve this by directly affecting His37 protonation by altering proton sensitivity/affinity as a result of an allosteric change induced upon rimantadine binding.

As pH was lowered, fluorescence increased, for both M2 and nM2 (Figure 3.24). The λ_{max} shifted 4nm in M2 from 337nm at pH 8 to 341nm at pH 5. nM2, lacking Trp15 in the N-terminus, gave a larger λ_{max} shift of 6nm from 334nm to 340nm. The majority of the λ_{max} shift in emission was seen below 6.5 for both proteins, while no λ_{max} shift was seen from pH 8 to 7 when the channel is supposedly closed. The λ_{max} at pH 5 for both M2 and nM2 was similar. The channel environment therefore seems to change in response to activation by lower pH.

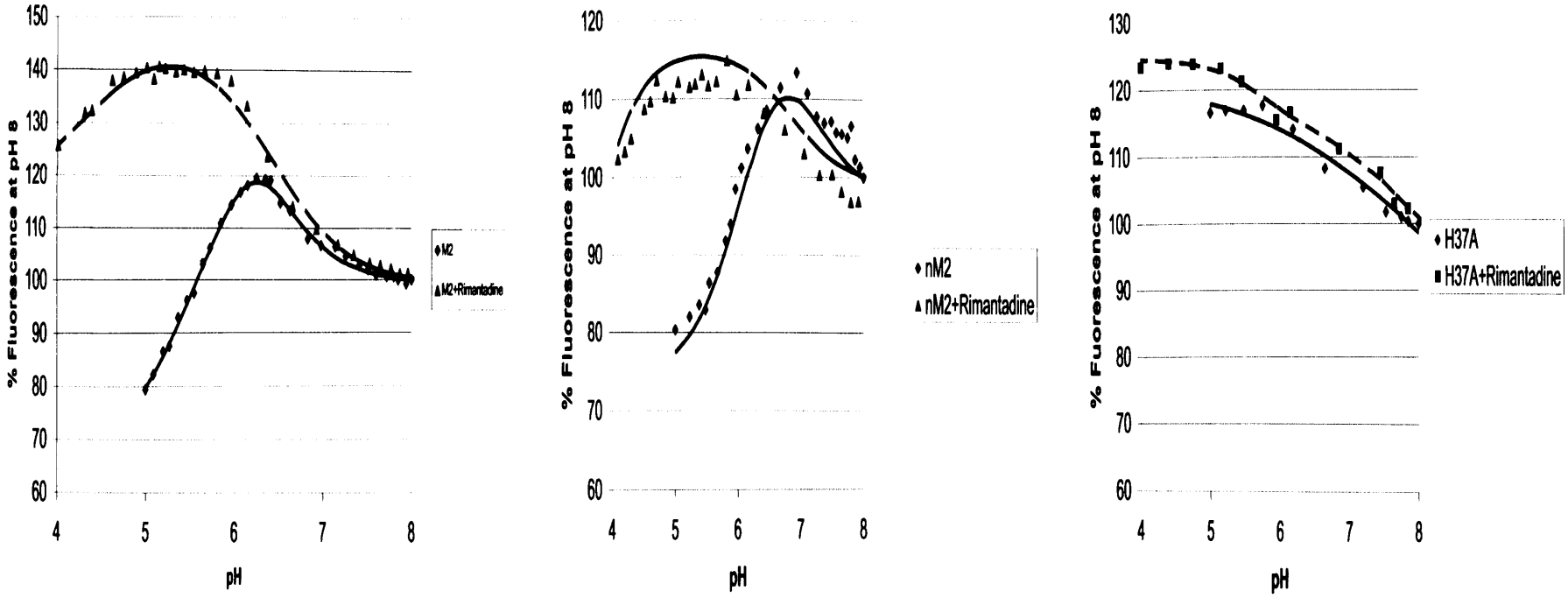

Figure 3.23: pH titration with and without 50μM rimantadine of 0.33μM protein of M2, nM2 and H37A between pH 8 and 4. Large increases in fluorescence were seen in the case of M2, nM2 and H37A in the presence of rimantadine. Fluorescence intensities were normalized against intensity at pH 8 to produce a relative fluorescence values. Data points were then fitted to curves using a ligand protonation profile described in section 2.4 of the methods.

No shift in λ_{max} was observed in M2H37A (data not shown). The channel environment, surrounding the tryptophan 41 residue is therefore changing in response to changes in the state of the His37 residues, possibly in relation to the changing channel open probability. When the λ_{max} values were fitted to a ligand protonation curve, pKa values of 5.88 for M2 and 5.75 for nM2, were calculated (Figure 3.24). Both of these values are close to the pKa value for proton permeation through M2. The close correspondence of the pKa values for fluorescence quenching to those for the λ_{max} shifts suggest that they both derive from effects created by protonation of His37.

However, the λ_{max} derives directly from Trp41; therefore it is acting as a reporter for histidine protonation. Furthermore, Trp15 probably masks some of the λ_{max} shift, although this is not shown conclusively. Increases in λ_{max} are indicative of an increasing solvent exposure of tryptophan. The reason for the peak shifts is probably due to an electronic interaction between histidine and tryptophan.

Rimantadine addition fully reversed the peak shift of M2 and nM2 pH titrations from 341nm to below 337nm (data not shown) in the case of M2 and from 340nm to 334nm for nM2 therefore suggesting a full reversal of the His37-Trp41 interaction by rimantadine (data not shown). As a shift in λ_{max} is usually indicative of an environmental change emanating from a structural rearrangement within the protein these pH-induced internal structural alterations of the M2 pore were further studied using acrylamide quenching. This technique measures accessibility of the indole ring of tryptophan to fluorescence quenchers such as acrylamide in the external solvent.

If the tryptophan is exposed it will have a high Stern-Volmer (Ksv) constant, which is a measure of the photophysical intramolecular deactivation process defined by the Stern-Volmer equation (refer to sections 1.8 and 2.4). If the tryptophan is buried then this value will be low. Measurements were done from pH 8 to 5, which equate with changing open probability of the M2 channel (Figure 3.25). Ksv values for M2 and nM2 at pH 8 were 2.47±0.13 and 1.51±0.01, respectively. These values reflect the highly inaccessible nature of both Trp15 and 41 at high pH. When pH was lowered to 5, Stern-Volmer constants increased to Ksv=4.06± 0.25 in the case of M2 and Ksv=2.44± 0.23 for nM2. The increases in Stern-Volmer constant for both M2 and nM2 indicate that at low pH, the accessibility to the external solution containing acrylamide has increased. M2H37A on the other hand gave a Ksv value of 2.99±0.13 at pH 8, which did not change significantly when pH was lowered to 5 suggesting that the changes seen in both M2 and nM2 are related to changes associated with the histidine side-chain. The Ksv values for M2H37A are between the Ksv values for M2 at low and high pH indicating that in the absence of His37 the tryptophans, in particular, Trp41 in M2H37A are in a more open conformation within the channel pore at high pH. The addition of rimantadine reduced exposure of the M2 Trps with a Ksv=2.74±0.04. Consequently, in M2 lowering pH seems to lead to a change in the environment of the tryptophans in the M2 protein, which is mediated by histidine. However these changes are small and may also be indicative of a His37/Trp41 interaction rather than a change in the bulk solvent exposure of Trp41. Rimantadine addition to the M2 protein and its mutants at pH 5 in all proteins reduced the accessibility of tryptophans (Table 3.1). In the case of M2, Ksv= 3.25± 0.12, nM2 Ksv=1.91± 0.09 and in M2H37A

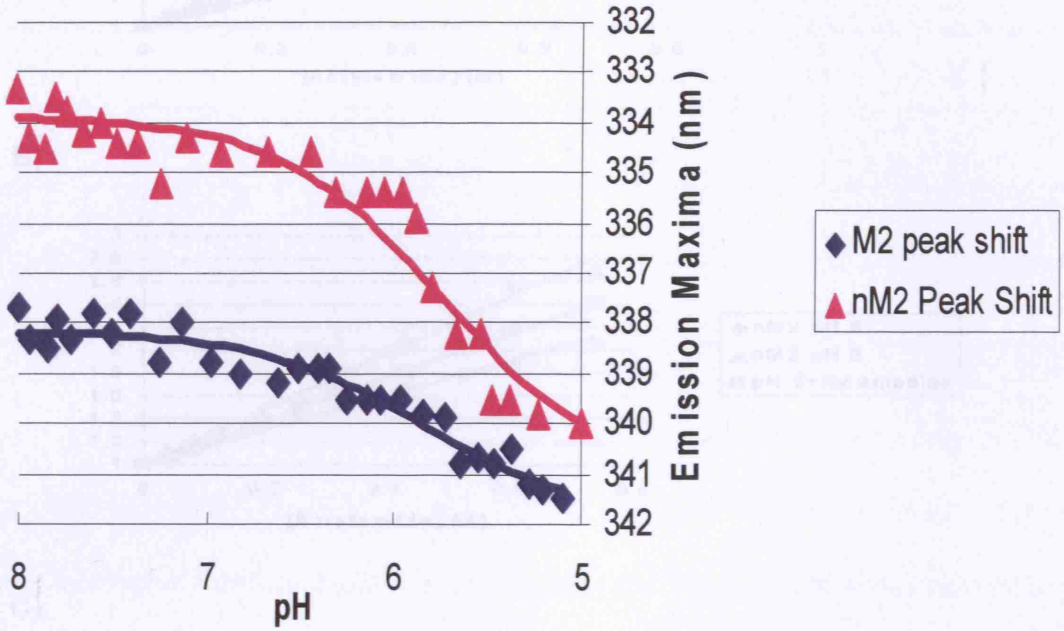

Figure 3.24: Shifts in λ_{max} of tryptophan fluorescence of 0.33μM M2 and nM2 proteins with pH. pH was titrated from 8 to 5 and the λ_{max} was calculated from the first derivative (refer to section 2.4). Data points were then fitted to curves using a ligand protonation profile described in section 2.4 of the methods.

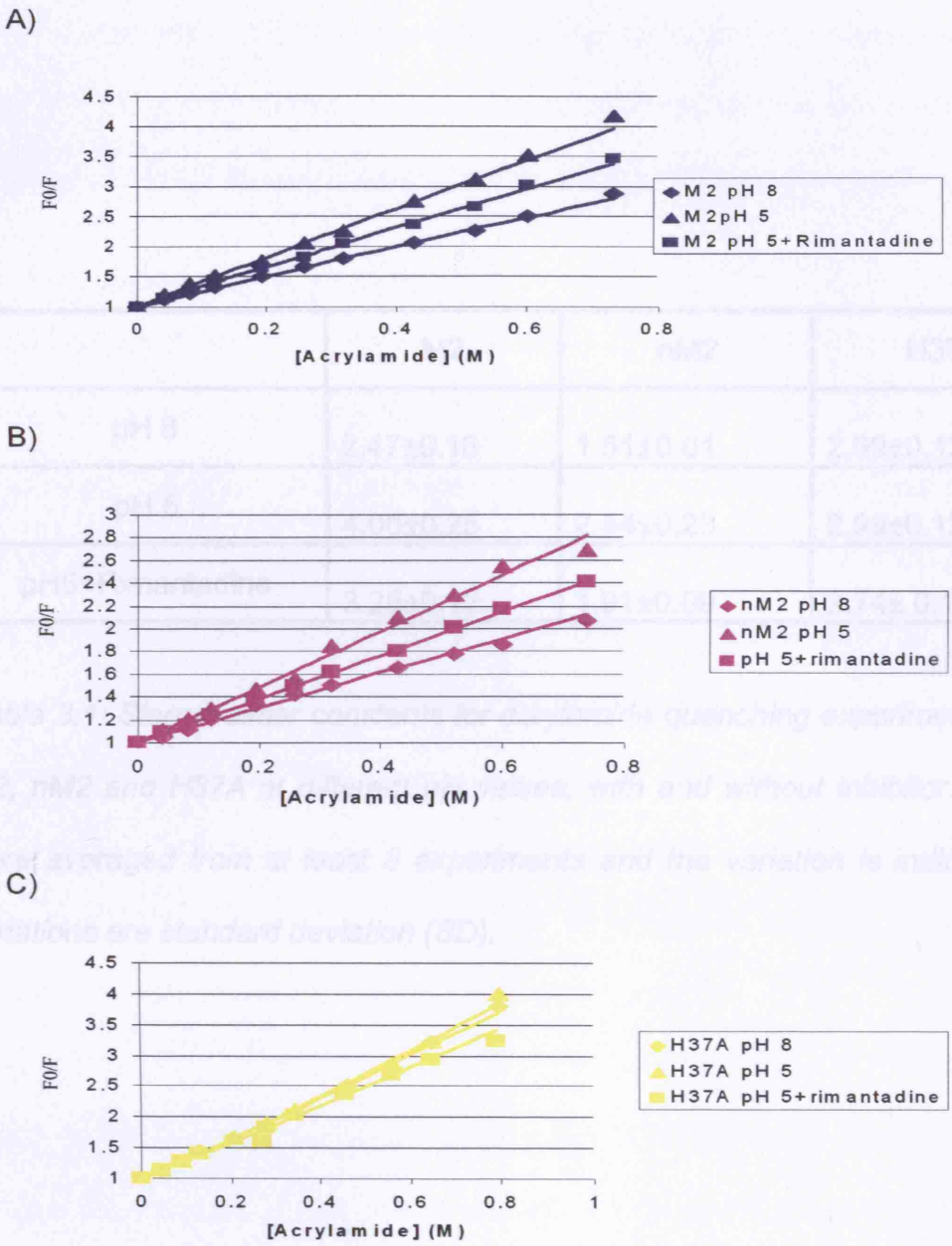

Figure 3.25: Effects of pH and rimantadine on acrylamide quenching of M2, nM2 and M2H37A. 1ml volumes of 2M acrylamide+protein at the original protein concentration were added in order to prevent dilution and fluorescence intensity measured.

	M2	nM2	H37A
pH 8	2.47±0.13	1.51±0.01	2.99±0.13
pH 5	4.06±0.25	2.44±0.23	2.99±0.13
pH5+Rimantadine	3.25±0.12	1.91±0.09	2.74± 0.13

Table 3.1: Stern-Volmer constants for acrylamide quenching experiments using M2, nM2 and H37A at different pH values, with and without inhibitor. Values were averaged from at least 3 experiments and the variation is indicated. All variations are standard deviation (SD).

the Stern-Volmer constant was 2.74± 0.13. The addition of rimantadine reduced accessibility of Trp41 in nM2 to acrylamide by 56% relative to that at pH 5, and 50% in the case of M2. Interestingly, the reduction in accessibility within M2H37A suggests that this effect of rimantadine may be due to it binding within the pore of the M2 channel rather than mediating inhibition via His37.

3.2.3.1: Red-Edge Excitation Shift

Red-Edge Excitation Shift (REES) was used to gauge the conditions of water molecules within the pore. REES is a technique in which, when excitation wavelength is shifted towards longer wavelengths, emission maxima change in the same direction. This phenomenon is seen only with polar fluorophores in motionally restricted environments, where the dipolar relaxation time for the solvent shell around the fluorophore is comparable to, or longer than, the fluorescence lifetime. REES arises from slow solvent reorientation around an excited state fluorophore. The parameter measured is therefore the fluorophore solvent/environment itself therefore, this technique is suitable to study the behavior of water molecules in the M2 channel pore.

REES measurements (between 280nm and 300nm) were made using the various M2 proteins at both pH 8 and pH 5 with and without drug bound, to observe changes in solvent conditions within the M2 pore (Figure 3.26 and Table 3.2). For M2 upon lowering pH from 8 to 5 the REES changed from 3.45nm to 1.45nm indicating a more dynamic environment for the tryptophans within M2 at low pH. Water molecules were able to move quickly re-orientating at low pH when the channel is open, possibly in response to water wire formation. When the same experiments were done with nM2 a REES shift reduction of 3.6nm to 2.3nm was seen showing that the solvent shell around

Trp41 is less viscous at low pH. Trp41, is located in the channel pore and therefore reflects the environmental changes, which occur there.

M2H37A gives a REES of approximately 2.1nm, which did not vary with pH. This value is close to that found at low pH in M2 indicating water molecules are free to re-orientate in the M2H37A pore as in the open channel at low pH. Therefore the presence of His37 seems to mediate the viscosity of the water environment of the M2 pore possibly through hydrogen bonding water molecules at high pH, preventing reorientation, and at low pH forming an interaction with Trp41 making the solvent environment within the M2 channel more freely moveable.

The addition of rimantadine at pH 5 produced an increase in REES to 6.85nm in nM2 and 2.47nm in M2 and M2H37A. The restoration of the REES is probably due to rimantadine reversing/preventing histidine protonation. Therefore rimantadine addition restored the immobility of water molecules found characteristically at high pH, whether it does this by returning the channel to the closed channel state or moving it to a different "M2/drug" complex state remains undefined.

REES Shift (nm)	M2	nM2	H37A
pH 8	3.45±0.07	3.60±0.02	2.10±0.12
pH 5	1.45±0.11	2.30±0.03	2.10±0.05
pH5+Rimantadine	2.47±0.09	6.85±0.23	2.47±0.08

Table 3.2: REES measurements of M2, nM2 and H37A at different pH values, with and without inhibitor. Values were averaged from at least 3 experiments and the variation is indicated.

A)

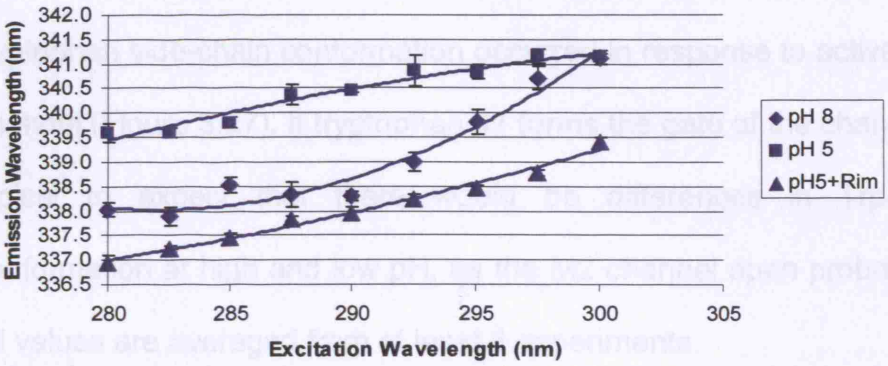

B)

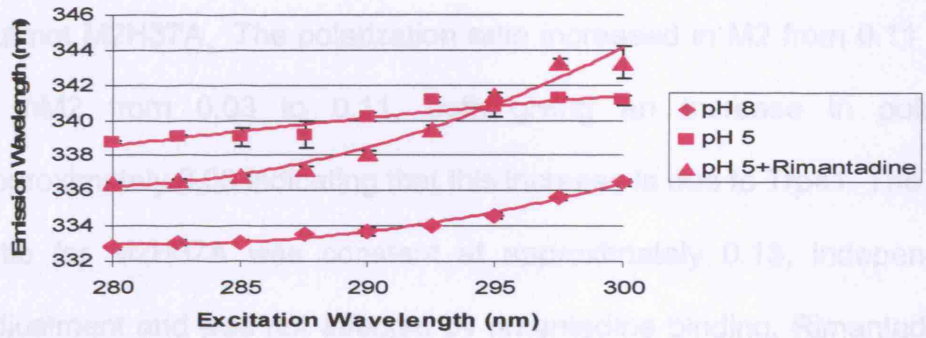

C)

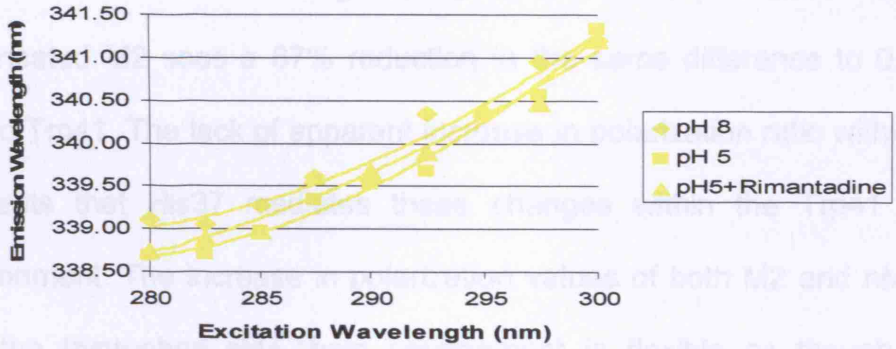

Figure 3.26: REES measurements of M2 (A), nM2 (B) and M2H37A (C) measuring the reorientation of water molecules within the M2 pore.

3.2.3.2: Fluorescence Polarization

Polarization measurements were used to establish whether any change in tryptophan side-chain conformation occurred in response to activation of the M2 channel (Figure 3.27). If tryptophan 41 forms the gate of the channel it would be logical to expect that there would be differences in Trp41 side-chain conformation at high and low pH, as the M2 channel open probability changes. All values are averaged from at least 3 experiments.

Upon lowering pH from 8 to 5 the polarization ratio increased for M2 and nM2 but not M2H37A. The polarization ratio increased in M2 from 0.11 to 0.18 and in nM2 from 0.03 to 0.11, both giving an increase in polarization of approximately 0.08 indicating that this increase is due to Trp41. The polarization ratio for M2H37A was constant at approximately 0.13, independent of pH adjustment and was not affected by rimantadine binding. Rimantadine addition to M2 and nM2 caused a decrease in polarization. In the case of M2 a 62% reduction is seen of the change from pH 8 to 5 with a polarization ratio of 0.13. N-truncated M2 sees a 67% reduction in the same difference to 0.055 again due to Trp41. The lack of apparent increase in polarization ratio within M2H37A suggests that His37 mediates these changes within the Trp41 side-chain environment. The increase in polarization values of both M2 and nM2 suggest that the tryptophan side-chain environment is flexible as though it was in solution. Protonation of His37 caused the polarization value to increase giving the tryptophan 41 a more rigid environment which is probably concomitant with proton conduction through M2. M2H37A polarization indicates a state for the tryptophans which is similar to that found in the open M2 channel at low pH - a rigid conformation allowing proton conduction. His37 therefore appears to have

an effect on the environment and conformation of Trp41 at both high and low pH. These results suggest segmental motion occurs in the tryptophan side-chains upon activation of M2 through His37 protonation. The tryptophan side-chain environment changes from being freely flexible to a defined rigid conformation, possibly due to molecular interaction with His37. These results could also be indicative of a change in fluorescent lifetime within the tryptophans of M2. Another noticeable feature is that the polarization values for nM2 are low in comparison to M2. A reason for this is the possibility of homo-fret between the Trps located at position 41 in the M2 pore due to their close proximity.

To test this hypothesis, polarization values were measured at pH 8, pH 5 and pH 5+rimantadine while moving excitation λ_{max} to the red-edge (Figure 3.27). Homo-fret leads to depolarization of tryptophans. As the excitation λ_{max} is moved to the red-edge, a reduction in the homo-fret effect should be seen by an increase in polarization values. Not only did polarization values increase as excitation was shifted to the red-edge, this shift varied with the conditions of the channel. At pH 8 a shift in polarization of 0.15 was observed while at pH 5 and with drug a reduction in polarization shifts of 0.12 and 0.08, respectively were seen. This change in the effect of homo-fret due to pH and drug binding suggests once again that the environment of the Trp at position 41 is changing. More notably, the homo-fret contribution changes with distance, therefore, these measurements suggest tryptophan movement which, when combined with other polarization measurements indicate a different environment for the tryptophans of M2.

All of the above measurements are indicative of effects of pH and drug binding which lead to unique conformations and either/or unique conformational environments with the M2 channel. It is logical to deduce that these changes are linked with the function of the M2 channel. Therefore, these differences possibly correspond to three distinct forms of M2 with unique channel architecture, a closed form, and open proton conducting form and an inhibited drug-bound form. These forms are predominantly linked with the state of the two crucial residues within the M2 channel, His37 and Trp41 that undoubtedly have roles in both the closed and open form of the channel. Further time-resolved measurements may be better able to characterise these defined states and any intermediates that may exist.

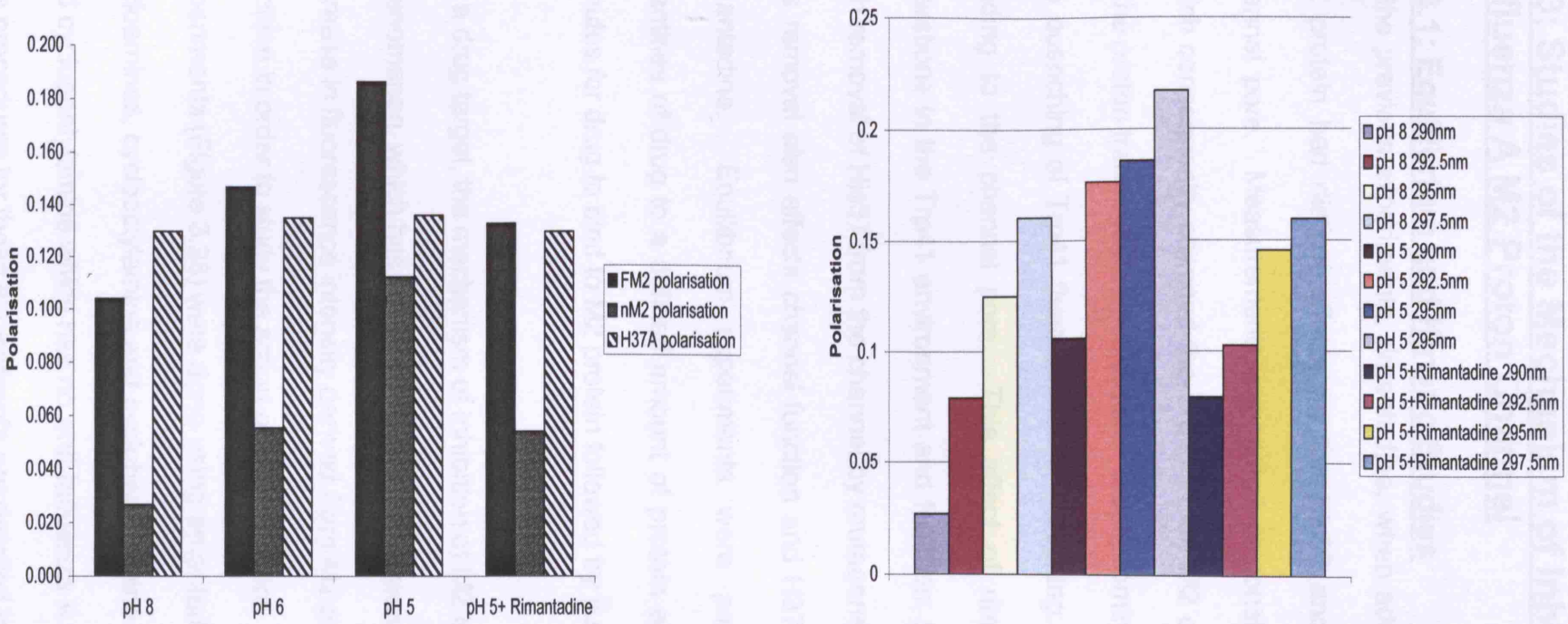

Figure 3.27: Polarization measurements, taken at defined pH values for M2, nM2 and H37A (left diagram) indicating segmental motion in Trp41 and at different excitation wavelengths right diagram) measuring the effect of homo-fret on depolarization of Trp41 in M2

3.3: Studies of the Mechanism of Inhibition of the Influenza A M2 Proton Channel

3.3.1: Equilibrium and Kinetic Studies

In the previous experiments, rimantadine, when added to purified recombinant M2 protein had distinct effects on the His37 and Trp41 side-chains in the channel pore. Measurements suggested protonation of His37 was affected which consequently changed the Trp41 in the M2 channel leading to inhibition of the proton translocation mechanism. Most prominently, rimantadine reversed the quenching of Trp41 fluorescence by inhibiting protonation of His37 when binding to the channel pore. This effect of rimantadine on His37 led to alterations in the Trp41 environment and function. However, this was negated with removal of His37 from the channel by mutagenesis. It should be noted that this removal also affects channel function and H37A is reversibly inhibited by rimantadine. Equilibrium experiments were performed by adding small quantities of drug to a defined amount of protein at pH 5 and then allowing 5 minutes for drug to bind to M2 protein followed by fluorescence measurements.

As a drug target, the mechanism of inhibition of M2 is an important biological phenomenon, which has yet to be elucidated. It was decided to use the increase in fluorescence intensity derived from M2 protein upon inhibitor addition in order to study the action of M2 inhibitors. Equilibrium binding experiments (Figure 3.28) were done using amantadine, rimantadine and the cycloamines, cyclooctylamine and cycloheptylamine with known antiviral activity and cyclopentylamine which has no anti-Influenza A activity (Hay *et al.,* 1985). The procedures for these experiments are detailed in section 2.4 but for context they are also briefly described here.

Small additions of the M2 inhibitors were made to 0.33μM M2 tetramer at pH 5 until saturation, whereby all M2 tetramers had been converted to an inhibitor bound form. Approximately 5 minutes was left between each measurement to allow time for the cuvette to reach equilibrium. The equation which defines the reversal of pH 5-induced quenching of M2 Trp fluorescence is:

(3.1) Obs Flu = F(M).[M] + F(MD).[MD]

The observed fluorescence change (Obs Flu) is the sum of the M2 tetramer concentration times its fluorescence at pH 5 (F(M).[M]) and with the amantadine bound M2 tetramer concentration times its "inhibited" fluorescence (F(MD).[MD]). K_d values were calculated from the M2 tetramer concentration times drug concentration divided by their concentration when in complex. This value then gave the drug concentration at which 50% of M2 tetramers were in complex with drug. The experiment therefore had three parameters for consideration, two optical and the K_d.

All compounds used in equilibrium binding experiments, which had a known antiviral activity, suggested an interaction of 1:1 stiochmetry, with one M2 tetramer binding one drug molecule. Cyclopentylamine a compound that has no antiviral activity caused no fluorescence increase when added to purified M2 protein at pH 5 further demonstrating the specificity of the drug-induced effect.

Cycloheptylamine gave a high K_d value of 16.2μM while cyclooctylamine gave a fairly low K_d value of 1.83μM. Changes in the carbon ring size to a smaller structure than cyclooctylamine led to a gradual loss of inhibition with decreasing ringsize (data not shown). An increase in ring size again decreased K_d and led to the eventual elimination of all inhibition increases by the cycloamine compounds. Ranking of the cycloamine equilibrium K_d values according to strength of binding affinity correlated with antiviral activity of the compound (Table 3.3). The stronger the antiviral activity, the higher the binding affinity.

Compounds with an adamantyl cage, such as amantadine and rimantadine had higher affinities. Amantadine gave a K_d of 324nM, a 5x stronger affinity than that of cyclooctylamine. This may be due to the variance in structure, between an adamantyl cage and a cyclic carbon ring. Rimantadine gave the lowest K_d of all with 16nM. Adamantol, which has no amine group and instead carries an hydroxyl group, caused no fluorescent increase. This suggests an amine group is an important requirement for binding to M2 inducing an increase in fluorescence. Interestingly when all compounds (both cycloamines and adamantly structures) were ranked by K_d values from equilibrium experiments (Table 3.3) they all correlated with the ranking of the antiviral activity each compound reported in the seminal study of *Hay et al.,* 1985.

These experiments also reflect the importance of the two composite parts of the molecule, the uncharged/charged amine group and the carbon-based frame to which it is attached. The active amine group may be important for interaction

Inhibitor	Equilibrium K_d (μM)	Kinetic K_d (μM)
Rimantadine	0.016 (±0.005)	14
Amantadine	0.324 (±0.031)	18
Cyclooctylamine	1.83 (±0.29)	15
Cycloheptylamine	16.2 (±4.5)	10
Cyclopentylamine	No Effect	No Effect

Table 3.3: Dissociation constants derived from equilibrium and kinetic binding experiments. The relative equilibrium K_d values reflect the relative antiviral activity ranking for these compounds

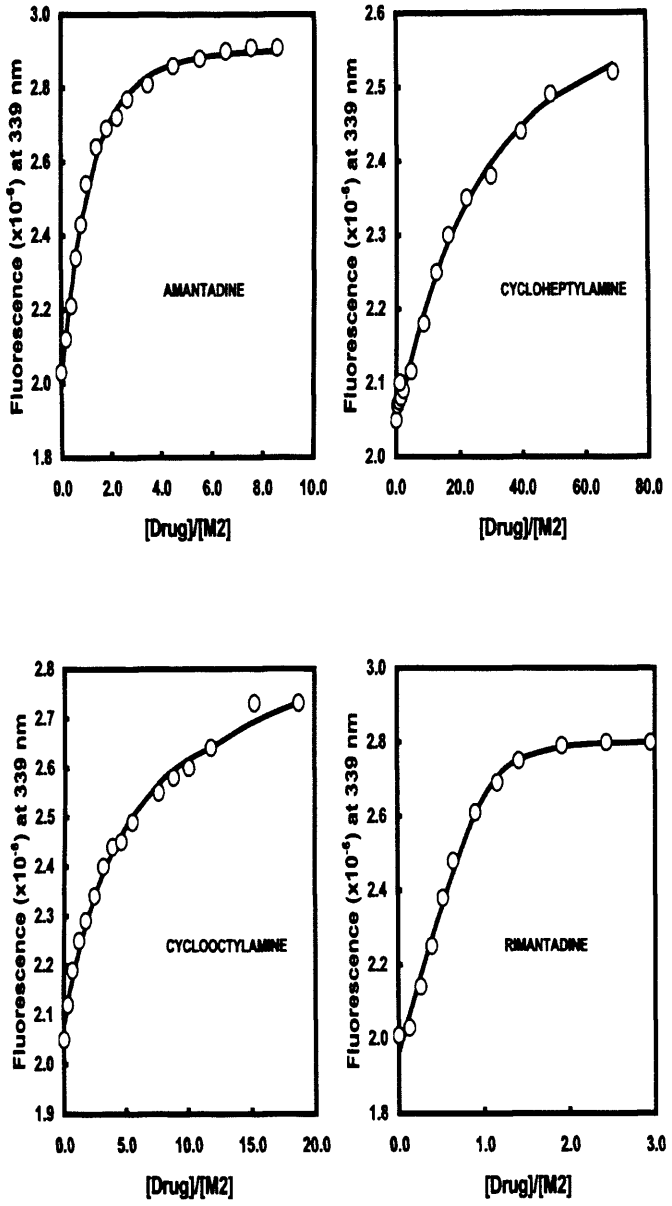

Figure 3.28: Equilibrium measurements of amantadine, rimantadine and cycloamine inhibition of pH-induced quenching of Trp fluorescence of M2. Increasing compound was added to 0.33μM tetramer until saturation. Experiments were fitted to the following scheme: $M + D \leftrightarrow MD$ *with* K_d*=([M][D])/[MD] with the optical signal is calculated by: Signal=εd[D]+εmd[MD]. Note that cycloheptylamine and cyclooctylamine are nearing their maximums.*

directly with the proton translocation mechanism of the M2 channel and whereas the frame (adamantyl cage or cyclic ring structure) will either affect the positioning of the amine group or interact with the channel in a distinct manner possibly altering tetramer configuration. The high K_d values are lower than those reported in previous studies (Wang *et al.,* 1993; Astrahan *et al.,* 2004) and probably reflect more accurately the irreversible nature of drug binding within the M2 channel. Previous studies have either used electrophysiology to determine isochronic inhibitory constants for M2 expressed in cells or used surface plasmon resonance with M2TM in liposomes to study M2 inhibitor binding (Wang *et al.,* 1993; Astrahan *et al.,* 2004). To gain further insight into the kinetics of drug binding time resolved experiments were conducted under pseudo-first order conditions. An excess of drug was added to M2 tetramer and the increase in fluorescence signal (k_{obs}) was followed as a function of time. The formula for this reaction is:

(3.2) $\mathbf{k_{obs} = k_{on}[D] + k_{off}}$

To understand the binding kinetics, the observed association rate of amantadine with M2 (k_{obs}) was used to derive the K_d value. k_{obs} is the product of the on rate (k_{on}) (i.e. the rate at which drug binds to M2) times drug concentration, plus the off rate (k_{off}) (the rate at which inhibitor dissociates from M2 tetramer) which is drug concentration independent. This is why the reaction is under pseudo-first order conditions. To derive the dissociation constant (K_d) from these data both of the above values must be known. k_{on} is derived from the slope of the plot of k_{obs} against [drug] while the k_{off} is given by the y-axis

intercept (Figure 3.29). All the anti-influenza drugs inhibited M2 with slow on and off rates, which is consistent with the irreversible nature of inhibitor binding to M2. Once again cyclopentylamine was used as a negative control Cycloheptylamine gave a K_d 0f 10μM while cyclooctylamine gave a value of 15μM. All the inhibitors gave similar K_d values (Table 3.3).

Amantadine and rimantadine gave K_d values of 18μM and 14μM, respectively. The relative values do not correlate with the relative antiviral activities of these compounds. Furthermore, the linear increase of k_{obs} with drug concentration is descriptive of a simple one-step bi-molecular process for inhibitor binding to M2 (i.e. the drug binds in the channel and proton flow is inhibited as per a non-competitive channel blocker). However, unexpectedly the K_d values obtained from these time-resolved experiments were much higher than those obtained from the equilibrium experiments (Table 3.3). The difference in K_d values between equilibrium and kinetic experiments is hard to rationalize in terms of a simple one-step bi-molecular process for drug binding to M2. If this were the case, then the K_d values from the two types of data should be similar. To explore this difference in K_d values further, the amplitudes that would be

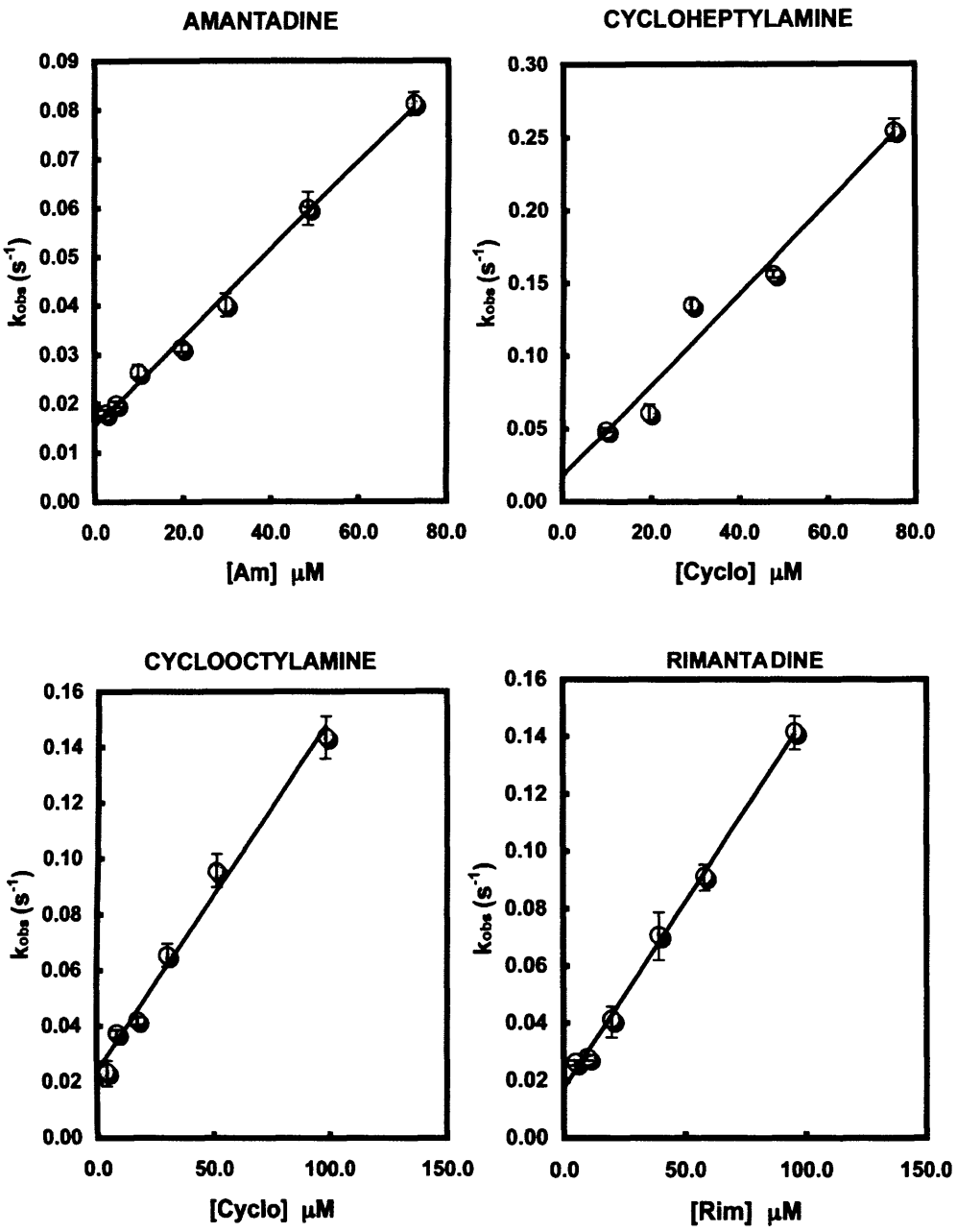

Figure 3.29: Kinetic measurements of amantadine, rimantadine and cycloamine inhibition of low pH-induced quenching of Trp fluorescence of M2. Please refer to section 2.4.1 for information regarding fitting parameters for the above experiment and raw k_{on} and k_{off} data in a table contained in equation 3.2.

	Amantadine	Rimantadine	Cyclooctylamine	Cycloheptylamine
k_{on}	920 $M^{-1}S^{-1}$	1350 $M^{-1}S^{-1}$	1400 $M^{-1}S^{-1}$	3100 $M^{-1}S^{-1}$
k_{off}	0.017	0.019	0.021	0.018

Table 3.4: Raw data for k_{on} and k_{off} values to perform k_{obs} calculations.

expected from the kinetic data for the two K_d values for amantadine binding were predicted and plotted along with the experimental kinetic amplitude increases (Figure 3.30). The experimental amplitude increases seen for amantadine did not correspond to the K_d value of 18μM extrapolated from the k_{on} and k_{off} values from these experiments. In fact the experimental amplitude increases were much closer to the predicted amplitude for the equilibrium experiment K_d of 0.32μM indicating that these are the true values that represent the affinities for inhibitor binding of M2. Furthermore the deviation of the K_d values from the two types of experiments is indicative of a more complex binding process of amantadine and similar compounds to the M2 pore. Binding appears to involve an optically silent step, which cannot be observed in time-resolved fluorescent kinetic experiments. This extra step that is induced after amantadine binding is most likely a fast conformational change, which would be indicative of an allosteric mechanism of inhibition of the M2 channel by amantadine. This led to a proposal for a mechanism for the binding of the M2 inhibitor to the M2 channel (figure 3.31). One M2 tetramer is capable of complexing with one drug molecule at a rate of K_{d1}. Upon inhibitor binding a conformational change is induced within the M2 protein, which is both fast and optically silent, locking the M2 and drug together in an almost irreversible form, at a rate constant of K*. Therefore, in this case K_d is equal to K_{d1} divided by 1 over K*, explaining why values from equilibrium and kinetic experiments are so different. Although this describes the most likely and plausible mechanism, it

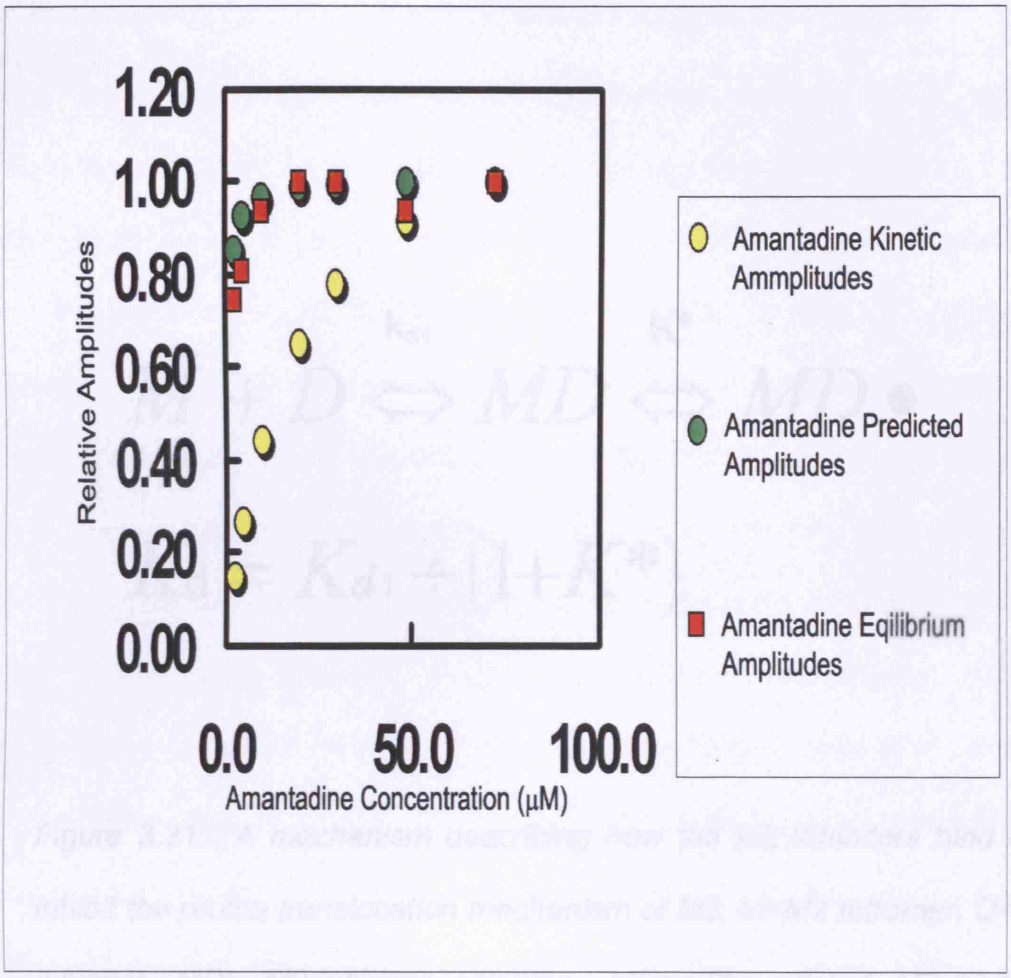

Figure 3.30: Comparison of predicted and experimentally determined amplitudes of amantadine inhibition from equilibrium and kinetic experiments.

$$M + D \overset{k_{d1}}{\Leftrightarrow} MD \overset{K^*}{\Leftrightarrow} MD\bullet$$

$$K_d = K_{d1} \div (1 + K^*)$$

Figure 3.31: A mechanism describing how the M2 inhibitors bind and inhibit the proton translocation mechanism of M2. M=M2 tetramer, D=M2 inhibitor, MD= M2-inhibitor complex, $MD\bullet$ *=The altered M2-inhibitor complex induced, by an optically silent, fast conformational change.* K_{d1}*=equilibrium constant for association/dissociation of inhibitor and M2 tetramer (*$K_{d1}=k_{off} / k_{on}$*) and K*=equilibrium constant for conformational change of complex (*$K^*=k_{=+MD} / k_{-MD}$*). It is possible that kinetic or equilibrium measurements may have a systematic error.*

should be noted that this is just one scheme which could be formulated for inhibitor binding to the M2 channel.

3.3.2: Structure-Activity Relationship Studies of Anti-M2 Inhibitors

M2 is a well-defined drug target; however resistance develops easily, due to single amino-acid changes within the transmembrane domain. Therefore it is of importance to consider what constituents of potential inhibitors enhance or reduce binding/inhibition of the M2 channel, in order to produce alternative inhibitors. A series of compounds, synthesized by Antonios Kolocouris as potential M2 inhibitors were studied using the fluorescence assay to analyse binding characteristics. The structures of the compounds are listed in Figure 3.32. The adamantane cage provided the core structure to which different reactive groups were attached in different positions. Equilibrium binding measurements were performed with all compounds titrated against a constant amount of M2 protein. and the K_d values were calculated from the drug-induced fluorescence increase. K_d values were then compared to published antiviral activities of compounds where available, or inferences were made about antiviral activity from the K_d (Table 3.4). All titrations were performed a minimum of 3 times. Spiro-piperidine-2,2'-adamantane (K_d=0.39μM similar to amantadine) gave the highest K_d. Other compounds showed reduced affinities with K_d's of between 3 to 20-fold lower Compounds 1-7, 12 and 28 produced no fluorescent increase in this assay. In some instances they actually caused a reduction in fluorescence; however this effect was not readily repeatable. Compounds 10,11,17,18,20, 22, 23 and 30 all gave K_d of between 5- 25μM. and

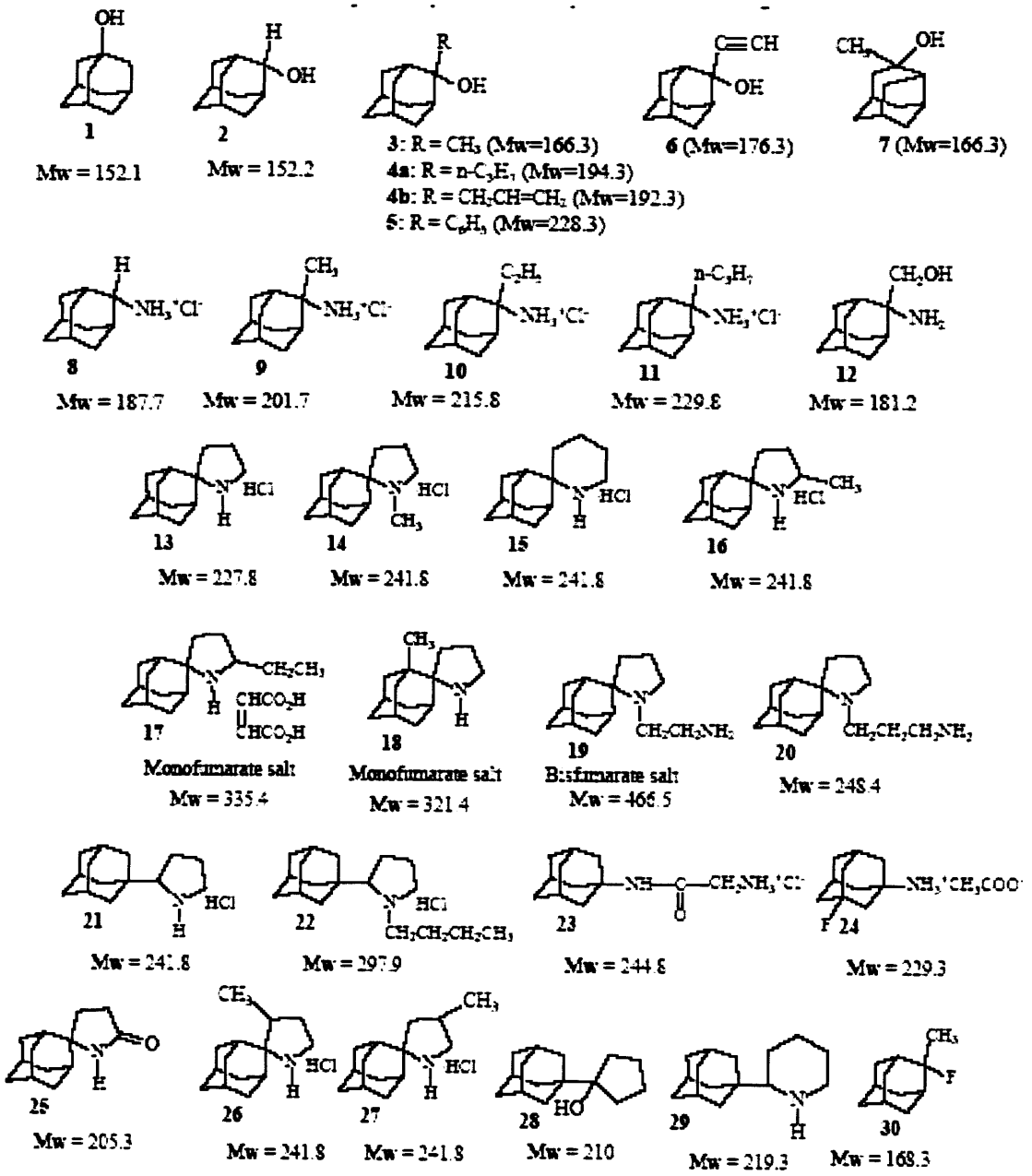

Figure 3.32: Structures, of adamantanes provided by Antonios Kolocouris of the University of Athens, Greece for studies of structure-activity of M2 inhibition.

were reported to have no antiviral effect, Most contained hydroxyl groups attached directly to the amantadane cage, which may produce the inability to bind the M2 protein. The features of these molecules included long carbon chains attached to the adamantane cage via a piperidine ring and amine groups co-localized with methyl groups at various points around the same structure. In the case of amine groups being present on an adamantane cage structure it would be expected for these compounds to have a high affinity for M2. It is likely that either the positioning of the amine group around the structure inhibits the amine groups interaction with the M2 protein or the presence of methyl groups has the opposite effect to that of an amine group. From these data it is inconclusive which of these is more plausible. Certainly the addition of methyl groups to compounds, which already exhibited high affinity, caused a decrease in the Kd value, or compounds, which contained a methyl group as the main active group, showed lower affinity than other compounds. Increasing alkyl chain lengths on the pyrrolidine ring also led to a reduction in binding affinities. Other compounds gave a range of K_d values from 2-5μM; these either contained single hydrogen atoms or amine groups attached to either the adamantane cage or piperidine ring structure attached to the cage.

The presence of amino groups or any active chemical entities with delocalized electrons showed both higher affinities for M2 binding and increased antiviral activity such as compound 8. The localization of these groups seemed to be important, with increased activity in those compounds where the active group was directly attached to the adamantane cage. There was also broad

agreement once again with the K_d values relating to the published antiviral activities of these compounds, although there were exceptions, such as in the case of compound 29. Spiro-piperidine-2,2'-adamantane (compound 15) gave the highest affinity, for M2 comparable with that of amantadine (K_d 0.32μM). 2-(1-adamantyl) pyrrolidine (compound 21) was next with an affinity also close to amantadine and then Spiro-pyrrolidine-2,2'-adamantane (compound 13) whose K_d was some 2-fold less than the other high affinity compounds. Interestingly, these compounds all contained a nitrogen and hydrogen atom at the same point in the piperidine ring. Certain chemical side-chains however, had pronounced affects when located in various parts of the adamantane cage, giving information about the chemical requirements for binding and the possible orientation of the adamantane molecule in the channel pore. Unfortunately no information has been published on any of these compounds so it is difficult to form a conclusion from this analysis. The mode of action for these compounds is thought to be the same as that for amantadine and rimantadine.

Compound Number	K_d value (μM)	Published MIC_{50} (μg/ml)
1	N/E	n/k
2	N/E	n/k
3	N/E	n/k
4a	N/E	n/k
4b	N/E	n/k
5	N/E	n/k
6	N/E	n/k
7	N/E	n/k
8	2.36	n/k
9	3.6	n/k
10	6.7	n/k
11	8.71	n/k
12	N/E	n/k
13	1.1625	1.8 (1.1)
14	2.93	2.9 (1.1)
15	0.39	n/k
16	1.5	2.5 (1.1)
17	5.58	n/k
18	5.8	n/k
19	3.72	n/k
20	10.5	n/k
21	0.508	2.5 (45)
22	10.61	>26.9 (12.8)
23	7.5	n/k
24	4.86	n/k
25	1.49	n/k
26	4.21	3.7 (1.1)
27	2.64	3.3 (1.1)
28	N/E	n/k
29	1.51	3.3 (45)
30	>26	n/k

Table 3.5: K_d and MIC_{50} values for the adamantane compounds. The abbreviation N/E means no inhibitors effect. All values are given in μM. MIC_{50} were obtained from the literature. Where the value is not known n/k is used in place of a value.

Chapter 4: Discussion

The studies discussed in this thesis used two methods to investigate the structure-function relationship of the M2 channel. Firstly, a pH-sensitive green fluorescent fusion protein, M2-GFP was investigated as a probe for M2 activity, to measure directly proton passage through M2 as a possible assay for mutant channel specific activity and the action of M2 inhibitors. Secondly, tryptophan fluorescence of recombinant purified M2 protein was used to study the biophysical basis of channel activation, permeation and the mechanism of action for the anti-M2 inhibitors amantadine and rimantadine. The latter provided the basis of an assay to measure inhibitor binding affinity and perform structure-function studies of the M2 channel, to contribute to the development of other anti-influenza drugs.

4.1: M2-GFP Fusion Protein as a Probe for M2 Channel Activity

Initial data from experiments using the HA protection assay had indicated that the activity of the M2-GFP proton channel expressed in HeLa cells was comparable to that of wild type WM2 in Hela cells. Subsequent direct measurements of proton currents by patch clamp confirmed the M2 channel fused to GFP retained activity, but that the specific activity was reduced by approximately 3-fold relative to that of the WM2 channel protein.

It was decided to use the MEL cell system, which had been used to characterize the proton conductance so exquisitely, in conjunction

with a fluorescent technique which may give better estimation of M2 specific activity than previously obtained with other fluorescent techniques, such as SNARF-1AM.

The M2-GFP protein was expressed in stably transfected MEL cells at similar levels to WM2 when compared by Western-Blot. The protein was of the expected size and ran as a single band. Thus, as observed in other studies when GFP has been fused to ion channels, both within the structure (Siegel and Isacoff, 1997) and to their C-terminus, to look at cellular trafficking of Kv channels (Marshall *et al.,* 1995), GFP could be attached to M2 without reducing expression or transport of the fusion protein in the MEL cell expression system.

As GFP is attached on a one to one ratio with the M2 monomer, the level of GFP expression is directly related to that of the M2 protein and the level of GFP fluorescence could be used to measure the amount of M2 and determine the specific activity of M2 in single cells. In addition a technique such as FACS could provide a quick method for selection of high expressing MEL cells.

Fluorescence imaging showed that M2-GFP localised predominantly, in an evenly distributed fashion, on the plasma membrane. This is similar to previous studies of the Kv channel which was shown to be evenly distributed in the plasma membrane of expressing cells (Kupper, 1998). The wild-type M2 channel is known to localise at the apical domain of polarised cells, surrounding

lipid rafts in which the HA and NA are found (Leser and Lamb, 2005) thereby giving an even spread of M2 in the cell membrane.

Various experiments were performed to study the two facets of the M2-GFP protein, the pH sensitivity of the GFP portion of the fusion protein and ability of the M2 protein to modify intracellular pH.

The GFP protein has distinct properties which allows it to partner other proteins in fusion complexes without loss of activity. It has a β-barrel structure which is extremely resilient, and remains intact when fused to a number of different partner proteins allowing it to function. The GFP chromophore is protected by this β-barrel structure. The chromophore itself is fairly resilient with local amino acid changes altering but not halting its fluorescence properties. Amino acid changes in the chromophore can alter fundamentally the properties of GFP fluorescence such as in the case of the pHluorin (Miesenbock *et al.,* 1998).

Firstly, the pH-sensitive properties of the GFP were tested using the K^+/H^+ ionophore nigericin to equilibrate extracellular and intracellular pH. The calibration curve obtained for the fused GFP was very similar to that reported for GPI-anchored GFP (Miesenbock *et al.,* 1998). Various experiments showed that the probe could monitor changing intracellular pH due to a variety of stimuli and it proved highly sensitive in detecting relatively small changes. With a sensitive GFP probe, attention now turned to the activity of the M2 channel. The M2-GFP fusion protein showed an ability to affect the "steady-state" pH

gradient across the MEL cell plasma membrane, but reduced intracellular pH by only 0.05 pH units. Previous experiments showed that WM2 was capable of reducing (and abolishing) this pH gradient, by nearly 0.3 pH units. This suggests that the M2-GFP has a lower channel activity than WM2. "Ion flux" experiments which monitored changes in pH in M2-GFP cells, in response to large changes in extracellular pH to the K^+/H^+ ionophore nigericin failed to reveal any substantial or abrupt changes in pH due to M2-GFP. For example following reduction of external pH from 7 to 6 saw a small difference between rimantadine treated and untreated cells indicating only a small influence rimantadine-sensitive of M2 activity on the reduction of intracellular pH. Experiments in which pH was kept constant, rimantadine addition led to a gradual increase in intracellular pH of 0.1 units at pH 6 again demonstrating M2-GFP had the ability to alter the transmembrane pH gradient but not to abolish it.

Valinomycin-induced K^+ gradient experiments again showed a rimantadine-blockable M2 channel activity comparable to those detected under other ionic conditions.

The results indicate that M2-GFP retains proton channel activity that is blocked by rimantadine but that was estimated to be 3-5X fold lower than that of WM2. Thus although the GFP probe was functional as expected, the evident reduction in M2 activity indicated that this fusion protein would not be obtained for mutagenesis studies. Furthermore, the limited effect M2-GFP had on the local pH and the inability of the probe to detect proton flux through the M2 channel, or

rapid changes in local pH, showed this approach offered no advantage over the use of SNARF-1 to monitor changes in cytoplasmic pH.

WM2 had the ability to modify the cytoplasmic pH of MEL cells; although the physiological significance of this is unclear, the electrochemical pH gradient across the plasma membrane is abolished. The reason for reduced M2-GFP activity is also unclear but it is undoubtedly linked to the fusion of the GFP to the C-terminus of M2. It is known that removal of the C-terminus of M2 can lead to a reduction in activity in *Xenopus Laevis* but the exact role of the C-terminus in channel activity is not fully understood. The C-terminus is also likely to stabilise the entire channel structure and therefore affect the conformation of the histidine and tryptophan side-chains which are crucial for proton conduction. One possible scenario for how the GFP has affected M2 is with the helical tilt (Figure 4.1). Alteration of the C-terminus does not affect rimantadine inhibition in both the M2-GFP protein or when the C-terminus is removed. The M2 transmembrane domain is therefore capable of binding drug.

M2 is a membrane protein with an α-helical structure rather than β-barrel. Its homotetrameric complex is a delicate interplay between hydrophobic interactions and disulphide bridges. Previous work suggests that M2 evolution has selected amino acids in the transmembrane domain on the basis of channel functionality rather than stability (Stouffer *et al.*, 2005). The C-terminus to which the GFP is attached is also thought to contain α-helical structural elements (Howard K and Cross T, personal communication). It is also being found that this area of the M2 protein not only stabilizes the channel structure but also has

functions independent of the protein's ion channel activity (McCown and Pekosz, 2006). GFP is also larger than M2. With all these factors combined, it is highly likely that the attachment of GFP to the C-terminus causes a structural alteration which leads to disruption of channel activity.

Although the arguments above suggest that GFP might have affected the channel structurally it is important to note that the channel is still functional and capable of being inhibited. Therefore any structural rearrangement cannot have affected the channel from the N-terminus side of the channel on a gross scale. It is likely that a small conformational change has been caused by the fusion of these two proteins. This may have altered the environment within the channel pore leading to an altered conformation of perhaps His37 side-chain leading to a varied ability to passage protons through the pore (Figures 4.1). Activation characteristics could also have been altered during fusion of M2 and GFP. M2-GFP experiments regarding activation were not performed here due to the small currents produced by the M2-GFP channel.

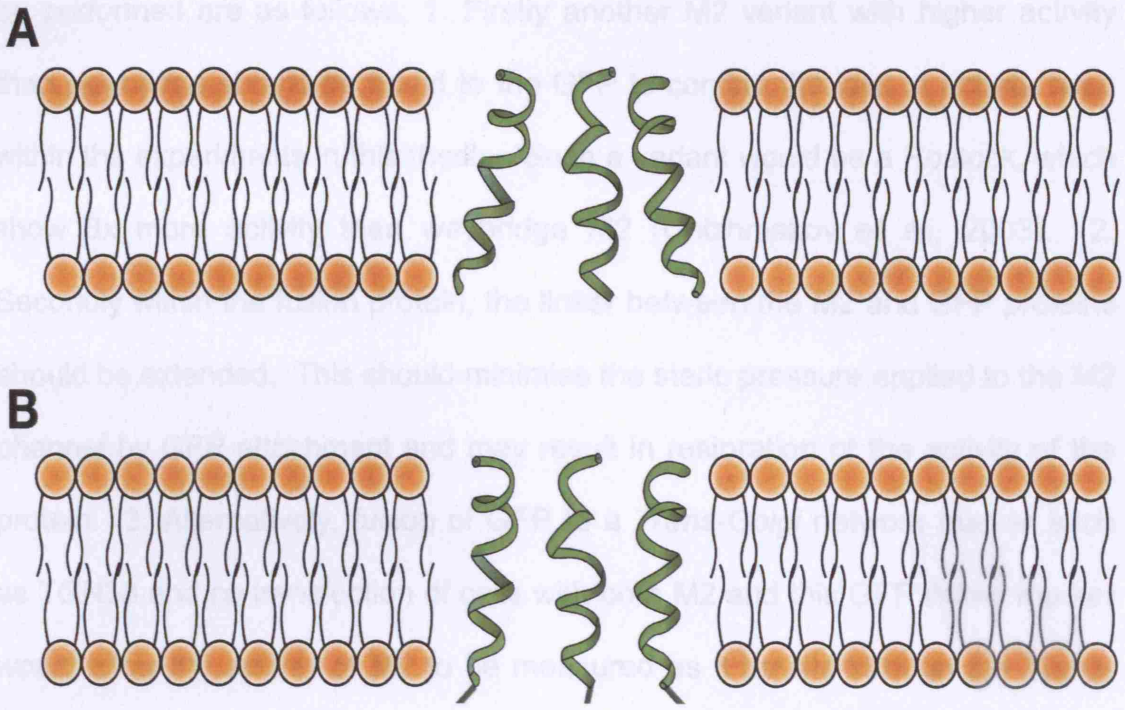

Figure 4.1: A cartoon showing M2 transmembrane domains with different helical tilts in a lipid bilayer without (A) and with (B) GFP attached. The diagram illustrates a possible alteration of helix tilt through attachment of GFP to the M2 C-terminus.

Future work could focus on modifications to the assay, which either avoid the decrease in M2 activity of the fusion or decouple the M2 and GFP by using them separately in a joint assay. Therefore further experiments which should be performed are as follows: 1. Firstly another M2 variant with higher activity than weybridge should be fused to the GFP to confirm the loss of activity seen within the experiments in this thesis. Such a variant would be a Rostock, which show 8x more activity than weybridge M2 (Chizhmakov *et al.,* 2003). 2. Secondly within the fusion protein, the linker between the M2 and GFP proteins should be extended. This should minimise the steric pressure applied to the M2 channel by GFP attachment and may result in restoration of the activity of the protein. 3. Alternatively, fusion of GFP to a *Trans-Golgi* network marker such as TGN38 and co-transfection of cells with both M2 and this GFP linked marker would allow the activity of M2 to be measured as it travels through the *Trans-Golgi* network where it is known to modify pH and is blockable by rimantadine. An advantage of this method is the fact that the GFP is closely localized with the M2, thereby allowing more direct measurement of activity using a whole cell cytoplasmic indicator such as SNARF.

4.2: Spectroscopic Studies of the Influenza M2 Protein

Tryptophan fluorescence studies have provided information on two facets of the M2 channel:

1. Structural changes related to activation and permeation of M2.
2. How inhibitors interact with the channel to limit proton conduction.

4.2.1: Tryptophan Fluorescence Studies of M2 Channel Functionality

The experiments performed here emphasized several responses to pH. M2 protein was expressed in *E.Coli* at high levels and successfully purified. The protein was correctly folded in a tetrameric form as shown by Western Blot and CD spectroscopy and, in particular, rimantadine binding showed a 1:1 stoichiometry with drug. All of these characteristics are important when considering the validity of measurements in relating them to functional characteristics. Attempts were made to purify single tryptophan M2 mutants, W15F and W41F. This would have allowed deconvolution of the two tryptophan signals from WM2 permitting characterization of the fluorescence increase at pH 6.2 and the quenching of Trp41 fluroescence in isolation. Although these proteins did not give enough yield for purification the N-truncated mutant provided an alternative means to study Trp41 quenching.

Fluorescent emission spectra suggested the predominant signal was produced from Trp41 in the M2 pore. Trp41 gave a highly buried spectrum while Trp15 was highly exposed. Different mutants gave different λ_{max} values suggesting a different environment for the M2 Trps at high pH. Removal of His37 led to a small shift in emission maximum of the tryptophans in M2 making them more accessible to the solvent. Although only a 1nm shift was observed it is interesting that His37 seems to influence the environment of Trp41 at high pH.

When pH was lowered, fluorescence quenching was observed due to His37 protonation. This occurred all they way down to pH 3 when quenching stopped.

A red-shift in λ_{max} of several nanometers was also seen to accompany the quenching as pH was lowered, suggesting that a His37-dependent change in Trp environment occurs upon protonation. Acrylamide quenching experiments confirmed this and showed that Trp41 was highly inaccessible to solvent at high pH or when rimantadine was added. When pH was lowered however, Trp41 became more accessible. REES measurements suggested that at high pH His37 restricted water molecule motion within the channel pore, but as pH was lowered water molecules were able to reorientate in a freely moving environment. Combined with polarization measurements, which suggest a rigid environment for Trp41 at low pH, all experiments suggest that upon lowering pH major changes occur in His37 and Trp 41.

The His37 tetrad in ssNMR measurements occludes the pore of M2TM (Nishimura *et al.,* 2002). Other data has suggested a hydrogen-bonded format for His37, which leads to channel occlusion. Two separate studies have proposed either a cyclic hydrogen bonded network, or two linked dimers forming a "histidine-lock" for the imidazole tetrad formation occluding the pore (Okada *et al.,* 2001; Hu *et al.,* 2006). Our data cannot differentiate between these two formations but does suggest that His37 acts as a barrier. Upon pH activation of the channel, which is mediated by His37 protonation, it acts as a proton sensor and mediates the opening and closing of the M2 channel either itself or through control of the putative gate Trp41 by a cation-π interaction.

Furthermore, all of the above are not shown with a H37A mutant. This suggests the four histidines form a blockade of the pore from the N-terminal side at high pH probably through a hydrogen-bonded formation. Histidine 37, as also mentioned above, activates M2 with pH-dependency. Its role in proton conduction is discussed below. The exact steps in channel activation cannot be seen from our data. However the state of the hydrogen-bonded histidine tetrad is probably broken by a protonation event. Interestingly, in the M2TM peptide, Hu *et al.* observed altered proton sensitivity due to the "histidine lock" formation. Our data set does not see this during channel activation. Below pH 6.2 a continuous quenching phenomenon is observed, therefore, resolution of single protonation events associated with His37 are not possible.

Trp41 at high pH is also known to occlude the channel pore and acts as the putative gate of the channel (Nishimura *et al.,* 2002; Tang *et al.,* 2002). At high pH the conformation of the tryptophans is loose, sitting in the channel pore acting as a physical barrier to stop proton flow. It may also limit accessibility to His37 from one side of the channel, hence the unique activation characteristics of "Weybridge" when compared to "Rostock" M2 (Chizhmakov *et al.,* 2003). At high external pH, Weybridge M2 has a small outward conductance while Rostock M2 gives a high conductance under these conditions. When internal pH is high the opposite is seen with Weybridge M2 giving large internal conductance while Rostock gives a small conductance.

The H37A protein is described by Wang *et al.*1995 as an open pore which allows passage of multiple ion types. Interestingly, all values in H37A measurements are found intermediate what one would classify as the non-conducting form and conducting form of M2. Consistency in measurements of H37A and the lack of response to pH in our experiments suggest that this protein equates to a single, permanently open conformation of the M2 pore, one which is non-selective for protons. Through the loss of quenching, peak shift with pH, polarization, REES shift and increased acrylamide accessibility due to lack of His37 it is possible that our biophysical measurements reflect the conditions found in a non-selective pore. This would differentiate it from the selective pore.

As the non-conducting form of M2 is characterised by a hydrogen-bonded network of histidines, the conducting form involves another type of interaction between His37 and Trp41. A cation-π interaction involving these two residues was shown by UVRR spectroscopy of M2TM (Okada *et al.,* 2001). Cation-π interactions have previously been reported to produce increased emission intensities with red-shifted emission maxima in the case of tryptophan (Lee *et al.,* 2002). Both of these phenomena are seen in the case of our measurements and when combined with previous UVRR measurements, a cation-π interaction appears to be involved in the formation of the conducting state of the full length protein. The alternative answer would be an increase in tryptophan solvent exposure. Increases in acrylamide quenching exposure would indicate this however only a small increase in solvent exposure was seen

within M2, although a larger one in nM2. This does not correlate with a red shift of several nanometers in both proteins which are indicative of a larger increase in solvent exposure than that indicated by acrylamide quenching. Hence the red-shift that emanates from Trp41 may be due to an electronic transition and not just to changes in solvency. The solvent exposure seen in acrylamide quenching may be related to a structural rearrangement in tryptophan side-chain environments as a consequence of the His37-Trp41 interaction.

Further to this, a cation-π interaction would produce a polar, rigid environment for any tryptophan involved. Polarisation measurements of M2 and nM2 suggest that at low pH Trp41 is rigid in conformation while peak shifts suggest a more polar environment. pKa values for peak shifts and quenching of Trps in M2 give values of between 5.7 and 6 close to the value for proton permeation of M2 (Chizmakov *et al.,* 1996), and are associated with histidine protonation causing quenching of Trp fluorescence. It seems that peak shifts, fluorescence and acrylamide quenching, and polarization measurements indicate that, as pH is lowered, Trp41 undergoes a change in conformation mediated by His37, which may well lead to a structural alteration in the tryptophans, leading to proton conduction. A diagram (Figure 4.3) demonstrates how this interaction might occur.

His37 would seem to initiate the cation-π interaction and act as a proton sensor, which then interacts with Trp41 as the gate. There is no evidence to suggest in our measurements that His37 act directly in the actual translocation of protons

during conduction. Our data would implicate His37 acting indirectly with the tryptophan to change side-chain conformation and allow formation of a transient water-wire (indicated by REES measurements at low pH).

Tryptophan 41 plays the role of the gate within the channel. Solid-state NMR has shown that the four Trp residues at high pH, like His37, face into the tetrameric pore in the closed state. Measurements have given some insight into the state of the Trp residues. Like His37, Trp41 residues in the channel are in rather a lose conformation as shown by polarization measurements. Their occlusion of the pore is confirmed by their relative inaccessibility to acrylamide in quenching experiments and the fact that water molecules surrounding Trp41 in REES experiments showed no fluidity. There is also no data to indicate that His37 has an effect on Trp41 conformation at high pH.

Conversion of M2 to the conducting state leads to profound changes in the environmental, chemical and possibly the conformational state of Trp41. Upon activation of the M2 at pH 7, the hydrogen-bonded formation of His37 is broken by protonation of the imidazole ring which forms cation-π interactions with Trp41 on adjacent helices. pKa's of λ_{max} shifts reflects the value at which 50% of

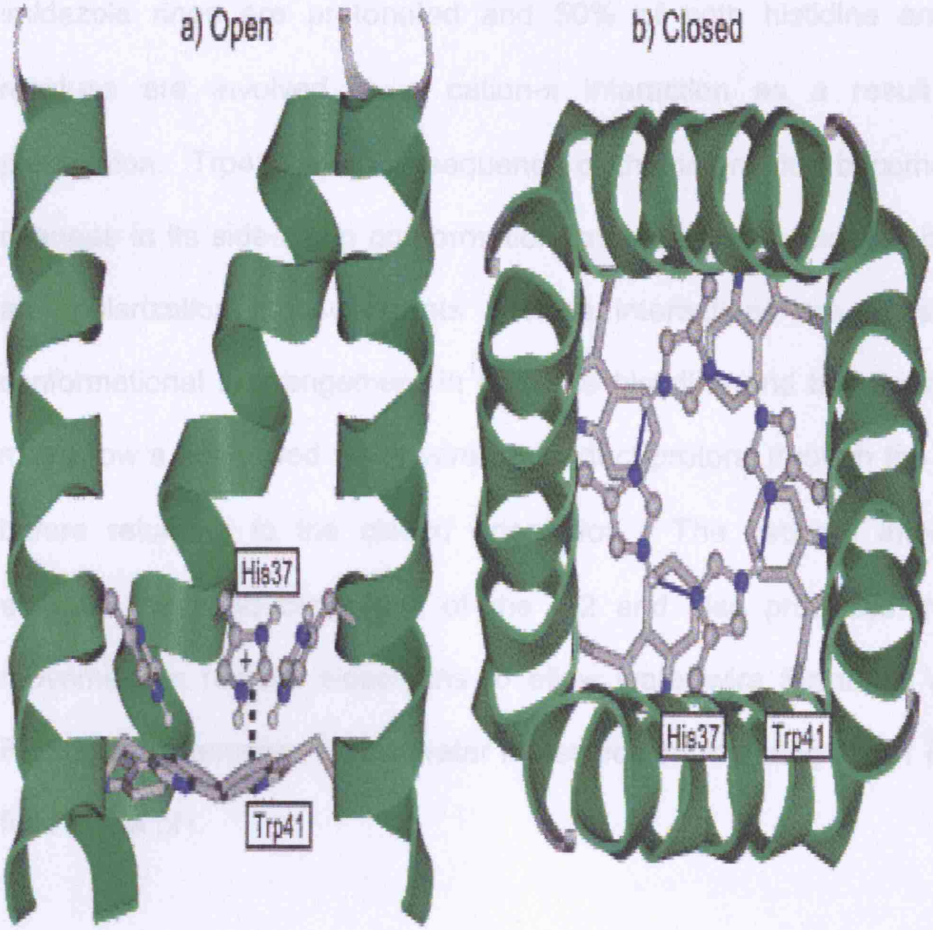

Figure 4.2: A) The open form (side view) of the M2 channel involving a cation-π interaction between His37 and Trp41 on adjacent helices and B) the closed form (top view) involving a hydrogen bonded network (Takeuchi et al., 2003).

imidazole rings are protonated and 50% of both histidine and tryptophan residues are involved in a cation-π interaction as a result of histidine protonation. Trp41, as a consequence of this interaction becomes polar, and changes in its side-chain conformation, as indicated by acrylamide quenching and polarization measurements These interactions are transient and the conformational rearrangement in both the histidine and tryptophan sidechains may allow a short-lived water-wire to conduct protons through the resulting gap before returning to the closed orientation. The cation-π interaction helps stabilise the conducting form of the M2 and also produces the necessary movement in residue sidechains to allow water-wire formation as shown by REES measurements, where water molecules surrounding Trp41 become more fluid at low pH.

If all of the above is correct, Trp41 may act as the putative gate of the channel, occluding it at high pH and moving to both open the channel to allow water-wire formation, but also stabilizing the conformation by interacting with His37.

Therefore these results suggest that histidine protonation plays a role in proton permeation of M2. Combined with acrylamide quenching measurements which imply a more exposed environment for Trps at low pH due to an alteration in either:

a) Conformation rearrangement in the imidazole ring of histidine 37
b) Conformation rearrangement in the indole ring of Trp41
c) Conformation rearrangement in both

as a consequence of an electronic interaction between His37-Trp41.

Data from our studies indicate two distinct forms of the M2 channel. One is a conducting form which involves inter side-chain interactions between the crucial residues His37 and Trp41, stabilising an open channel. The other, non-conducting form is where these side-chains interact with side-chains on the adjacent helices leading to a closed form. This does not rule out the possibility of transition states between the conducting and non-conducting forms of M2

Rimantadine addition inhibits and reverses fluorescence quenching and peak shifts fully. However, REES measurements were not fully restored, indicating that solvent molecules still maintain some fluidity within the channel pore while acrylamide quenching measurement changes related to pH were only reversed by 50% in both M2 and nM2. This may not be due to rimantadine inhibition of M2 proton translocation but to a decrease in tryptophan solvent exposure by rimantadine binding in the pore. Polarisation measurements also do not show a full reversal to their original state suggesting that rimantadine binding may produce a conformational change in M2 that produced a distinct M2/rimantadine bound state incapable of proton conduction.

4.2.2: Inhibition of the M2 Channel

How amantadine inhibits the M2 channel has been a question that research in this field has tried to address for some time. Several theories have been put forward as to the possible mechanism by which this occurs. Initially it was

thought that amantadine inhibited the channel by acting as a steric blocker sitting within the channel pore forming a physical barrier to block the passage of protons.

However, various data gathered do not support this proposal. Two facets of a channel blocker which acts in this way is that the on rate is extremely quick and block is both reversible and independent of membrane potential. Amantadine inhibition of M2 is slow and irreversible and shows no dependency on voltage therefore it is unlikely that amantadine inhibits M2 proton translocation like a typical non-competitive blocker. A second theory which has been put forward is that amantadine binds at a site external to the channel pore and causes inhibition by an allosteric conformational change in the protein. This is unlikely because resistance mutations occur in the amino acids within the physical pore of M2, and neutron diffraction studies showed that amantadine binds within the channel pore between V27 and G34 of a TM peptide (Astrahan *et al.,* 2004). A third scenario is that amantadine interacts with the channel pore with the hydrophobic cage interacting with the pore-lining residues perhaps alanine 30 and glycine 34. The ammonium nitrogen may then interact with the imidazole ring of His37 through hydrogen bonding to inhibit the proton translocation mechanism of M2.

Our studies which gave different K_d values from kinetic and equilibrium measurements suggest an allosteric mechanism for M2 inhibition by amantadine/rimantadine. This mechanism has several consequences for the

His and Trp side-chains within the channel pore. It would seem that His37 becomes deprotonated as shown by the increase in Trp fluorescence on rimantadine binding and actually demonstrates a lower affinity for protons. This is shown by fluorescence quenching at lower pH in WM2 and nM2 when rimantadine is bound. This is due to disruption of interactions at the various pH values caused by a structural change.

From the above information it is possible to postulate about the way amantadine and rimantadine bind and inhibit M2. Fluorescence equilibrium measurements which reflected true K_d values for inhibitors gave good agreements with previously reported values. For example K_i values measured electrophysiologically gave a inhibitory constant of 0.3μM (Wang *et al.*,1993) for amantadine while our experiments gave a value of 0.32μM. Results also suggested a 1:1 stiochmetry with one drug molecule binding to one tetramer in both our and Wang's experiments. Again this is in agreement with previously published results. Of note these measurements were done at high and low pH respectively. Wang *et al.* conducted experiments at high pH (non-conducting form of M2) while our experiments were done at low pH (conducting form). This would indicate a lack of pH sensitivity for amantadine binding not as previously reported and that amantadine binds to both the open and closed form of M2 (Wang *et al.*,1993; Salom *et al.*, 2000).

In agreement with previous information, acrylamide quenching experiments suggest that amantadine binds in the channel pore. The first event that occurs

is the drug binds to the channel pore. From our drug structure-function studies, both the adamantane cage and the active group are required for binding of any inhibitor to M2 therefore insinuating two points of contact. This binding then leads to the induction of an optically silent step, which may be a structural change in M2 as reported recently by Hu *et al.,* 2007 in M2TM by ssNMR. The data shown here would indicate that this change occurs in the full-length protein. The exact structural rearrangement shows a small kink within the M2 transmembrane helix. This type of kink would probably require two points of contact with the M2 helices leading to the amantadine molecule "hugging" the transmembrane helices as shown below (Figure 4.4). One of the following things then occurs. Either the amine group interacts with His37 as a surrogate proton acceptor leading to its deprotonation, or the structural change leads to breaking of the His37 tetrad symmetry leading to its deprotonation. Both of these events could lead to a reduction in the proton sensitivity of the His37, which is shown by our experiments. The breaking of the His37 tetrad symmetry may also affect the activation mechanism of M2, thereby inhibiting proton conduction. Our data cannot differentiate as to which of these events might occur. Certainly NMR data would indicate the structural change leads to breaking of His37 dimer formation thereby lowering proton affinity for M2 (Hu *et al.,* 2007). The adamantane cage therefore acts somewhat as a physical restriction through its own bulk and structural rearrangement of the channel also changing the His and Trp side-chain conformation. Further the amine group acts as a surrogate proton acceptor preventing histidine protonation completing channel inhibition. Therefore inhibition of proton translocation is a two-step

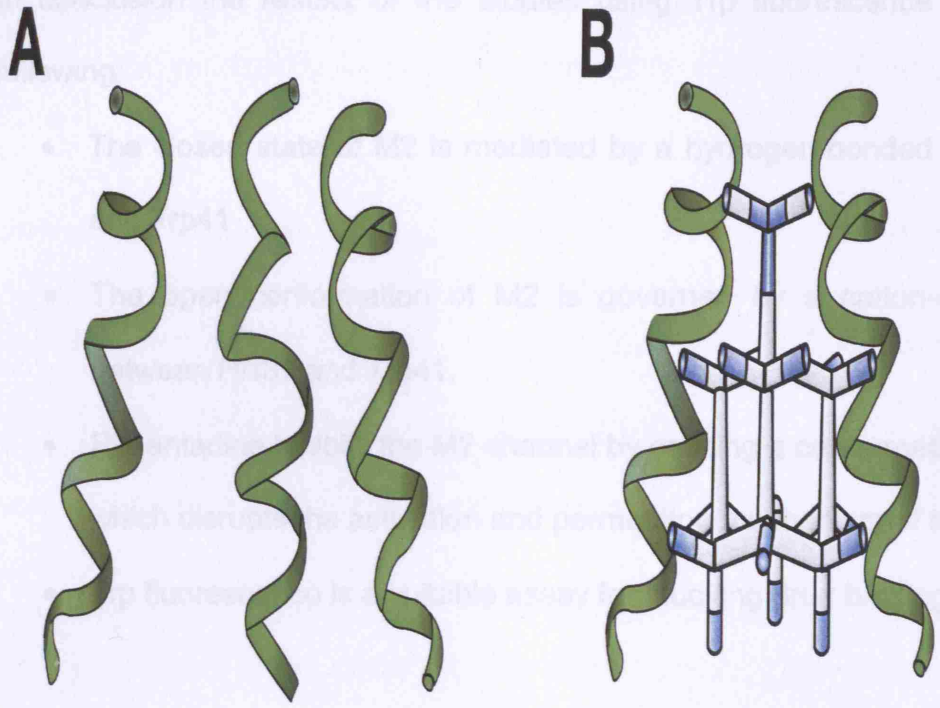

Figure 4.3: A ribbon representation of the M2 transmembrane domain with (B) and without (A) amantadine. In A, the transmembrane domain is orientated with a tilt depending on the thickness of the membrane occupied. In B, amantadine is bound in the channel and the helices bind at the amino group and adamantyl cage producing a kink in the helices.

process as reflected by our kinetic data and is a combination of previously extrapolated theories.

In conclusion the results of the studies using Trp fluorescence showed the following:

- The closed state of M2 is mediated by a hydrogen-bonded His37 tetrad and Trp41
- The open conformation of M2 is governed by a cation-π interaction between His37 and Trp41.
- Rimantadine inhibits the M2 channel by causing a conformational change which disrupts the activation and permeation mechanism of the channel.
- Trp fluorescence is a suitable assay for studying drug binding to M2.

Chapter 5: References

Astrahan, P., I. Kass, M. A. Cooper and I. T. Arkin (2004). "A novel method of resistance for influenza against a channel-blocking antiviral drug." Proteins, **55**:251-257.

Avigliano, L., P. Aducci, P. Sirianni and A. Finazzi-Agro (1984) "A fluorimetric study of the lanthanides binding to concanavalin A." Int J of Biochem, **16**:1409-1413.

Beaton, A.R. and R.M, Krug (1986) "Transcription antitermination during influenza viral template RNA synthesis requires the nucleocapsid protein and the absence of a 5' capped end." Proc Natl Acad Sci U S A, **83**: 6282-6286.

Betakova, T., M. V. Nermut and A. J. Hay (1996). "The NB protein is an integral component of the membrane of influenza B virus." J Gen Virol, **77**: 2689-94.

Betakova, T., F. Ciampor and A. J. Hay (2005) "Influence of residue 44 on the activity of the M2 proton channel of influenza A virus." J Gen Virol, **86**:181-184.

Benne, C. A., F. P. Kroon, M. Harmsen, L. Tavares, C. A. Kraaijeveld and J. C. De Jong (1998). "Comparison of neutralizing and hemagglutination-inhibiting antibody responses to influenza A virus vaccination of human immunodeficiency virus-infected individuals." Clin Diagn Lab Immunol, **5**: 114-7.

Birks, J.B (1973) "Organic Molecular Physics." John Wiley & Sons, New York.

Both, G.W., C.H. Shi and E.D. Kilbourne (1983) "Hemagglutinin of swine influenza virus: a single amino acid change pleiotropically affects viral antigenicity and replication." Proc Natl Acad Sci U S A, **80**: 6996-7000.

Braam, J., I. Ulmanen and R.M. Krug (1983) "Molecular model of a eucaryotic transcription complex: functions and movements of influenza P proteins during capped RNA-primed transcription." Cell, **34**: 609-618.

Brassard, D. L., G. P. Leser and R. A. Lamb (1996). "Influenza B virus NB glycoprotein is a component of the virion." Virology, **220**: 350-60.

Bui, M., G. Whittaker and A. Helenius (1996) "Effect of M1 protein and low pH on nuclear transport of influenza virus ribonucleoproteins." J Virol, **70**: 8391-8401.

Bukrinskaya, A.G., N.K. Vorkunova, G.V. Kornilayeva, R.A Narmanbetova and G.V. Vorkunova (1982) "Influenza virus uncoating in infected cells and effect of rimantadine." J Gen Virol, **60**, 49-59.

Burnet, F.M. and P.E. Lind (1949) "Recombination of characters between two influenza virus strains." Aust. J. Sci,**12**:109-110.

Bush, R.M., C.A. Bender, K. Subbarao, N.J. Cox, and N.W. Fitch (1999) "Predicting the evolution of human influenza A." Science, **286**:1921-1925.

Bushueva, O. A. and V. D. Kuznetsov (1974)"Vliianie uslovi khraneniia na antibioticheskuiu aktivnost' i sostav populiatsii Actinomyces roseolus produtsenta linkomitsina." Antibiotiki, **19**:1099-1100.

Carrasco, M., M. J. Amorim and P. Digard (2004). "Lipid raft-dependent targeting of the influenza A virus nucleoprotein to the apical plasma membrane." Traffic, **5**: 979-92.

Chalfie, M., Y. Tu, G. Euskirchen, W. W. Ward and D. C. Prasher (1994) "Green fluorescent protein as a marker for gene expression." Science, **263**:802-805.

Chattoraj, M., B. A. King, G. U. Bublitz and S. G. Boxer (1996) "Ultra-fast excited state dynamics in green fluorescent protein: multiple states and proton transfer" Proc of the Natl Acad of Sci USA, **93**:8362-8367.

Chizhmakov, I. V., F. M. Geraghty, D. C. Ogden, A. Hayhurst, M. Antoniou, and A.J. Hay (1996). "Selective proton permeability and pH regulation of the influenza virus M2 channel expressed in mouse erythroleukaemia cells." Journal of Physiology, **494**:329-336.

Chizhmakov, I. V., D. C. Ogden, F. M. Geraghty, A. Hayhurst, A. Skinner, T. Betakova and A. J. Hay (2003). "Differences in conductance of M2 proton channels of two influenza viruses at low and high pH." J Physiol, **546**: 427-38.

Choppin, P.W. and I.Tamm (1960) "Studies of two kinds of virus particles which comprise influenza A2 strains. I. Characterization of stable homogeneous strains in reaction with specific antibody, mucoprotein inhibitors and erythrocytes." J. Exp. Med, **112**: 895-920.

Chu, C.M., I.M. Dawson and W.J. Elford (1949) "Filamentous forms associated with newly isolated influenza virus." Lancet,: 602-603.

Ciampor, F., C. A. Thompson, S. Grambas and A. J. Hay (1992). "Regulation of pH by the M2 protein of influenza A viruses." Virus Res, **22**: 247-58.

Cody, C. W., D. C. Prasher, W. M. Westler, F. G. Prendergast and W. W. Ward (1993) "Chemical structure of the hexapeptide chromophore of the Aequorea green-fluorescent protein." Biochemistry, **32**:1212-1218.

Colman, P.M., J.N. Varghese and W.G. Laver (1983) "Structure of the catalytic and antigenic sites in influenza virus neuraminidase." Nature, **303**: 41-44.

Compans, R.W. (1973) "Distinct carbohydrate components of influenza virus glycoproteins in smooth and rough cytoplasmic membranes." Virology, **55**: 541-545

Cubitt, A. B., R. Heim, S. R. Adams, A. E. Boyd, L. A. Gross and R. Y. Tsien (1995) "Understanding, improving and using green fluorescent proteins." T Biochem Sci, **20**: 448-455.

Czabotar, P. E., S. R. Martin and A. J. Hay (2004). "Studies of structural changes in the M2 proton channel of influenza A virus by tryptophan fluorescence." Virus Res, **99**: 57-61.

Deisseroth, A., R. Burk, D. Picciano, W. F. Anderson, A. Nienhuis and J. Minna (1975) "Hemoglobin synthesis in somatic cell hybrids: globin gene expression in hybrids between mouse erythroleukemia and human marrow cells or fibroblasts." Proc Natl Acad Sci USA, **72**:1102-1106.

Domingo, E., A. Mas, E. Yuste, N. Pariente, S. Sierra, N.S Gutierrez-Riva and L. Menendez-Arias (2001) "Virus population dynamics, fitness variations and the control of viral disease: an update." Prog Drug Res, **57**: 77-115.

Domingo, E. (2003) "Quasispecies and the development of new antiviral strategies." Prog Drug Res, **60**: 133-158

Duff, K. C. and R. H. Ashley (1992). "The transmembrane domain of influenza A M2 protein forms amantadine-sensitive proton channels in planar lipid bilayers." Virology, **190**: 485-9.

Duff, K. C., S. M. Kelly, N. C. Price and J. P. Bradshaw (1992). "The secondary structure of influenza A M2 transmembrane domain. A circular dichroism study." FEBS Lett, **311**: 256-8.

Duff, K. C., P. J. Gilchrist, A. M. Saxena and J. P. Bradshaw (1994). "Neutron diffraction reveals the site of amantadine blockade in the influenza A M2 ion channel." Virology, **202**: 287-93.

Eftink, M. R. and C. A. Ghiron (1981) "Fluorescence quenching studies with proteins." Anal Biochem, **114**:199-227.

Eftink, M. R., C. A. Ghiron, R. A. Kautz and R. O. Fox (1991) "Fluorescence and conformational stability studies of Staphylococcus nuclease and its mutants, including the less stable nuclease-concanavalin A hybrids." Biochemistry, **30**:1193-1199.

Fischer, W. B., M. Pitkeathly, B. A. Wallace, L. R. Forrest, G. R. Smith, and M. S. Sansom (2000) "Transmembrane peptide NB of influenza B: a simulation, structure, and conductance study." Biochemistry, **39**:12708-12716.

Fischer, W. B., M. Pitkeathly and M. S. Sansom (2001). "Amantadine blocks channel activity of the transmembrane segment of the NB protein from influenza B." Eur Biophys J, **30**: 416-20.

Fitch, W.M., J.M. Leiter, X.Q. Li and P. Palese (1991) "Positive Darwinian evolution in human influenza A viruses." Proc Natl Acad Sci U S A, **88**: 4270-4274.

Fitch, W.M., R.M. Bush, C.A. Bender and N.J. Cox (1997) "Long term trends in the evolution of H(3) HA1 human influenza type A." Proc Natl Acad Sci U S A, **94**: 7712-7718.

Főrster, T. (1948) "Intermolecular energy Migration and Fluorescence." Ann Phys. **2**:55-75.

Fouchier, R.A.M., V. Munster, R.A. Wallensten, T.M. Bestebroer, S. Herfst, S. Smith, G.F. Rimmelzwaan, B. Olsen and A.D. Osterhaus (2005) "Characterization of a novel Influenza A virus hemagglutinin subtype (H16) obtained from black-headed gulls." J Virol, **79**: 2814-2822.

Gallagher, P.J., J.M. Henneberry, J.F. Sambrook and J.M. Gething (1992) "Glycosylation requirements for intracellular transport and function of the hemagglutinin of influenza virus." J Virol, **66**:7136-7145.

Gandhi, C. S., K. Shuck, J. D. Lear, G. R. Dieckmann, W. F. DeGrado, R. A. Lamb and L. H. Pinto (1999). "Cu(II) inhibition of the proton translocation machinery of the influenza A virus M2 protein." J Biol Chem, **274**: 5474-82.

Glezen, W.P. (1982) "Serious morbidity and mortality associated with influenza epidemics." Epidemiol Rev, **4**: 25-44.

Gottschalk, A. (1959) "On the mechanism underlying initiation of influenza virus infection." Ergeb Mikrobiol Immunitatsforsch Exp Ther, **32**: 1-22.

Grambas, S., M. S. Bennett and A. J. Hay (1992). "Influence of amantadine resistance mutations on the pH regulatory function of the M2 protein of influenza A viruses." Virology, **191**: 541-9.

Gryczynski, I., H. Cherek and J. R. Lakowicz (1988) "Detection of three rotational correlation times for a rigid asymmetric molecule using frequency-domain fluorometry." Biophys Chem, **30**:271-277.

Hagen, M., T.D. Chung, J.A. Butcher and M Krystal (1994) "Recombinant influenza virus polymerase: requirement of both 5' and 3' viral ends for endonuclease activity." J Virol, **68**:1509-1515.

Hatta, M. and Y. Kawaoka (2003). "The NB protein of influenza B virus is not necessary for virus replication in vitro." J Virol, **77**: 6050-4.

Hay, A.J. (1974) "Studies on the formation of the influenza virus envelope." Virology, **60**: 398-418.

Hay, A.J., Lomniczi, B., Bellamy, A.R. and Skehel, J.J. (1977) Transcription of the influenza virus genome. Virology, **83**: 337-355.

Hay, A. J. and J. J. Skehel (1979). "Characterization of influenza virus RNA transcripts synthesized in vitro." J Gen Virol, **44**: 599-608.

Hay, A. J., A. J. Wolstenholme, J. J. Skehel and M. H. Smith (1985). "The molecular basis of the specific anti-influenza action of amantadine." Embo J, **4**: 3021-4.

Hayden, F. G., R. B. Belshe, R. D. Clover, A. J. Hay, M. G. Oakes and W. Soo (1989). "Emergence and apparent transmission of rimantadine-resistant influenza A virus in families." N Engl J Med, **321**: 1696-702.

Hayden, F. G. (2006). "Antivirals for influenza: historical perspectives and lessons learned." Antiviral Res, **71**: 372-8.

Heim, R., D. C. Prasher and R. Y. Tsien (1994) "Wavelength mutations and posttranslational autoxidation of green fluorescent protein." Proc Natl Acad Sci USA, **91**:12501-12504.

Holsinger, L. J. and R. A. Lamb (1991). "Influenza virus M2 integral membrane protein is a homotetramer stabilized by formation of disulfide bonds." Virology, **183**: 32-43.

Honda, A., K. Mizumoto and A. Ishihama (2002) "Minimum molecular architectures for transcription and replication of the influenza virus." Proc Natl Acad Sci U S A, **99**: 13166-13171

Hongo, S., K. Sugawara, H. Nishimura, Y. Muraki, F. Kitame and K. Nakamura1(994). "Identification of a second protein encoded by influenza C virus RNA segment 6." J Gen Virol, **75**:3503-3510.

Hongo, S., K. Sugawara, Y. Muraki, F. Kitame and K. Nakamura (1997) "Characterization of a second protein (CM2) encoded by RNA segment 6 of influenza C virus." J Virol, **71**:2786-2792.

Hongo, S., P. Gao, K. Sugawara, Y. Muraki, Y. Matsuzaki, Y. Tada, F. Kitame and K. Nakamura (1998) "Identification of a 374 amino acid protein encoded by RNA segment 6 of influenza C virus." J Gen Virol, **79**:2207-2213.

Hongo, S., K. Ishii, K. Mori, E. Takashita, Y. Muraki, Y. Matsuzaki and K. Sugawara (2004)" Detection of ion channel activity in Xenopus laevis oocytes expressing Influenza C virus CM2 protein" Arch Virol, **149**:35-50.

Horvath, C. M., M. A. Williams, and R. A. Lamb (1990)"Eukaryotic coupled translation of tandem cistrons: identification of the influenza B virus BM2 polypeptide." EMBO J, **9**:2639-2647.

Hu, J., R. Fu, K. Nishimura, L. Zhang, H. X. Zhou, D. D. Busath, V. Vijayvergiya and T. A. Cross (2006). "Histidines, heart of the hydrogen ion channel from influenza A virus: toward an understanding of conductance and proton selectivity." Proc Natl Acad Sci U S A, **103**: 6865-70.

Hu, J., R. Fu and T. A. Cross (2007) "The chemical and dynamical influence of tanti-viral drug amantadine on the M2 proton channel transmembrane domain." Biophys J, **93**:276-283.

Ina, Y. and T. Gojobori (1994) "Statistical analysis of nucleotide sequences of the hemagglutinin gene of human influenza A viruses." Proc Natl Acad Sci U S A, **91**: 8388-8392.

Inouye, S., H. Ogawa, K. Yasuda, K. Umesono and F. I. Tsuji (1997) "A bacterial cloning vector using a mutated Aequorea green fluorescent protein as an indicator." Gene, **189**:159-162.

Jablonski ,A (1935) "Uber den Mechanisms des Photolumineszenz von Farbstoffphosphoren". Z.Phys, **94**: 38-46.

Johansson, B.E., D.J. Bucher and E.D. Kilbourne (1989) "Purified influenza virus hemagglutinin and neuraminidase are equivalent in stimulation of antibody response but induce contrasting types of immunity to infection." J Virol **63**: 1239-1246.

Kates, M., A.C. Allison, D.A.C. Tyrrell and A.T. James (1961) "Lipids of influenza virus and their relation to those of the host cell." Biochimica et Biophisica Acta, **52**: 455-466.

Kato, N., H. J. Eggers & H. Rolly (1969). Inhibition of release of vaccinia virus by N_1-isonicotinoyl-N_2-3-methyl-4-chlorobenzoylhydrazine. J Exp Med **129**: 795–808.

Kautsky, H. (1939) "Quenching of luminescence by oxygen." Trans Faraday Soc, **35:** 216-219.

Kawaoka, Y., S. Krauss and R.G. Webster (1989) "Avian-to-human transmission of the PB1 gene of influenza A viruses in the 1957 and 1968 pandemics." J Virol, **63**: 4603-4608.

Knibbe, H., D. Rehm and A. Weller (1968) "Intermediates and kinetics of fluorescence quenching by electron transfer." Phys Chem, **72**:257-263.

Kemble, G. and H. Greenberg (2003) "Novel generations of influenza vaccines." Vaccine, **21**: 1789-1795.

Kochendoerfer, G. G., D. Salom, J. D. Lear, R. Wilk-Orescan, S. B. Kent and W. F. DeGrado (1999). "Total chemical synthesis of the integral membrane protein influenza A virus M2: role of its C-terminal domain in tetramer assembly." Biochemistry, **38**: 11905-13.

Kupper, J (1998) Functional expression of GFP-tagged Kv1.3 and Kv1.4 channels in HEK 293 cells." Euro J of Neuro, **10**:3908-3912.

Kukol, A., P. D. Adams, L. M. Rice, A. T. Brunger and T. I. Arkin (1999). "Experimentally based orientational refinement of membrane protein models: A structure for the Influenza A M2 H+ channel." J Mol Biol, **286**: 951-62.

Lakowicz, J. R. and I. Gryczynski (1993) "Characterization of p-bis(O-methylstyryl)benzene as a lifetime and anisotropy decay standard for two-photon induced fluorescence." Biophys Chem, **47**:1-7.

Lakowicz, J.R. (1999) "Principles of Fluorescence Spectroscopy" Second Edition. Kluwer Academic/Plenum Publishers.

Lamb, R. A. and P. W. Choppin (1981). "Identification of a second protein (M2) encoded by RNA segment 7 of influenza virus." Virology, **112**: 729-37.

Lamb, R. A., S.L. Zebedee & C.D. Richardson (1985). "Influenza Virus M2 protein is an integral membrane protein ezpressed on the infected cell surface." Cell **40:** 627-33.

Le, Q. M., M. Kiso, K. Someya, Y. T. Sakai, T. H. Nguyen, K. H. Nguyen, N. D. Pham, H. H. Ngyen, S. Yamada, Y. Muramoto, T. Horimoto, A. Takada, H. Goto, T. Suzuki, Y. Suzuki and Y. Kawaoka (2005). "Avian flu: isolation of drug-resistant H5N1 virus." Nature, **437**: 1108.

Leser, G. P. and R. A. Lamb (2005) "Influenza virus assembly and budding in raft-derived microdomains: a quantitative analysis of the surface distribution of HA, NA and M2 proteins." Virology, **342**:215-227.

Li, Z. N., S. Hongo, K. Sugawara, K. Sugahara, E. Tsuchiya, Y. Matsuzaki and K. Nakamura (2001) "The sites for fatty acylation, phosphorylation and intermolecular disulphide bond formation of influenza C virus CM2 protein." J Gen Virol, **82**:1085-1093.

Lin, T. I. and C. Schroeder (2001). "Definitive assignment of proton selectivity and attoampere unitary current to the M2 ion channel protein of influenza A virus." J Virol, **75**: 3647-56.

Liu, J., T. E. Hughes and W. C. Sessa (1997) "The first 35 amino acids and fatty acylation sites determine the molecular targeting of endothelial nitric oxide synthase into the Golgi region of cells: a green fluorescent protein study." J Cell Biol, **137**:1525-1535.

Loewenthal, R., J. Sancho and A. R. Fersht (1991) "Fluorescence spectrum of barnase: contributions of three tryptophan residues and a histidine-related pH dependence." Biochemistry, **30**:6775-6779.

Matlin, K.S., H. Reggio, A. Helenius and K. Simons (1981) "Infectious entry pathway of influenza virus in a canine kidney cell line." J Cell Biol, 91: 601-613.

Martin, K. and A. Helenius (1991). "Nuclear transport of influenza virus ribonucleoproteins: the viral matrix protein (M1) promotes export and inhibits import." Cell, **67**: 117-30.

Marshall, W. S., S. E. Bryson, A. Midelfart and W. F. Hamilton (1995) "Low-conductance anion channel activated by cAMP in teleost Cl- -secreting cells." Am J Physiol, **268**:R963-969.

McCown, M. F. and A. Pekosz (2006). "Distinct domains of the influenza a virus M2 protein cytoplasmic tail mediate binding to the M1 protein and facilitate infectious virus production." J Virol **80**: 8178-89.

Miesenbock, G., D. A. De Angelis and J. E. Rothman (1998) "Visualizing secretion and synaptic transmission with pH-sensitive green fluorescent proteins." Nature, **394**:192-195.

Miroux, B. and J. E. Walker (1996) "Over-production of proteins in Escherichia coli: mutant hosts that allow synthesis of some membrane proteins and globular proteins at high levels." J Mol Biol, **260**:289-298.

Mosley, V.M. and R.W.G. Wyckoff (1946) "Electron micrography of the virus of influenza." Nature: 157-263.

Mould, J. A., J. E. Drury, S. M. Frings, U. B. Kaupp, A. Pekosz, R. A. Lamb and L. H. Pinto (2000). "Permeation and activation of the M2 ion channel of influenza A virus." J Biol Chem, **275**: 31038-50.

Mould, J. A., R. G. Paterson, M. Takeda, Y. Ohigashi, P. Venkataraman, R. A. Lamb and L. H. Pinto (2003). "Influenza B virus BM2 protein has ion channel activity that conducts protons across membranes." Dev Cell, **5**: 175-84.

Mura, M., R. G. Webster and F. A. Ennis (1991). "Antibodies to HA and NA augment uptake of influenza A viruses into cells via Fc receptor entry." Virology, **182**: 211-9.

Nayak, D. P., E. K. Hui and S. Barman (2004). "Assembly and budding of influenza virus." Virus Res, **106**: 147-65.

Needham, M., C. Gooding, K. Hudson, M. Antoniou, F. Grosveld and M. Hollis (1992) "LCR/MEL: a versatile system for high-level expression of heterologous proteins in erythroid cells." Nucl Aci Res, **20**:997-1003.

Neumann, G., G. G. Brownlee, E. Fodor and Y. Kawaoka (2004). "Orthomyxovirus replication, transcription, and polyadenylation." Curr Top Microbiol Immunol, **283**: 121-43.

Nishimura, K., S. Kim, L. Zhang and T. A. Cross (2002). "The closed state of a H+ channel helical bundle combining precise orientational and distance restraints from solid state NMR." Biochemistry, **41**: 13170-7.

Niwa, H., S. Inouye, T. Hirano, T. Matsuno, S. Kojima, M. Kubota, M. Ohashi and F. I. Tsuji 1(996) "Chemical nature of the light emitter of the Aequorea green fluorescent protein." Proc Natl Acad Sci USA, **93**:13617-13622.

Odagiri, T., J. Hong, and Y. Ohara (1999) "The BM2 protein of influenza B virus is synthesized in the late phase of infection and incorporated into virions as a subviral component." J Gen Virol, **80**:2573-2581.

Okada, A., T. Miura and H. Takeuchi (2001). "Protonation of histidine and histidine-tryptophan interaction in the activation of the M2 ion channel from influenza a virus." Biochemistry, **40**: 6053-60.

Takeuchi, H., A. Okada and T. Miura (2003) "Roles of the histidine and tryptophan side chains in the M2 proton channel from influenza A virus." FEBS Lett, **552**:35-38.

Palese, P., J.L. Schulman, G. Bodo and P Meindl (1974) "Inhibition of influenza and parainfluenza virus replication in tissue culture by 2-deoxy-2,3-dehydro-N-trifluoroacetylneuraminic acid (FANA)." Virology, **59**: 490-498.

Paterson, R. G., M. Takeda, Y. Ohigashi, L. H. Pinto, and R. A. Lamb (2003) "Influenza B virus BM2 protein is an oligomeric integral membrane protein expressed at the cell surface." Virology, **306**:7-17.

Peiris, M., K.Y. Yuen, C.W. Leung, K.H Chan, P.L. Ip, R.W. Lai, W.K. Orr and K.F. Shortridge (1999) "Human infection with influenza H9N2." Lancet, **354**: 916-917.

Permyakov, E. A., I. L. Reyzer and L. J. Berliner 1(993) "Effects of Zn(II) on galactosyltransferase activity." J Prot Chem, **12**:633-638.

Petrich, J. W., J. L. Martin, D. Houde, C. Poyart and A. Orszag (1987) "Time-resolved Raman spectroscopy with subpicosecond resolution: vibrational cooling and delocalization of strain energy in photodissociated (carbonmonoxy)hemoglobin." Biochemistry, **26**:7914-7923.

Pinto, L. H., L. J. Holsinger and R. A. Lamb (1992). "Influenza virus M2 protein has ion channel activity." Cell, **69**: 517-28.

Pinto, L. H., G. R. Dieckmann, C. S. Gandhi, C. G. Papworth, J. Braman, M. A. Shaughnessy, J. D. Lear, R. A. Lamb and W. F. DeGrado (1997). "A functionally defined model for the M2 proton channel of influenza A virus suggests a mechanism for its ion selectivity." Proc Natl Acad Sci U S A, **94**: 11301-6.

Pons, M.W., I.T. Schulze, G.K. Hirst and R. Hauser (1969) "Isolation and characterization of the ribonucleoprotein of influenza virus." Virology, **39**: 250-259.

Portela, A. and P. Digard (2002) "The influenza virus nucleoprotein: a multifunctional RNA-binding protein pivotal to virus replication." J Gen Virol, **83**: 723-734.

Prasher, D. C., V. K. Eckenrode, W. W. Ward, F. G. Prendergast and M. J. Cormier (1992) "Primary structure of the Aequorea victoria green-fluorescent protein." Gene, **111**:229-233.

Roberts, P. C., R. A. Lamb and R. W. Compans (1998). "The M1 and M2 proteins of influenza A virus are important determinants in filamentous particle formation." Virology, **240**: 127-37.

Ruigrok, R.W., P.J. Andree, R.A. Hooft van Huysduynen and J.E. Mellema (1984) "Characterization of three highly purified influenza virus strains by electron microscopy." J Gen Virol, **65**: 799-802.

Ruigrok, R.W. (1998) "Structure of Influenza A, B and C viruses. In K.G. Nicholson, R.G. Webster and A.J. Hay (eds.), Textbook of Influenza. Blackwell Science, Oxford, pp. 29-42.

Saito, T., G. Taylor and R.G. Webster (1995) "Steps in maturation of influenza A virus neuraminidase." J Virol, **69**: 5011-5017.

Sakaguchi, T., Q. Tu, L. H. Pinto and R. A. Lamb (1997). "The active oligomeric state of the minimalistic influenza virus M2 ion channel is a tetramer." Proc Natl Acad Sci U S A, **94**: 5000-5.

Sakurai, H., S. Shimomura, Y. Sugiura and K. Ishizu (1979) "A model of the heme site of cytochrome P-450: characterization of a sulfhydryl- and imidazole-containing peptide-heme system in solution." Chem Pharm Bull, **27**:3022-3028.

Salom, D., B. R. Hill, J. D. Lear and W. F. DeGrado (2000). "pH-dependent tetramerization and amantadine binding of the transmembrane helix of M2 from the influenza A virus." Biochemistry, **39**: 14160-70.

Sanger, F., G. M. Air, B. G. Barrell, N. L. Brown, A. R. Coulson, C. A. Fiddes, C. A. Hutchison, P. M. Slocombe and M. Smith (1977) "Nucleotide sequence of bacteriophage phi X174 DNA." Nature, **265**:687-695.

Sansom, M. S. and I. D. Kerr (1993). "Influenza virus M2 protein: a molecular modelling study of the ion channel." Protein Eng, **6**: 65-74.

Sansom, M. S., I. D. Kerr, G. R. Smith and H. S. Son (1997). "The influenza A virus M2 channel: a molecular modeling and simulation study." Virology, **233**: 163-73.

Schild, G.C., J.S. Oxford, D.C. de Jong and R.G. Webster (1983) "Evidence for host-cell selection of influenza virus antigenic variants." Nature, **303**: 706-709.

Schroeder, C., C. M. Ford, S. A. Wharton and A. J. Hay (1994). "Functional reconstitution in lipid vesicles of influenza virus M2 protein expressed by baculovirus: evidence for proton transfer activity." J Gen Virol, **75** : 3477-84.

Schulman, J.L., M. Khakpour and E.D. Kilbourne (1968) "Protective effects of specific immunity to viral neuraminidase on influenza virus infection of mice." J Virol, 2: 778-786.

Schulze, I.T. (1970) "The structure of influenza virus. I. The polypeptides of the virion." Virology, **42**: 890-904.

Schulze, I.T. (1972) "The structure of influenza virus. II. A model based on the morphology and composition of subviral particles." Virology, **47**: 181-196.

Seidel, C.A.M., A. Schulz and M.H.M Sauer (1993) "Nucleotide base-specific sequencing of fluorescent dyes. 1.Nucleobase one-electron redox potentials and their correlation with static and dynamic quenching efficiencies." J Phys Chem, **100**:5541-5553.

Shaw, M. W., P. W. Choppin and R. A. Lamb (1983). "A previously unrecognized influenza B virus glycoprotein from a bicistronic mRNA that also encodes the viral neuraminidase." Proc Natl Acad Sci U S A, **80**: 4879-83.

Shimbo, K., D. L. Brassard, R. A. Lamb and L. H. Pinto (1995). "Viral and cellular small integral membrane proteins can modify ion channels endogenous to Xenopus oocytes." Biophys J, **69**: 1819-29.

Shinitzky, M. and R. Goldman (1967) "Fluorometric detection of histiine-tryptophan complexes in peptides and proteins." Euro J of Biochem, **3**:139-144.

Sieczkarski, S.B. and G.W. Whittaker (2002) "Influenza virus can enter and infect cells in the absence of clathrin-mediated endocytosis." J Virol, **76**: 10455-10464.

Siegel, M. S. and E. Y. Isacoff 1(997) "A genetically encoded optical probe of membrane voltage." Neuron, **19**:735-741.

Skehel, J.J., P.M. Bayley, E.B. Brown, S.R. Martin, M.D. Waterfield, J.M. White, I.A. Wilson and D.C. Wiley (1982) "Changes in the conformation of influenza virus hemagglutinin at the pH optimum of virus-mediated membrane fusion." Proc Natl Acad Sci U S A, **79**: 968-972.

Smith, W., C.H. Andrewes and P.P. Laidlaw (1933) "A virus obtained from influenza patients." Lancet: 66-68.

Smith, W. and C.H. Stuart-Harris (1936) "Influenza infection of man from the ferret." Lancet:121-123.

Song, Z., F. A. Kovacs, J. Wang, J. K. Denny, S. C. Shekar, J. R. Quine and T. A. Cross (2000). "Transmembrane domain of M2 protein from influenza A virus studied by solid-state (15)N polarization inversion spin exchange at magic angle NMR." Biophys J, **79**: 767-75.

Spencer, T. A. and L. D. Eisenhauer (1970) "A study of amine-catalyzed epimerization of 2-beta-methylcholestan-3-one." J Org Chem, **35**:2632-2635.

Sreerama, N. and R. W. Woody (2000) "Estimation of protein secondary structure from circular dichroism spectra: comparison of CONTIN, SELCON, and CDSSTR methods with an expanded reference set." Anal Biochem, **287**:252-260.

Stieneke-Grober, A., M. Vey, H. Angliker, E. Shaw, G. Thomas, C. Roberts, H.D. Klenk, and W. Garten (1992) "Influenza virus hemagglutinin with multibasic cleavage site is activated by furin, a subtilisin-like endoprotease." Embo J, **11**: 2407-2414.

Stouffer, A. L., V. Nanda, J. D. Lear and W. F. DeGrado (2005) "Sequence determinants of a transmembrane proton channel: an inverse relationship between stability and function." J Mol Biol, **347**:169-179.

Strickland, E. H., C. Billups and E. Kay (1972) "Effects of hydrogen bonding and solvents upon the tryptophanyl 1 L a absorption band. Studies using 2,3-dimethylindole." Biochemistry, **11**:3657-3662.

Strickler, S.J. and R.A. Berg (1962) "Relationship between absorption intensity and fluorescence lifetime of molecules." J. Chem Phys, **37**:814-822.

Sugrue, R.J., G. Bahadur, M.C. Zambon, M. Hall-Smith, A.R. Douglas & A.J. Hay (1990) "Specific structural alteration of the Influenza haemagglutinin by amantadine." EMBO J, 9:3469-3476.

Sugrue, R.J., R.B. Belshe and A.J. Hay (1990) "Palmitoylation of the influenza A virus M2 protein." Virology, 179: 51-56.

Sugrue, R. J. and A. J. Hay (1991). "Structural characteristics of the M2 protein of influenza A viruses: evidence that it forms a tetrameric channel." Virology, **180**: 617-24.

Sunstrom, N. A., L. S. Premkumar, A. Premkumar, G. Ewart, G. B. Cox and P. W. Gage (1996). "Ion channels formed by NB, an influenza B virus protein." J Membr Biol, **150**: 127-32.

Tang, Y., F. Zaitseva, R. A. Lamb and L. H. Pinto (2002). "The gate of the influenza virus M2 proton channel is formed by a single tryptophan residue." J Biol Chem, **277**: 39880-6.

Taylor, H.P. and N.J. Dimmock (1985) "Mechanism of neutralization of influenza virus by secretory IgA is different from that of monomeric IgA or IgG." J Exp Med, **161**:198-209.

Taylor, A.R., D.G. Sharp, D. Beard, W.J. Beard, D.H. Dingle and A.E. Feller (1943) "Isolation and characterisation of influenza A virus (PR8 strain)." J. Immunolgy, **47:** 261-282.

Tian, C., K. Tobler, R. A. Lamb, L. H. Pinto and T. A. Cross (2002). "Expression and initial structural insights from solid-state NMR of the M2 proton channel from influenza A virus." Biochemistry, **41**: 11294-300.

Tillett, H. E., J. W. Smith and R. E. Clifford (1980). "Excess morbidity and mortality associated with influenza in England and Wales." Lancet,: 793-5.

Thompson C. (1994)"" PhD Thesis

Torres, J., A. Kukol and I. T. Arkin (2000). "Use of a single glycine residue to determine the tilt and orientation of a transmembrane helix. A new structural label for infrared spectroscopy." Biophys J, **79**: 3139-43.

Tu, Q., L. H. Pinto, G. Luo, M. A. Shaughnessy, D. Mullaney, S. Kurtz, M. Krystal and R. A. Lamb (1996). "Characterization of inhibition of M2 ion channel activity by BL-1743, an inhibitor of influenza A virus." J Virol, **70**: 4246-52.

van Thor, J. J., A. J. Pierik, I. Nugteren-Roodzant, A. Xie and K. J. Hellingwerf (1998) "Characterization of the photoconversion of green fluorescent protein with FTIR spectroscopy." Biochemistry, **37**:16915-16921.

Venkataraman, P., R. A. Lamb and L. H. Pinto (2005). "Chemical rescue of histidine selectivity filter mutants of the M2 ion channel of influenza A virus." J Biol Chem, **280**: 21463-72.

Vijayvergiya, V., R. Wilson, A. Chorak, P. F. Gao, T. A. Cross and D. D. Busath (2004). "Proton conductance of influenza virus M2 protein in planar lipid bilayers." Biophys J, **87**: 1697-704.

Virelizier, J.L. (1975) "Host defenses against influenza virus: the role of anti-hemagglutinin antibody." J Immunol, 115: 434-439.

Virelizier, J.L., J.S. Oxford and G.C. Schild (1976) "The role of humoral immunity in host defence against influenza A infection in mice." Postgrad Med J, 52: 332-337.

von Itzstein, M., W.Y. Wu, G.B. Kok, M.S. Pegg, J.C. Dyason, B. Jin, T. Van Phan, M.L. Smythe, H.F. White, S.W Oliver and et al. (1993) "Rational design of

potent sialidase-based inhibitors of influenza virus replication." Nature, 363: 418-423.

Wang, C., K. Takeuchi, L. H. Pinto and R. A. Lamb (1993). "Ion channel activity of influenza A virus M2 protein: characterization of the amantadine block." J Virol, **67**: 5585-94.

Wang, C., R. A. Lamb and L. H. Pinto (1995). "Activation of the M2 ion channel of influenza virus: a role for the transmembrane domain histidine residue." Biophys J, **69**: 1363-71.

Wang, S. and T. Hazelrigg (1994) "Implications for bcd mRNA localization from spatial distribution of exu protein in Drosophila oogenesis." Nature, **369**:400-403.

Ward, W. W. and S. H. Bokman (1982) "Reversible denaturation of Aequorea green-fluorescent protein: physical separation and characterization of the renatured protein." Biochemistry, **21**:4535-4540.

Weber, G. (1966) "Polarization of the fluorescence of solutions." Fluorescence and Phosphorescence Analysis, D.M. Hercules (ed.), John Wiley and Sons, New York: 217-240.

Webster, R. G., W. J. Bean, O. T. Gorman, T. M. Chambers and Y. Kawaoka (1992). "Evolution and ecology of influenza A viruses." Microbiol Rev, **56**: 152-79.

Wharton, S. A., R. B. Belshe, J. J. Skehel and A. J. Hay (1994). "Role of virion M2 protein in influenza virus uncoating: specific reduction in the rate of membrane fusion between virus and liposomes by amantadine." J Gen Virol, **75**: 945-8.

Willaert, K., R. Loewenthal, J. Sancho, M. Froeyen, A. Fersht and Y. Engelborghs (1992) "Determination of the excited-state lifetimes of the tryptophan residues in barnase, via multifrequency phase fluorometry of tryptophan mutants. Biochemistry. **31**:711-716.

WHO. (1953) World Health. Organ. Tech. Rep. Ser. 64.

Yang, F., L. G. Moss and G. N. Phillips, Jr (1996) "The molecular structure of green fluorescent protein." Nat Biotech, **14**:1246-1251.

Zebedee, S. L., C. D. Richardson and R. A. Lamb (1985). "Characterization of the influenza virus M2 integral membrane protein and expression at the infected-cell surface from cloned cDNA." J Virol, **56**: 502-11.

Zhirnov, O. P. (1992). "Isolation of matrix protein M1 from influenza viruses by acid-dependent extraction with nonionic detergent." Virology, **186**: 324-30.

Zimmer, M (2002) "Green fluorescent protein (GFP): applications, structure, and related photophysical behavior." Chem Rev, **102**:759-781.

Zlydnikov, D. M., L. Z. Sterninson, A. Romanov Iu, M. G. Shamanova and O. I. Kubar (1982). "[Rendering medical care to patients with influenza and other acute viral diseases complicated by pneumonia]." Klin Med (Mosk), **60**: 27-30.

Chapter 1

Introductionn